Finite element methods for multicomponent flow problems

Aaron Matthew Baier-Reinio

Hertford College

University of Oxford

A thesis submitted for the degree of

Doctor of Philosophy

Trinity 2026

This thesis is dedicated to my parents.

Acknowledgements

First and foremost, I would like to thank my superb DPhil supervisor, Patrick Farrell, for his guidance and mentorship over these last few years. His vision and immense wealth of mathematical knowledge have been invaluable in my journey to complete this thesis. Of equal importance have been the many opportunities and lessons he has imparted on me regarding how to successfully navigate with confidence in research and academia. I am excited for what the future holds, and equipped with this background, feel prepared as ever to tackle the challenges that lie ahead.

I am immensely grateful to Charles Monroe, for the many hours spent having enlightening discussions on physics and engineering. These have shaped my mindset on the importance and great fun of interdisciplinary research. I owe great thanks to Yuji Nakatsukasa, for inviting me to all of his stimulating research group meetings, and for his frequent words of encouragement. I am incredibly grateful to Endre Süli, for the numerous enlightening mathematical discussions over the years, and especially for taking the time to carefully read through my thesis and for serving as my internal examiner. Likewise, I am incredibly grateful to Clément Cancès, also for taking the time to read through my thesis in great detail, and for visiting Oxford to serve as my external examiner.

As always, words cannot express my gratitude towards my family for their unwavering support. Finally, I wish to thank all of my friends and academic colleagues, especially those in the Numerical Analysis group. It was my absolute greatest pleasure to spend the last four years with you. Not a day went past where I did not forward to going into the office, which was always great fun and full of stimulating discussions. I feel incredibly privileged and grateful to have worked with such an amazing group of people for my DPhil degree.

Abstract

Multicomponent flows consist of multiple distinct chemical species in a common thermodynamic phase. This thesis develops a general framework for the numerical simulation of such flows using finite element methods. The partial differential equations that we employ are the Onsager–Stefan–Maxwell (OSM) equations of irreversible thermodynamics, coupled with the Navier–Stokes equations. These yield a thermodynamically consistent framework for capturing a wide variety of coupled physical phenomena, including momentum transport, cross-diffusion, thermodynamic non-idealities, electrochemical effects, local electroneutrality, heat transport, and thermodiffusion. Such phenomena appear ubiquitously in scientific applications, but the numerical analysis literature studying their coupling is extremely limited.

Chapter 2 of this thesis devises a family of high-order finite element algorithms for the stationary isothermal Stokes–OSM equations. This enables their efficient numerical solution by finite element methods in three dimensions for the first time. We also prove well-posedness and quasi-optimality of these discretisations in a Picard linearised setting. Chapter 3 extends these algorithms to handle transient, Navier–Stokes–OSM flow in electrolyte mixtures that are locally electroneutral. Here, a subtle interplay between the boundary conditions and volumetric equation of state arises, which we identify and address for the first time. Finally, chapter 4 extends the algorithms further by capturing heat transport and thermodiffusion in anisothermal multicomponent flows. Therein we also show, for the first time, that it is possible to obtain structure-preserving discretisations in the sense of energy preservation and entropy dissipation.

Throughout the thesis, numerical simulations demonstrate the scientific applicability of the methods. These simulations include (i) the non-ideal microfluidic mixing of hydrocarbons, (ii) electrolytic flow around a microfluidic rotating disk electrode, and (iii) ion, heat and momentum transport in electrolyte mixtures used in lithium-ion batteries.

Contents

List of figures

Chapter 1

Introduction

Section 1.1 of this chapter is adapted from the introduction sections in [6, 7].

1.1 Introduction to multicomponent flows

This thesis is concerned with the numerical simulation of *multicomponent fluids* (or *mixtures*) using finite element methods. Mixtures are fluids comprised of $n \geq 2$ distinct chemical species (or *components*) in a common thermodynamic phase (e.g. liquid or gas). The defining challenge in modelling mixtures is that the different components are not independent; they are instead coupled through physical processes such as diffusion or reaction. Air, for example, is a mixture of oxygen, carbon dioxide, water vapour, nitrogen and other species, and when modelling airflow in the lungs for heliox therapy, it is important to track these different components and model their diffusive interactions [77].

A common but limiting assumption in multicomponent fluid modelling is that the mixture is in the *dilute regime*. In this regime the concentration of one component (the *solvent*) dominates that of all others (the *solutes*). Consequently, the solvent velocity field can be solved for independently of the solutes, using, for example, the Navier–Stokes equations. The solute concentrations can then be modelled using decoupled advection-diffusion equations in which the solvent velocity field is used for advection and the diffusive fluxes are modelled using Fick's law [53]. However, in *non-dilute* (or *concentrated*) mixtures, this approach can fail drastically. In the concentrated regime all components are present in similar amounts, and Fick's law breaks down as it fails to capture the appreciable diffusional forces that the components can exert on one another [77, 78, 123]. This behavior, known as *cross-diffusion* [28, 69, 108], plays an important role in many areas of science; examples include physiology [30], combustion [56], electrochemistry [86], geosciences [110] and separation processes [119].

We model cross-diffusion using the *Onsager–Stefan–Maxwell*[1] *(OSM) equations* [14, 77, 78, 86, 87, 123]. These are named after Onsager, who developed the theory of irreversible thermodynamics [88, 89, 90], and Stefan and Maxwell, who independently derived the *Stefan–Maxwell (SM) equations* [82, 107] which model cross-diffusion in ideal gaseous mixtures. It was first realised in [79] that Onsager's theory and the SM equations are compatible; their reconciliation yields the more general OSM equations. The OSM equations are applicable to gases and condensed phases, are valid in the dilute and concentrated regimes, and can account for a range of physical phenomena including pressure diffusion and thermal diffusion [14, 123]. Moreover, the OSM equations can handle thermodynamic non-idealities (arising in mixtures with a nonzero excess Gibbs free energy of mixing [60]), the effects of which are important in the non-dilute regime [78]. The OSM equations also obey the second law of thermodynamics, which states that entropy generation in a closed system is non-negative. This ensures that the *thermodiffusion transport matrix*, defined in section 1.6, is positive-semidefinite [90, 112, 113], which will be crucial in our subsequent mathematical analysis.

The OSM equations are of particular importance in electrochemistry. In this context, the equations were popularised by Newman [86, 87] for modelling electrolytes, and the resulting framework is sometimes known as *concentrated solution theory*. The OSM equations provide a thermodynamically rigorous model for electrolytic mass transport by convection, cross-diffusion and electromigration. The equations are also compatible with the principle of local electroneutrality [114]. In many applications, momentum transport plays an important role (e.g. fuel cells, electrodialysis). In such cases it is necessary to couple the OSM equations to momentum conservation laws such as the Stokes or Navier–Stokes equations.

Despite being ubiquitous in many scientific applications, the OSM equations have received limited attention in the numerical analysis literature. This is especially true regarding discretisation by finite element methods; we are only aware of a handful of papers in this direction [4, 24, 26, 46, 80]. However, finite element methods are a natural candidate for tackling real-world scientific applications, owing to their ability to handle complex geometries and boundary conditions. High-order finite element methods are especially appealing because of their ability to exploit the high arithmetic intensity of modern computer architectures. Moreover, almost all of the existing OSM numerics literature relies on limiting physical assumptions, such as: a thermodynamically ideal gaseous mixture; that the equations for momentum transport can

[1]Sometimes in the literature called the *generalised Stefan–Maxwell* or *Maxwell–Stefan* equations.

be decoupled from the OSM equations; that the mixture is quasi-incompressible; or the Boussinesq approximation holds. It would be desirable to overcome the need for such assumptions, since they limit the scientific applicability of existing methods.

The purpose of this thesis is to develop a robust numerical framework for multicomponent fluids, based on the OSM equations and finite element methods, that does not rely on limiting physical assumptions such as those mentioned above. As we shall see in the forthcoming chapters, this shall enable the simulation of scientific applications that were previously inaccessible.

1.2 Mathematical summary of equilibrium thermodynamics of multicomponent systems

A natural starting point in the study of multicomponent systems is the theory of equilibrium thermodynamics. This concerns systems that are in *thermodynamic equilibrium*, a concept that is physically intuitive but difficult to rigorously define in full generality. For the purposes of our discussion here, an isolated system can be considered to be in thermodynamic equilibrium if all of its macroscopically measurable properties do not vary in space or in time. Equilibrium thermodynamics establishes a large collection of macroscopic quantities for characterising the state of mixtures and describing their physical behaviour. Examples that will be encountered often are temperature, pressure, chemical potentials and concentrations. These quantities and their mathematical relationships remain foundational in mixtures that are out of equilibrium, as we shall discuss in section 1.4. Crucially, for scientific applications it is necessary to have a physical understanding of thermodynamic properties and their relationships to experiment. However, it is not our purpose to discuss this in detail here. The purpose of this section is to briefly summarise the mathematical aspects of equilibrium thermodynamics that are relevant to this thesis; we use these tools ubiquitously in the following chapters. For further detail, and especially for physical insight on the ideas discussed in this section, we refer to standard textbooks on thermodynamics and chemistry [2, 60, 61].

We begin by considering a multicomponent system of $n \geq 2$ species, which is in thermodynamic equilibrium, at temperature $T > 0$ (K) and pressure $p > 0$ (Pa). We denote by $n_1, \dots, n_n > 0$ (mol) the number of moles of each species present. Throughout this thesis, we use the letter $i \in \{1 : n\} := \{1, \dots, n\}$ to index the species. The molar masses of the species are denoted by $m_1, \dots, m_n > 0$ ($\mathrm{kg\,mol^{-1}}$). We treat $T, p, n_1, \dots, n_n$ as being the fundamental $n + 2$ variables that characterise

the macroscopic equilibrium state of our multicomponent system. This means that it is possible to independently vary these $n+2$ variables (in either a real experiment, or in a thought experiment), and by doing so any possible macroscopic equilibrium state of the system can be realised. For simplicity, we assume that the species are electrically uncharged, since in the charged case the electrical state of the system must also be taken into account (see chapters 3 and 4), a complication we avoid for the sake of this discussion.

We have chosen to work with the state variables T and p because these quantities are *intensive*, meaning that they are independent of the size of the system. This will be helpful in section 1.4 when we introduce the partial differential equations governing systems out of thermodynamic equilibrium, since these equations are naturally formulated using intensive quantities. Having decided on a choice of state variables, the next step is to introduce a so-called *thermodynamic potential*, which is a property that quantifies the energy of the system. There are numerous thermodynamic potentials that one can choose to work with, including the *Gibbs free energy*, *Helmholtz free energy*, *internal energy* and *enthalpy*. When using T and p as state variables it is most convenient to work with the Gibbs free energy, and we shall do so throughout this work. Importantly, this choice comes with no loss of generality, since the different thermodynamic potentials can be related to one another using formulae derived from Legendre transformations.

The Gibbs free energy has the remarkable property that, by taking its partial derivatives, one can derive expressions for nearly all of the equilibrium properties of interest in the multicomponent system at hand. It therefore serves as the starting point for our mathematical discussion of equilibrium thermodynamics. The Gibbs free energy (J) is denoted by

$$G = G(T, p, n_1, \ldots, n_n), \tag{1.1}$$

and it is a function of the state variables $T, p, n_1, \ldots, n_n$. The reader can imagine that, for a given multicomponent system, the functional dependence of G on these variables is known; it differs depending on the system at hand. Of course, exact knowledge of G is scarcely possible in practice. In any real-world mixture, the functional dependence of G on $T, p, n_1, \ldots, n_n$ can at best only be known approximately, either through analytical formulae derived from physical idealisations, or through phenomenological laws based on experimental measurements. Fortunately, the extent to which G is actually known is rarely important in practice, since it usually suffices to work with formulae for quantities which are derived from G. Let us now give examples of

such quantities. The most crucial property of G is that it satisfies a *fundamental thermodynamic relation*, phrased in terms of differentials,

$$\mathrm{d}G = -S\,\mathrm{d}T + V\,\mathrm{d}p + \sum_{i=1}^{n} \mu_i\,\mathrm{d}n_i. \tag{1.2}$$

Here, S is the entropy of the system, V is its volume, and μ_i is the chemical potential of species $i \in \{1:n\}$. Hence from eq. (1.2) we can identify the relationships

$$S = -\frac{\partial G}{\partial T}, \quad V = \frac{\partial G}{\partial p}, \quad \mu_i = \frac{\partial G}{\partial n_i}, \tag{1.3}$$

and these are all functions of $T, p, n_1, \ldots, n_n$[2]. Note that whenever we differentiate G, we implicitly assume that it is smooth enough for all relevant derivatives to exist.

Much of the mathematical structure of equilibrium thermodynamics comes from the fact that physical quantities of interest are often either *extensive* or *intensive*, as alluded to already. Suppose $Q = Q(T, p, n_1, \ldots, n_n)$ is a physical quantity which can be expressed as a function of the state variables $T, p, n_1, \ldots, n_n$. We say that Q is *extensive* if

$$Q(T, p, \lambda n_1, \ldots, \lambda n_n) = \lambda Q(T, p, n_1, \ldots, n_n) \quad \text{for all} \quad \lambda > 0. \tag{1.4}$$

Similarly, we say that $q = q(T, p, n_1, \ldots, n_n)$ is *intensive* if

$$q(T, p, \lambda n_1, \ldots, \lambda n_n) = q(T, p, n_1, \ldots, n_n) \quad \text{for all} \quad \lambda > 0. \tag{1.5}$$

Physically, an extensive quantity is one whose value doubles when the size of the system doubles, while an intensive quantity is one whose value is independent of the size of the system. In particular, as already mentioned both T and p are intensive, whereas n_i is extensive for each $i \in \{1:n\}$.

Two basic but important extensive quantities are the total mass M_T and total number of moles n_T of the system. We denote these by

$$M_T = \sum_{i=1}^{n} m_i n_i \quad \text{and} \quad n_T = \sum_{i=1}^{n} n_i. \tag{1.6}$$

We make the customary assumption that G is extensive[3]. Moreover, one verifies that if Q is extensive then so are $\frac{\partial Q}{\partial T}$ and $\frac{\partial Q}{\partial p}$. Hence by eq. (1.3), both S and V are

[2]The reader might find it surprising or unintuitive that the volume V of the system can be expressed as a function of $T, p, n_1, \ldots, n_n$. One way of developing an intuition for this fact is to consider the special case of an ideal gaseous mixture. Such mixtures satisfy the ideal gas law $pV = n_T RT$ where $n_T = \sum_{i=1}^{n} n_i$ is the total number of moles and R is the gas constant. Hence in this special case one has a simple explicit formula for V as a function of $T, p, n_1, \ldots, n_n$.

[3]This assumption is ubiquitous in classical thermodynamics and it holds in most systems of practical interest. There are, however, pathological systems in which it can fail to hold [111].

extensive, matching physical intuition. Other extensive quantites we shall encounter are the internal energy E_{int}, enthalpy H and heat capacity at constant pressure C_p:

$$E_{\text{int}} = G + TS - pV, \quad H = G + TS, \quad C_p = \frac{\partial H}{\partial T} = T\frac{\partial S}{\partial T}. \tag{1.7}$$

Intensive quantities are usually derived in two ways. The first way is to take a ratio of extensive quantities. In particular, if Q is extensive, then Q/V denotes the amount of Q per unit volume (sometimes the word *volumetric* is used) while Q/M_T denotes the amount of Q per unit mass (sometimes the word *specific* is used) and Q/n_T denotes the amount of Q per unit molar content (sometimes the word *molar* is used). Hence for example G/V is called the *volumetric Gibbs free energy* while G/M_T is called the *specific Gibbs free energy* and G/n_T the *molar Gibbs free energy*. Other examples of quantities formed in this way include the *(mass) density* $\rho = M_T/V$ and the *molarity* or *total (molar) concentration* $c_T = n_T/V$. The density reciprocal is $\Psi = 1/\rho = V/M_T$ which we identify as the *specific volume*. Finally, the *(molar) concentrations* of the species are given by $c_i = n_i/V$ and the *(mass) densities* of the species are $\rho_i = m_i c_i = m_i n_i/V$. These quantities appear ubiquitously in the chapters to follow.

The second (and more interesting) way of producing an intensive quantity from a given extensive quantity Q is to differentiate it with respect to n_i. We call such properties the *partial molar properties* derived from Q, and we denote them by

$$\overline{Q_i} := \frac{\partial Q}{\partial n_i}, \quad i \in \{1 : n\}. \tag{1.8}$$

Hence from eq. (1.3) we see that the chemical potential of species i is nothing more than the partial molar Gibbs free energy, which is to say that

$$\mu_i = \overline{G_i}. \tag{1.9}$$

Other partial molar properties that we shall encounter in this work are the partial molar volumes, entropies, enthalpies and heat capacities, respectively denoted by:

$$\overline{V_i} = \frac{\partial V}{\partial n_i}, \quad \overline{S_i} = \frac{\partial S}{\partial n_i}, \quad \overline{H_i} = \frac{\partial H}{\partial n_i}, \quad \overline{C_{p,i}} = \frac{\partial C_p}{\partial n_i}. \tag{1.10}$$

Since partial derivatives commute (always assuming sufficient smoothness), one can readily derive many relationships between partial molar properties. These are referred to as *Maxwell relations*. Two important examples of Maxwell relations are

$$\overline{V_i} = \frac{\partial \mu_i}{\partial p}, \tag{1.11a}$$

$$\overline{S_i} = -\frac{\partial \mu_i}{\partial T}, \tag{1.11b}$$

and these hold owing to eqs. (1.3), (1.9), and (1.10).

Euler's homogenous function theorem implies that every extensive quantity Q is intimately related to its partial molar properties $\overline{Q_i}$ by means of

$$Q = \sum_{i=1}^{n} n_i \overline{Q_i}. \tag{1.12}$$

The Euler relation eq. (1.12) can be recast purely in terms of intensive quantities, if one divides the equation by an extensive quantity. For example, taking Q to be the volume V in eq. (1.12) and dividing by the total number of moles n_T yields

$$\frac{1}{c_T} = \sum_{i=1}^{n} x_i \overline{V_i}, \tag{1.13}$$

where $x_i := n_i/n_T = c_i/c_T$ denotes the *mole fraction* of species i. Notice that $\sum_{i=1}^{n} x_i = 1$ by definition. We refer to eq. (1.13) as a *volumetric equation of state*, since it expresses the total concentration c_T in terms of the intensive quantities x_i and $\overline{V_i}$. To give a concrete example, in an ideal gaseous mixture it holds that $\overline{V_i} = \frac{RT}{p}$ where R is the gas constant. Since $\sum_{i=1}^{n} x_i = 1$ one then verifies that eq. (1.13) reduces to $\frac{V}{n_T} = \frac{RT}{p}$, which is equivalent to the familiar ideal gas law $pV = n_T RT$.

The Euler relation eq. (1.12) is also important because it leads to a constraint on the partial molar properties $\overline{Q_i}$, which we refer to as a *Gibbs–Duhem relation*. The Gibbs–Duhem relation is derived by taking a total differential of eq. (1.12), i.e.

$$\mathrm{d}Q = \mathrm{d}\left(\sum_{i=1}^{n} n_i \overline{Q_i} \right). \tag{1.14}$$

Since $Q = Q(T, p, n_1, \ldots, n_n)$, the left-hand side of eq. (1.14) can be evaluated using the chain rule,

$$\mathrm{d}Q = \frac{\partial Q}{\partial T}\,\mathrm{d}T + \frac{\partial Q}{\partial p}\,\mathrm{d}p + \sum_{i=1}^{n} \frac{\partial Q}{\partial n_i}\,\mathrm{d}n_i = \frac{\partial Q}{\partial T}\,\mathrm{d}T + \frac{\partial Q}{\partial p}\,\mathrm{d}p + \sum_{i=1}^{n} \overline{Q_i}\,\mathrm{d}n_i, \tag{1.15}$$

while the right-hand side of eq. (1.14) can be evaluated using the product rule

$$\mathrm{d}\left(\sum_{i=1}^{n} n_i \overline{Q}_i \right) = \sum_{i=1}^{n} \left(\overline{Q_i}\,\mathrm{d}n_i + n_i\,\mathrm{d}\overline{Q}_i \right). \tag{1.16}$$

Equating eqs. (1.15) and (1.16) and cancelling terms yields

$$\frac{\partial Q}{\partial T}\,\mathrm{d}T + \frac{\partial Q}{\partial p}\,\mathrm{d}p = \sum_{i=1}^{n} n_i\,\mathrm{d}\overline{Q_i}, \tag{1.17}$$

which is the *Gibbs–Duhem relation*. Similar to eq. (1.12), this relation can be expressed in terms of intensive quantities only, by dividing by an extensive quantity. The most common form of eq. (1.17) that we encounter in this work is obtained by taking $Q = G$ and dividing by the volume V. This results in

$$-s_V \, \mathrm{d}T + \mathrm{d}p = \sum_{i=1}^{n} c_i \, \mathrm{d}\mu_i, \tag{1.18}$$

where $s_V = S/V$ is the volumetric entropy. The Gibbs–Duhem relation eq. (1.18) will be crucial in section 1.5 when we consider the forces that drive mass diffusion in non-equilibrium systems.

Several more general remarks on eq. (1.17) are in order. First, an implication of eq. (1.17) is that the $n+2$ intensive quantities $T, p, \overline{Q_1}, \ldots, \overline{Q_n}$ are not all independent, since their infinitesimal changes must be related by eq. (1.17). This is a manifestation of a more general phenomenon known as the *Gibbs phase rule*, which in our present setting states that intensive quantities depend on at most $n+1$ independent degrees of freedom. Indeed, if $q = q(T, p, n_1, \ldots, n_n)$ is intensive, then we in fact have:

$$q = q(T, p, x_1, \ldots, x_n), \tag{1.19}$$

by taking $\lambda = 1/n_T$ in eq. (1.5) and recalling that the mole fractions are defined by $x_i := n_i/n_T = c_i/c_T$. Since $\sum_{i=1}^{n} x_i = 1$, only $n+1$ of the variables $T, p, x_1, \ldots, x_n$ in eq. (1.19) are independent. The most important consequence of eq. (1.19) is that intensive quantities can be viewed as functions of $T, p, x_1, \ldots, x_n$ instead of $T, p, n_1, \ldots, n_n$. Adopting this viewpoint is convenient since the variables $T, p, x_1, \ldots, x_n$ are all intensive. To emphasise this point and avoid any possible confusion, we stress that throughout this work (and in much of the literature) intensive quantities are by default viewed as being functions of $T, p, x_1, \ldots, x_n$ and not $T, p, n_1, \ldots, n_n$. **The default state variables we work with for intensive quantities are $\boldsymbol{T, p, x_1, \ldots, x_n}$.** The word *composition* is often used to refer to the values of the mole fractions $x_1, \ldots, x_n$.

We now discuss how the Gibbs free energy G can be modelled for various multicomponent systems. Since G can be recovered from the chemical potentials by an Euler relation (recall eq. (1.12)),

$$G = \sum_{i=1}^{n} n_i \mu_i, \tag{1.20}$$

we see that it suffices to describe how each μ_i varies as a function of $T, p, x_1, \ldots, x_n$. It is, however, worth mentioning that this functional dependence cannot be chosen

entirely arbitrarily. For instance, if we temporarily revert to viewing μ_i as a function of $T, p, n_1, \ldots, n_n$ then by a Maxwell relation it must hold that $\frac{\partial \mu_i}{\partial n_j} = \frac{\partial \mu_j}{\partial n_i}$. More generally, if T and p are held fixed, then the vector field $\vec{\mu} : (0, \infty)^n \to \mathbb{R}^n$ defined by $\vec{\mu}_i(n_1, \ldots, n_n) := \mu_i(T, p, n_1, \ldots, n_n)$ must be conservative (its scalar potential is the Gibbs free energy). Physical considerations place further restrictions on the functional form of the chemical potentials. For example, it is possible to have a negative partial molar volume $\overline{V_i} = \frac{\partial \mu_i}{\partial p}$ (e.g. dilute magnesium sulfate in water) but the total volume $V = \sum_{i=1}^n n_i \overline{V_i}$ must always be positive. Thermodynamic stability places further convexity requirements on various quantities derived from the Gibbs free energy, although such requirements are never utilised in this work.

The conceptually simplest multicomponent system is that of an *ideal gaseous mixture*. Here, the chemical potentials μ_i for $i \in \{1 : n\}$ are given by the formulae

$$\mu_i(T, p, x_1, \ldots, x_n) = \mu_i^*(T) + RT \ln(x_i p), \tag{1.21}$$

where $\mu_i^*(T)$ is some function of T alone, which must be specified. Sometimes in the literature eq. (1.21) is expressed in the equivalent but seemingly more complex form

$$\mu_i(T, p, x_1, \ldots, x_n) = \mu_i^\ominus(T, p^\ominus) + RT \ln(x_i p / p^\ominus), \tag{1.22}$$

where $p^\ominus$ is a fixed reference pressure and $\mu_i^\ominus(T, p^\ominus)$ a reference chemical potential. Comparing eqs. (1.21) and (1.22), we see that $\mu_i^*(T) = \mu_i^\ominus(T, p^\ominus) - RT \ln(p^\ominus)$. The advantage of using eq. (1.22) is that $\mu_i^\ominus(T, p^\ominus)$ then represents, by construction, the molar Gibbs free energy for pure species i (e.g. at $x_i = 1$) at pressure $p = p^\ominus$. Thus $\mu_i^\ominus(T, p^\ominus)$ is a quantity whose T dependence is readily connected to experiment.

One verifies from eq. (1.21) that the partial molar volumes in an ideal gaseous mixture are independent of composition (i.e. mole fractions), and are given by

$$\overline{V_i} = \frac{\partial \mu_i}{\partial p} = \frac{RT}{p}, \tag{1.23}$$

whence from eq. (1.13) we recover the ideal gas law $pV = n_T RT$. Since $x_i = c_i / c_T$, and $c_T = p/RT$ by the ideal gas law, it is common to see eq. (1.22) expressed as

$$\mu_i = \mu_i^\ominus(T, p^\ominus) + RT \ln(c_i RT / p^\ominus), \tag{1.24}$$

although caution should be applied when interpreting this equation[4].

[4]Based on eq. (1.24), it is tempting to believe that $T, c_1, \ldots, c_n$ can be used as state variables instead of $T, p, x_1, \ldots, x_n$. This is indeed true for ideal gaseous mixtures, but we caution that it is not true in general. In particular, for mixtures that are *incompressible* in the sense that the volume V is independent of p, one can show that $T, c_1, \ldots, c_n$ are not all independent, and that there is no way of recovering p from knowledge of $T, c_1, \ldots, c_n$.

To gain insight into how $\mu_i^*(T)$ might be modelled, we note that by a Maxwell relation the partial molar heat capacities are given by

$$\overline{C_{p,i}} = -T\frac{\partial^2 \mu_i}{\partial T^2} = -T\frac{\partial^2 \mu_i^*}{\partial T^2}. \tag{1.25}$$

This shows that for an ideal gaseous mixture, the partial molar heat capacities are functions of T alone. In many gases it is reasonable to approximate the partial molar heat capacities as being constant. In this case we say that the ideal gaseous mixture is *calorically perfect*. One can then recover $\mu_i^*(T)$ from eq. (1.25) by integration:

$$\mu_i^*(T) = \overline{C_{p,i}}T(A_i - \ln T) + B_i, \tag{1.26}$$

where A_i and B_i are constants of integration. When chemical reactions do not need to be modelled, as will be the case throughout this work, the values of A_i and B_i can be chosen arbitrarily[5]. Taking $A_i = B_i = 0$ therefore yields, for chemically non-reacting, calorically perfect ideal gaseous mixtures, that:

$$\mu_i(T, p, x_1, \ldots, x_n) = -\overline{C_{p,i}}T\ln T + RT\ln(x_i p). \tag{1.27}$$

From eq. (1.27) one can recover other quantities of interest. For example, the molar entropy density is found using the Euler relation eq. (1.12) and a Maxwell relation,

$$S/n_T = \sum_{i=1}^{n} x_i\overline{S_i} = -\sum_{i=1}^{n} x_i\frac{\partial \mu_i}{\partial T} = -R\sum_{i=1}^{n} x_i \ln x_i + (1 + \ln T)\sum_{i=1}^{n} x_i\overline{C_{p,i}}. \tag{1.28}$$

The first term $-R\sum_{i=1}^{n} x_i \ln x_i$ is sometimes referred to as the *ideal entropy of mixing*, and incidentally, it bears a striking resemblance to notions of entropy in other fields such as information theory. This concludes our discussion of ideal gaseous mixtures.

We now move on to discussing how liquid mixtures can be modelled. A liquid mixture is said to be *ideal* if its chemical potentials are of the form

$$\mu_i(T, p, x_1, \ldots, x_n) = \mu_i^0(T, p) + RT\ln x_i, \tag{1.29}$$

with $\mu_i^0(T, p)$ some function of (T, p) alone. By definition $\mu_i^0(T, p)$ represents the molar Gibbs free energy of pure species i (e.g. at $x_i = 1$) at temperature T and pressure p. Comparing eqs. (1.21) and (1.29) we see that at fixed temperature and pressure, the Gibbs free energies of ideal gases and liquids have the same dependence on composition, i.e. they share the same *ideal Gibbs free energy of mixing*. What

[5]Differences between species chemical potentials are the driving force for chemical reactions. Hence, when chemical reactions must be modelled, one must take care in properly choosing A_i and B_i.

differs between the two is how their free energies depend on pressure. This is made precise by introducing the *isothermal compressibility* α_T, which quantifies volumetric changes due to pressure,

$$\alpha_T = -\frac{1}{V}\frac{\partial V}{\partial p}. \tag{1.30}$$

The reciprocal of α_T is also known as the *isothermal bulk modulus*. Ideal gases are compressible; at a fixed temperature and molar content the volume of an ideal gas is inversely proportional to its pressure, and one has $\alpha_T = \frac{1}{p}$. By contrast, in liquids it is often appropriate to make an incompressibility assumption $\alpha_T = 0$, which is equivalent to asserting that V is independent of p. It follows that the partial molar volumes $\overline{V_i}$ are also independent of p. Moreover, differentiation of eq. (1.29) with respect to p shows that $\overline{V_i}$ is independent of $x_1, \ldots, x_n$. Hence, in an ideal incompressible liquid mixture, the partial molar volumes $\overline{V_i}$ are functions of T only. The extent to which $\overline{V_i}$ depends on T then apparently quantifies the effect of thermal expansion in the mixture. When this effect can be neglected it is expedient to approximate the partial molar volumes as being constants[6]. The word *quasi-incompressible* has been used in the literature to refer to mixtures with constant partial molar volumes [24, 41]. Altogether, in a chemically non-reacting ideal liquid mixture where the partial molar volumes and heat capacities are approximated as being constant, one has:

$$\mu_i(T, p, x_1, \ldots, x_n) = -\overline{C_{p,i}}T \ln T + \overline{V_i}p + RT \ln x_i. \tag{1.31}$$

While eq. (1.31) is based on numerous physical idealisations that will at best hold only approximately in real liquids, its simplicity makes it a useful starting point for more complicated models.

In many multicomponent systems of practical interest, thermodynamic ideality is a poor approximation. This is the case, for example, when modelling concentrated electrolytes, which is our focus in chapter 3. Thermodynamically non-ideal mixtures can be modelled through the introduction of *excess properties*. An excess property is defined to be the difference between the true property value of the mixture, and what the property value would be if the mixture were ideal. In particular, the *excess chemical potentials* μ_i^E satisfy the relation

$$\mu_i(T, p, x_1, \ldots, x_n) = \mu_i^0(T, p) + RT \ln x_i + \mu_i^E(T, p, x_1, \ldots, x_n). \tag{1.32}$$

Note that by construction $\mu_i^E = 0$ when $x_i = 1$ (i.e. at pure species i), since μ_i^0 is by definition the true chemical potential at pure species i. For liquid mixtures it is

[6]Interestingly, it has recently been argued that for any mixture with $\alpha_T = 0$, thermodynamic consistency requires the partial molar volumes to be constant [20].

common to neglect the pressure dependence of μ_i^E. Under this approximation, at a fixed temperature, μ_i^E becomes a function of composition only.

A simple model for the excess chemical potentials in the case of a binary mixture (i.e. $n = 2$ species) is the *Margules model* [60], wherein

$$\mu_1^E = RTx_2^2\big[A_{12} + 2(A_{21} - A_{12})x_1\big], \tag{1.33}$$

$$\mu_2^E = RTx_1^2\big[A_{21} + 2(A_{12} - A_{21})x_2\big], \tag{1.34}$$

where A_{12}, A_{21} are parameters that may depend on T and can be obtained by fitting experimental data. Many other models for excess chemical potentials exist, such as the equations of Van Laar or Wilson [60]. We will not delve into these here, as the numerical methods devised in this thesis are agnostic to what model is employed. Our numerical scheme in chapter 2 assumes that the functional relation for the chemical potentials is known, but it is not required to take any particular form. Our numerical scheme in chapter 3 does not even require one to have an explicit relation for the chemical potentials; all that is required is knowledge of the so-called *thermodynamic factors*, which are the partial derivatives of chemical potentials with respect to composition. This is convenient in electrolytic systems where it is often the thermodynamic factors and not the chemical potentials that are directly measurable through experiment.

1.3 Mole-based and mass-based formulations of equilibrium thermodynamics

Our formulation of equilibrium thermodynamics in section 1.2 is *mole-based*, since we employ $n_1, \ldots, n_n$ as the fundamental variables that characterise the amount of each species present. An entirely equivalent formulation can be obtained by using the species masses $M_i = m_i n_i$ (kg) as fundamental variables instead. Mole-based formulations are convenient for several reasons: the equations for ideal mixtures are based on mole fractions; stoichiometry is often conducted in terms of moles. Throughout this thesis we largely stick to the mole-based formulation. However, mass is arguably a more physically tangible notion than that of moles, since one can easily measure the mass of a given object, but measuring its molar content requires precise knowledge of its chemical composition. Moreover, in the literature one often encounters mass-based formulations. The purpose of this section is to give the reader a brief idea of how the two formulations can be interchanged with sufficient bookkeeping.

In the mass-based formulation, an extensive quantity Q is viewed as a function

$$Q = Q(T, p, M_1, \ldots, M_n). \tag{1.35}$$

Composition in the mass-based formulation is naturally described using *species mass fractions*, $\omega_i := M_i/M_T$, where we recall that $M_T = \sum_{i=1}^n M_i$ is the total mass. In analogy to eq. (1.19), an intensive quantity q can be viewed as a function

$$q = q(T, p, \omega_1, \ldots, \omega_n). \tag{1.36}$$

Partial specific properties $\overline{Q_i}^s$ are the analogue of partial molar properties (cf. eq. (1.8)):

$$\overline{Q_i}^s := \frac{\partial Q}{\partial M_i}, \quad i \in \{1 : n\}. \tag{1.37}$$

One verifies that $m_i \overline{Q_i}^s = \overline{Q_i}$. The analogue of the Euler relation eq. (1.12) is:

$$Q = \sum_{i=1}^n M_i \overline{Q_i}^s. \tag{1.38}$$

Hence, for example, the analogue of the volumetric equation of state eq. (1.13) is:

$$\frac{1}{\rho} = \sum_{i=1}^n \omega_i \overline{V_i}^s, \tag{1.39}$$

where ρ is the density. The analogue of the Gibbs–Duhem relation eq. (1.17) is:

$$\frac{\partial Q}{\partial T}\,\mathrm{d}T + \frac{\partial Q}{\partial p}\,\mathrm{d}p = \sum_{i=1}^n M_i\,\mathrm{d}\overline{Q_i}^s. \tag{1.40}$$

In particular, the analogue of the Gibbs–Duhem relation for G (recall eq. (1.18)) is:

$$-s_V\,\mathrm{d}T + \mathrm{d}p = \sum_{i=1}^n \rho_i\,\mathrm{d}\mu_i^s, \tag{1.41}$$

recalling that $\rho_i = m_i c_i = M_i/V$ is the density of species i, and $\mu_i^s := \overline{G_i}^s = \mu_i/m_i$ is the so-called *mass-based* (or *specific*) *chemical potential* of species i.

Finally, it is sometimes convenient to have formulae for converting between mole fractions and mass fractions. One can verify that these are given by:

$$\omega_i = \frac{m_i x_i}{\sum_{j=1}^n m_j x_j}, \quad \text{and} \quad x_i = \frac{\omega_i/m_i}{\sum_{j=1}^n \omega_j/m_j}. \tag{1.42}$$

1.4 Non-equilibrium thermodynamics of multicomponent systems

Most applications of multicomponent flows involve systems that are out of thermodynamic equilibrium. The purpose of this section, and also sections 1.5 and 1.6, is to present an overview of the relevant partial differential equations that we employ to model such systems, and to provide physical insight along the way.

Consider a mixture of $n \geq 2$ species that is out of thermodynamic equilibrium, in $d \in \{2, 3\}$ spatial dimensions. Our forthcoming treatment is based on three foundational assumptions. The first is the traditional *continuum assumption*, which is foundational in the theory of continuum mechanics. This assumption states that the microscopic state of the mixture (i.e. the state of its individual constituent molecules) does not need to be accounted for, and it instead suffices to work with macroscopically averaged quantities which can be treated as continuous fields. Consequently, our forthcoming models are posed as partial differential equations (PDEs) on $\mathbb{R}^d$.

Our second foundational assumption is that of *local thermodynamic equilibrium*. This postulates that every infinitesimal control volume in the mixture is locally in a state of thermodynamic equilibrium, even if this is not true globally. Hence intensive quantities may vary in space and time, but they must satisfy pointwise the relations of equilibrium thermodynamics, such as eq. (1.13). Note that one cannot speak of the value of extensive quantities at a point in space and time, but owing to the continuum assumption this notion is entirely sensible for intensive quantities. For this reason our governing PDEs only involve intensive quantities. Of course, extensive quantities can still be useful when performing intermediate calculations, because they allow one to derive relationships between intensive quantities such as eq. (1.13).

Our final foundational assumption, which shall be stated precisely in section 1.5, is the *linearity postulate*. This states that the fluxes in the system are linearly related to the so-called thermodynamic driving forces, which are, roughly speaking, gradients of particular state variables. For dilute gases, it is possible to derive this assumption from kinetic theory [56]. More generally, this assumption has been experimentally validated in many thermodynamically non-ideal gases, liquids and electrolytic mixtures [14, 78, 86].

We should mention that, while the three foundational assumptions above are applicable in a plethora of scientific applications, they are by no means universally true. When the continuum assumption or local thermodynamic equilibrium fails to hold, one must resort to microscopic theories, such as statistical mechanics [61],

kinetic theory [56], or rarefied gas dynamics [73]. In systems at *mesoscopic scales*, i.e. scales between the microscopic and macroscopic, one can still utilise the continuum assumption and local thermodynamic equilibrium, but microscopic effects must be accounted for using tools such as stochastic models [8, 39]. Finally, in systems that are far from thermodynamic equilibrium, the linearity postulate may be inaccurate; here, one can resort to nonlinear theories, such as GENERIC [91].

Our three foundational assumptions lay the groundwork for the classical theory of *non-equilibrium thermodynamics*[7][14, 34, 59]. The starting point in this theory are equations of continuity for mass, momentum and energy, which we now outline. The species molar concentrations are postulated to satisfy the equations of mass continuity

$$\frac{\partial c_i}{\partial t} + \nabla \cdot (c_i v_i) = 0 \quad \forall i \in \{1 : n\}, \tag{1.43}$$

which defines the *velocity* v_i of species i. The product $c_i v_i$ represents the *molar flux* of species i. Note that we have omitted reaction terms in eq. (1.43), since we do not model chemical reactions in this work. It is also worth keeping in mind that, although eq. (1.43) provides an evolution law for the concentrations, because we are assuming local thermodynamic equilibrium, the concentrations are still constrained to satisfy pointwise the relationships of equilibrium thermodynamics, such as the volumetric equation of state eq. (1.13). These algebraic constraints can lead to challenges when certain boundary conditions are imposed, as discussed in chapter 3 and appendix A.1.

The *barycentric* (or *mass-average*) *velocity* of the mixture is defined as

$$v = \sum_{i=1}^{n} \omega_i v_i, \tag{1.44}$$

recalling that $\omega_i = m_i c_i / \rho$ are the mass-fractions and $\rho = \sum_{i=1}^{n} m_i c_i$ is the density. The definition eq. (1.44) is natural because it implies that the density ρ satisfies the total mass continuity equation

$$\frac{\partial \rho}{\partial t} + \nabla \cdot (\rho v) = 0, \tag{1.45}$$

as verified by multiplying eq. (1.43) by m_i and summing over $i \in \{1 : n\}$. We refer to eq. (1.44) as the *mass-average constraint*, since special care will be taken to incorporate this constraint into our numerical schemes. The barycentric velocity can also be used to define the traditional *material derivative* operator

$$\frac{D}{Dt} := \frac{\partial}{\partial t} + v \cdot \nabla, \tag{1.46}$$

[7]Sometimes also called *linear irreversible thermodynamics*.

which will be used occasionally in this chapter.

Momentum continuity is expressed by the traditional Cauchy momentum equation

$$\frac{\partial(\rho v)}{\partial t} + \nabla \cdot (\rho v \otimes v) - \nabla \cdot \sigma = 0, \tag{1.47}$$

where σ is the *stress tensor*, which is assumed to be symmetric. To discuss energetics, note that the specific total energy e_{tot} is given by

$$e_{\text{tot}} = \frac{1}{2}(v \cdot v) + e_{\text{int}}, \tag{1.48}$$

where $\frac{1}{2}(v \cdot v)$ is the specific kinetic energy, and $e_{\text{int}} = E_{\text{int}}/M_T$ is the specific internal energy (recall eq. (1.7)). The energy continuity equation is given by

$$\frac{\partial(\rho e_{\text{tot}})}{\partial t} + \nabla \cdot (\rho e_{\text{tot}} v) - \nabla \cdot (\sigma v) + \nabla \cdot J_q = 0, \tag{1.49}$$

where J_q is the *heat flux*. The $\nabla \cdot (\rho e_{\text{tot}} v)$ term represents energy convected by v, while $\nabla \cdot (\sigma v)$ represents mechanical work, and $\nabla \cdot J_q$ represents heat transfer. Equation (1.49) can be viewed as defining J_q.

In summary, the crucial continuity equations (or *balance laws*) of non-equilibrium thermodynamics that we consider here are:

$$\frac{\partial c_i}{\partial t} + \nabla \cdot (c_i v_i) = 0 \quad \forall i \in \{1 : n\}, \tag{1.50a}$$

$$\frac{\partial(\rho v)}{\partial t} + \nabla \cdot (\rho v \otimes v) - \nabla \cdot \sigma = 0, \tag{1.50b}$$

$$\frac{\partial(\rho e_{\text{tot}})}{\partial t} + \nabla \cdot (\rho e_{\text{tot}} v) - \nabla \cdot (\sigma v) + \nabla \cdot J_q = 0. \tag{1.50c}$$

Note that in the forthcoming chapters, we will sometimes allow for source terms to be present on the right-hand sides of eqs. (1.50a) to (1.50c). However, we do not consider source terms here, since this would unnecessarily obfuscate our forthcoming derivation of the entropy balance in section 1.5.

It is worth noting that we have written eq. (1.50a) without explicitly including a convective term, but this is purely a matter of taste. One can define

$$v_i^d := v - v_i \quad \forall i \in \{1 : n\}, \tag{1.51}$$

the so-called *diffusive velocity* of species i, so that eq. (1.50a) becomes

$$\frac{\partial c_i}{\partial t} + \nabla \cdot (c_i v) + \nabla \cdot (c_i v_i^d) = 0. \tag{1.52}$$

Diffusive velocities (and fluxes) can be convenient to work with and are often used in the literature, although we mainly use species velocities in this work.

We close this section by noting that eq. (1.45) yields an equation for $\nabla \cdot v$,

$$\nabla \cdot v = \rho \frac{D\Psi}{Dt}. \tag{1.53}$$

Recall that $\Psi = 1/\rho = V/M_T$ is the specific volume; it is therefore a function of T, p and the mass-fractions $\omega_1, \ldots, \omega_n$ (recall section 1.3). Hence, one can expand $\frac{D\Psi}{Dt}$ by means of the chain rule. This ultimately leads to the insightful relation

$$\nabla \cdot v = \alpha_p \frac{DT}{Dt} - \alpha_T \frac{Dp}{Dt} + \rho \sum_{i=1}^{n} \overline{V_i}^s \frac{D\omega_i}{Dt}, \tag{1.54}$$

where $\alpha_p := \frac{1}{V}\frac{\partial V}{\partial T}$ is a thermal expansion coefficient, α_T is the isothermal compressibility (recall eq. (1.30)), and $\overline{V_i}^s$ is a partial specific volume (recall section 1.3). Equation (1.54) shows that for multicomponent systems, even in isothermal and isobaric conditions, it generally does not hold that $\nabla \cdot v = 0$, except in the exceptional case that the partial specific volumes $\overline{V_i}^s$ are all equal (e.g. an ideal gaseous mixture where all species have the same molar mass).

1.5 Derivation of Onsager–Stefan–Maxwell constitutive laws

The continuity equations eq. (1.50) are not closed, since we have not specified what σ, J_q or $v_1, \ldots, v_n$ are. This must be done by *constitutive laws*. Non-equilibrium thermodynamics provides a framework for developing such laws. The general philosophy is to derive an equation for the entropy balance, and then select constitutive laws that are consistent with the second law of thermodynamics (i.e. that entropy must be non-decreasing) [81], among other requirements such as Onsager reciprocal relations [88, 89]. For completeness, this section briefly outlines the key arguments and postulates that are invoked in this process. If desired, the reader may skip the following derivation and go directly to section 1.6, where the constitutive laws that we employ throughout this thesis are summarised.

Using eqs. (1.2) and (1.7), one verifies that the specific internal energy e_{int} satisfies

$$\mathrm{d}e_{\text{int}} = T\,\mathrm{d}s - p\,\mathrm{d}\Psi + \sum_{i=1}^{n} \frac{\mu_i}{m_i}\,\mathrm{d}\omega_i, \tag{1.55}$$

where $s = S/M_T$ is the specific entropy and $\Psi = V/M_T$ is the specific volume. Rearranging for $\rho\,\mathrm{d}s$, and replacing the total differentials $\mathrm{d}(\cdot)$ with material derivatives

$\frac{D}{Dt}(\cdot)$, one then finds

$$\rho\frac{Ds}{Dt} = \frac{1}{T}\left\{\rho\frac{De_{\text{int}}}{Dt} + p\rho\frac{D\Psi}{Dt} - \sum_{i=1}^{n}\frac{\mu_i}{m_i}\rho\frac{D\omega_i}{Dt}\right\}. \tag{1.56}$$

The various material derivatives on the right-hand side of eq. (1.56) can be computed using eqs. (1.43) to (1.49). In particular one can verify that

$$\rho\frac{De_{\text{int}}}{Dt} = \sigma : \nabla v - \nabla \cdot J_q, \tag{1.57a}$$

$$\rho\frac{D\Psi}{Dt} = \nabla \cdot v, \tag{1.57b}$$

$$\rho\frac{D\omega_i}{Dt} = -\nabla \cdot (m_i c_i v_i^d). \tag{1.57c}$$

In eq. (1.57a), : denotes tensor contraction. One then substitutes eq. (1.57) into eq. (1.56). Applying several manipulations (see [34] for more details) involving the vector calculus product rule, the relation $\overline{H_i} = \mu_i + T\overline{S_i}$ (recall eqs. (1.7) and (1.10)), and the Gibbs–Duhem relation eq. (1.18), one eventually can show that the entropy continuity equation is of the form

$$\rho\frac{Ds}{Dt} + \nabla \cdot J_s = g_S, \tag{1.58}$$

where J_s is the *entropy flux*, and g_S is the *rate of entropy generation*. Before we state the formulae for these, let us note that eq. (1.58) can equivalently be written as

$$\frac{\partial(\rho s)}{\partial t} + \nabla \cdot (\rho s v) + \nabla \cdot J_s = g_S, \tag{1.59}$$

since this is in a form more harmonious with the other continuity equations eq. (1.50).

To express the entropy flux and rate of entropy generation it is customary to introduce an *irreversible heat flux* J_q'. This quantifies the amount of heat flow that does not arise due to diffusion, by subtracting from J_q the enthalpy carried by the diffusive velocities:

$$J_q' := J_q - \sum_{i=1}^{n}\overline{H_i}c_i v_i^d. \tag{1.60}$$

Expressed in terms of the irreversible heat flux, the entropy flux works out to be

$$J_s = \frac{J_q'}{T} + \sum_{i=1}^{n}\overline{S_i}c_i v_i^d, \tag{1.61}$$

while the entropy production function g_S works out to be

$$g_S = \frac{1}{T}\Big\{\epsilon(v) : \big(p\mathbb{I} + \sigma\big) - \nabla \ln T \cdot J_q' + \sum_{i=1}^{n} d_i \cdot v_i^d\Big\}. \tag{1.62}$$

Here $\epsilon(v)$ is the symmetric gradient of v, $\mathbb{I}$ is the $d \times d$ identity matrix, and $d_1, \ldots, d_n$ are the so-called *diffusion driving forces*,

$$d_i = -c_i \nabla \mu_i - c_i \overline{S_i} \nabla T + \omega_i \nabla p \quad \forall i \in \{1 : n\}. \tag{1.63}$$

The diffusion driving forces sum to zero, which can be viewed as a statement of Newton's third law. To see this, note that by an Euler relation $\sum_{i=1}^n c_i \overline{S_i} = s_V$ where $s_V = S/V$ is the volumetric entropy. Moreover, the mass fractions satisfy $\sum_{i=1}^n \omega_i = 1$ by definition. Hence summation of eq. (1.63) yields

$$\sum_{i=1}^n d_i = -\sum_{i=1}^n c_i \nabla \mu_i - s_V \nabla T + \nabla p = 0, \tag{1.64}$$

where the second equality holds due to the Gibbs–Duhem relation eq. (1.18). Since $\sum_{i=1}^n d_i = 0$, the entropy production eq. (1.62) can equivalently be written using species velocities $v_i = v + v_i^d$ instead of diffusive velocities v_i^d. In particular, one has

$$g_S = \frac{1}{T}\Big\{ \epsilon(v) : \big(p\mathbb{I} + \sigma\big) - \nabla \ln T \cdot J_q' + \sum_{i=1}^n d_i \cdot v_i \Big\}. \tag{1.65}$$

To compactly write the entropy production we introduce the *viscous stress*,

$$\tau := p\mathbb{I} + \sigma. \tag{1.66}$$

Moreover, in non-equilibrium thermodynamics, heat transport and diffusion are coupled processes; we discuss this in more detail later. Following [113], it shall be notationally expedient to introduce a *thermal driving force* d_0 and *thermal velocity* v_0,

$$d_0 := -c_{p,V} \nabla T, \quad v_0 := \frac{J_q'}{c_{p,V} T}, \tag{1.67}$$

where $c_{p,V} := C_p/V$ is the volumetric heat capacity, included in eq. (1.67) for dimensional consistency. The entropy production can now be written compactly as

$$g_S = \frac{1}{T}\Big\{ \epsilon(v) : \tau + \sum_{i=0}^n d_i \cdot v_i \Big\}, \tag{1.68}$$

which involves a sum of products of so-called "fluxes" $\tau, v_0, \ldots, v_n$ and conjugate "forces" $\epsilon(v), d_0, \ldots, d_n$. Recall that our original goal was to derive a constitute law for σ, J_q and $v_1, \ldots, v_n$. This will be accomplished if we can establish an invertible relationship between the fluxes $\tau, v_0, \ldots, v_n$ and forces $\epsilon(v), d_0, \ldots, d_n$. Doing this is the next step in the programme of non-equilibrium thermodynamics.

The theory of linear non-equilibrium thermodynamics now proceeds by invoking the *linearity postulate*, which states that the fluxes and forces are related by a linear transformation. Further considerations constrain the precise form of the transformation. Firstly, the *Curie principle* states that fluxes and forces whose tensorial order differs by an odd number cannot be coupled. Hence, in the present setting, coupling only occurs between τ and $\epsilon(v)$ (second order tensors), and $(v_0, \dots, v_n)$ and $(d_0, \dots, d_n)$ (first order tensors). The linear coupling between τ and $\epsilon(v)$ can be expressed as

$$\tau = \mathscr{A}^{-1}\epsilon(v) \tag{1.69}$$

where $\mathscr{A} : \mathbb{R}^{d\times d}_{\text{sym}} \to \mathbb{R}^{d\times d}_{\text{sym}}$ is the *compliance tensor*. The linear coupling between $(v_0, \dots, v_n)$ and $(d_0, \dots, d_n)$ can be expressed as

$$d_i = \sum_{j=0}^{n} \mathfrak{M}_{ij} v_j \quad \forall i \in \{0 : n\}, \tag{1.70}$$

where $\mathfrak{M}$ is an $(n+1)\times(n+1)$ *thermodiffusion transport matrix*. Note that $\mathscr{A}$ and $\mathfrak{M}$ generally depend on the state variables $(T, p, x_1, \dots, x_n)$, but the linearity postulate requires that they are independent of the fluxes and forces.

Further physical insight places additional structure on $\mathscr{A}$ and $\mathfrak{M}$. Regarding $\mathscr{A}$, standard arguments from continuum fluid mechanics can be used to recover the usual Newtonian fluid law. In particular, if we assume an isotropic fluid, then $\mathscr{A}^{-1}$ can be expressed in terms of only two independent transport coefficients, the *shear viscosity* η and *bulk viscosity* ζ. In particular, the relation eq. (1.69) becomes

$$\tau = 2\eta\epsilon(v) + \big(\zeta - 2\eta/d\big)\,\mathrm{tr}(\epsilon(v))\mathbb{I}. \tag{1.71}$$

Regarding $\mathfrak{M}$, it is clear from eq. (1.70) that the entries $\mathfrak{M}_{ij}$ could potentially be $d\times d$ matrices. However, in an isotropic fluid the only possibility is that the $\mathfrak{M}_{ij}$ are scalars. Moreover, on the basis of microscopic time-reversibility, Onsager made the deep and non-trivial observation that $\mathfrak{M}$ must be symmetric, i.e. $\mathfrak{M}_{ij} = \mathfrak{M}_{ji}$. This is known as an *Onsager reciprocal relation* [88, 89]. Insertion of the constitutive laws eqs. (1.70) and (1.71) into eq. (1.68) then yields

$$g_S = \frac{1}{T}\Big\{2\eta\big(\epsilon^0(v) : \epsilon^0(v)\big) + \zeta(\nabla\cdot v)^2 + \sum_{i,j=0}^{n} v_i \cdot \mathfrak{M}_{ij} v_j\Big\}, \tag{1.72}$$

where $\epsilon^0(v) := \epsilon(v) - \frac{\mathbb{I}}{d}\nabla\cdot v$ denotes the traceless part of $\epsilon(v)$.

The second law of thermodynamics is implemented in traditional non-equilibrium thermodynamics by postulating that $g_S \geq 0$ must hold pointwise everywhere. Under

the additional physically reasonable assumption that $\epsilon^0(v), \nabla \cdot v$ and $v_0, \ldots, v_n$ can all in principle be varied independently, it is then clear from eq. (1.72) that η and ζ must be non-negative, and that $\mathfrak{M}_{ij}$ must be positive-semidefinite. Onsager further argued [90] that the matrix $\mathfrak{M}$ must be singular, with

$$\sum_{j=0}^{n} \mathfrak{M}_{ij} l_j = 0 \quad \forall i \in \{0 : n\}, \tag{1.73}$$

where $l \in \mathbb{R}^{n+1}$ is the vector whose entries are $l_0 = 0$ and $l_i = 1$ for $i \in \{1 : n\}$. This implies that $\sum_{i,j=0}^{n} v_i \cdot \mathfrak{M}_{ij} v_j = 0$ whenever $v_0 = 0$ and $v_i = v$ for all $i \in \{1 : n\}$, i.e. there is no entropy production due to thermodiffusion whenever the heat flux is zero and there is no relative motion between the species. Finally, and to conclude, it is postulated that the entropy production must be *strictly* positive whenever the system is out of equilibrium. Once again, under the assumption that $\epsilon^0(v), \nabla \cdot v$ and $v_0, \ldots, v_n$ can all in principle be varied independently, this implies that η and ζ must be *strictly* positive, and that $\mathfrak{M}$ must be *strictly* positive-definite on the orthogonal complement of l. Hence $\mathfrak{M}$ is an $(n+1) \times (n+1)$ symmetric positive-semidefinite matrix, with exactly one zero eigenvalue; its remaining eigenvalues are strictly positive, and the rank of $\mathfrak{M}$ is[8] n.

1.6 Summary of Onsager–Stefan–Maxwell constitutive laws

The constitutive laws derived in the previous section close the continuity equations eq. (1.50). For convenience, we summarise the constitutive laws as follows:

$$\tau = 2\eta\epsilon(v) + \big(\zeta - 2\eta/d\big) \operatorname{tr}(\epsilon(v))\mathbb{I}, \tag{1.74}$$

$$d_i = \sum_{j=0}^{n} \mathfrak{M}_{ij} v_j \quad \forall i \in \{0 : n\}. \tag{1.75}$$

We recall what all of these quantities are. Regarding eq. (1.74), the *viscous stress* is $\tau = p\mathbb{I} + \sigma$, where p is the pressure, $\mathbb{I}$ is the $d \times d$ identity matrix, σ is the total stress (recall eq. (1.47)), and $\epsilon(v)$ is the symmetric gradient of v. The shear and bulk viscosities are η and ζ respectively; these are strictly positive and can be functions of $T, p, x_1, \ldots, x_n$. Regarding eq. (1.75), for $i \in \{1 : n\}$, the species velocities v_i and

[8] In fact, if some of the species concentrations vanish, i.e. $c_i = 0$ for some i, it is possible for the rank of $\mathfrak{M}$ to be less than n. However, in this work we always consider the case of strictly positive species concentrations.

diffusion driving forces d_i were defined in eq. (1.43) and eq. (1.63). To define these for $i = 0$ we introduced the *thermal velocity* v_0, *irreversible heat flux* J'_q and *thermal driving force* d_0,

$$v_0 = \frac{J'_q}{c_{p,V}T}, \quad J'_q = J_q - \sum_{i=1}^{n} \overline{H_i} c_i v_i^d, \quad d_0 = -c_{p,V}\nabla T. \tag{1.76}$$

In eq. (1.76), we further recall that $c_{p,V} := C_p/V$ is the volumetric heat capacity, J_q is the heat flux (recall eq. (1.49)), the $\overline{H_i}$ are partial molar enthalpies (recall eq. (1.10)), and the v_i^d are diffusive velocities (recall eq. (1.52)). Finally, $\mathfrak{M}$ is an $(n+1)\times(n+1)$ *thermodiffusion transport matrix*, which is symmetric positive-semidefinite with rank n and nullspace given by eq. (1.73). The entries of $\mathfrak{M}$ are functions of $T, p, x_1, \ldots, x_n$.

Several comments on the constitutive laws are in order. Regarding the Newtonian fluid law eq. (1.74), it should be emphasised that the viscosities in general will not be constant, a possibility that we explore in the simulations of chapter 3. Moreover, since $\mathrm{tr}(\epsilon(v)) = \nabla \cdot v$ is generally non-zero (recall eq. (1.54)), the bulk viscosity ζ does generally contribute to the viscous stress, although for the mixtures considered in this work its contribution will typically be small compared to that of η.

Regarding eq. (1.75), the most urgent matter is to verify that this law actually uniquely determines the velocities $v_0, \ldots, v_n$. This can be seen as follows. First, since $\mathfrak{M}$ is symmetric, its range is the orthogonal complement of its nullspace. However, the nullspace of $\mathfrak{M}$ is one-dimensional and spanned by $l \in \mathbb{R}^{n+1}$, where $l_0 = 0$ and $l_i = 1$ for $i \in \{1 : n\}$ (recall eq. (1.73)). Hence, the linear system eq. (1.75) is consistent if and only if $\sum_{i=0}^{n} l_i d_i = 0$. This condition is indeed satisfied, owing to the form of l and the Gibbs–Duhem relation eq. (1.64). Thus eq. (1.75) can be solved non-uniquely for $v_0, \ldots, v_n$, but it leaves the species velocities $v_1, \ldots, v_n$ undetermined up to common shifts of the form $v_i \mapsto v_i + v'$ for $i \in \{1 : n\}$. This indeterminacy is removed, however, by additionally imposing that the species velocities satisfy the mass-average constraint eq. (1.44). From this perspective it is actually *beneficial* that $\mathfrak{M}$ is singular, since this ensures that the species velocities are always compatible with total mass continuity eq. (1.45). This property does not generally hold for more naïve diffusion models such as those given by Fick's law.

To conclude, it is worth mentioning that in the literature, the constitutive law eq. (1.75) is often expressed in numerous ways that are not obviously equivalent [113]. We wish to draw particular attention to the so-called *generalised Stefan–Maxwell*

equations, which can be written as [14]

$$d_i - \sum_{j=1}^{n} \frac{RTc_ic_j}{\mathscr{D}_{ij}c_T}\left(\frac{D_i^T}{\rho_i} - \frac{D_j^T}{\rho_j}\right)\nabla \ln T = \sum_{j=1}^{n} \frac{RTc_ic_j}{\mathscr{D}_{ij}c_T}(v_i^d - v_j^d) \quad \forall i \in \{1:n\}. \quad (1.77)$$

Here $\mathscr{D}_{ij}$ is a symmetric $n \times n$ matrix of so-called *Stefan–Maxwell* diffusivities; its diagonal entries $\mathscr{D}_{ii}$ are undefined. The quantities D_i^T are known as *thermal diffusion coefficients*. The irreversible heat flux can also be expressed using these quantities by

$$J_q' = -\kappa \nabla T - \sum_{i,j=1}^{n} \frac{RTc_ic_j}{c_T\mathscr{D}_{ij}}\left(\frac{D_i^T}{\rho_i} - \frac{D_j^T}{\rho_j}\right)v_j^d, \quad (1.78)$$

where κ is the *thermal conductivity*. The reciprocals of the diffusivities $\mathscr{D}_{ij}$ can be thought of as drag coefficients which quantify strength of cross-diffusion between species i and j. A detailed exposition on the extent to which one can recover Fick's law (and more generally, Nernst–Planck laws) from eq. (1.77) was recently presented in [99]. The thermal diffusion coefficients D_i^T quantify coupling between the transport of heat and mass. In particular, the terms involving D_i^T on the left-hand side of eq. (1.77) capture the *Soret effect*, where a temperature gradient can cause mass diffusion [105]. The reverse effect is the *Dufour effect*, where concentration gradients can cause heat transport [42], as captured by the terms involving D_i^T in eq. (1.78). When the diffusive fluxes v_i^d vanish, eq. (1.78) reduces to the traditional *Fourier's law* of heat transport. Fourier's law states that the heat flux is proportional to the negative temperature gradient, with constant of proportionality given by κ.

One can systematically derive eqs. (1.77) and (1.78) from the kinetic theory of dilute gases [56]. More generally, however, these equations are capable of modelling multicomponent thermodiffusion in thermodynamically non-ideal gases, liquids and electrolytic mixtures [14, 78, 79, 86]. Of crucial importance here, it is shown in [113] that eqs. (1.77) and (1.78) are equivalent to eq. (1.75), and it is possible to express the entries of $\mathfrak{M}$ in terms of $\mathscr{D}_{ij}, D_i^T$ and κ (see eq. (4.9) and the discussion thereafter). We therefore call (1.75) the *Onsager–Stefan–Maxwell (OSM) equations*, since they cast the generalised Stefan–Maxwell equations within the Onsager framework of irreversible thermodynamics. The numerical schemes developed in this thesis are based on the OSM framework eq. (1.75), not only because of its compact form, but also because the symmetric positive-semidefinite structure of $\mathfrak{M}$ facilitates the proof of well-posedness results.

Finally, we should mention that the transport coefficient values η, ζ and $\mathfrak{M}_{ij}$ can be obtained in several ways. In dilute gases, they can be determined from microscopic properties of the mixture using kinetic theory [56]. Determination of the

transport coefficients in more general mixtures can be challenging. This is especially true when n is large, since there are $\mathcal{O}(n^2)$ coefficients, and they can depend strongly on $T, p, x_1, \ldots, x_n$. Possible approaches are determination by experimental measurements [123], through empirical correlations [123], or by computational methods such as molecular dynamics [115].

1.7 Mixed finite element methods

The forthcoming chapters assume familiarity with the standard theory of *mixed finite element methods*. In particular, we assume familiarity with the theory of saddle point problems in Hilbert spaces, in both the infinite and finite dimensional settings. We also assume familiarity with the theory of mixed finite element methods for the incompressible Stokes equations, and for the mixed formulation of the Poisson equation. We shall not summarise this material here, since excellent expositions can be found in standard references, such as the textbook of Boffi, Brezzi and Fortin [18], and the textbook of Ern and Guermond [49].

1.8 Overview and main contributions of this thesis

Chapters 2 to 4 of this thesis systematically derive and analyse finite element algorithms for the governing equations eqs. (1.50), (1.74), and (1.75), in situations of increasing complexity and generality.

Chapter 2 begins by focussing on the case of stationary and isothermal flow, in the low Reynolds number regime where eq. (1.50b) reduces to the Stokes equations. In particular we derive, for the first time, high-order finite element discretisations for these equations that are applicable to non-ideal mixtures, and are straightforward to implement in two and three spatial dimensions. Several non-trivial steps are taken to accomplish this, including: the identification of an appropriate weak formulation of the governing equations; identification of the need for *integral constraints* to obtain unique solutions; and the efficient implementation of these constraints within Newton's method by means of the Woodbury identity. We also prove well-posedness and quasi-optimality of our discretisations, in a suitable Picard linearised setting. These discretisations form the basis for our extensions considered in the subsequent chapters.

In chapter 3 we extend on the discretisations of chapter 2 to handle the case of locally electroneutral mixtures of electrically charged species. This enables the

simulation of multicomponent electrolyte flows. This chapter additionally extends to the case of transient flow, and we allow for full Navier–Stokes flow in eq. (1.50b) with non-constant viscosities. Because we do not make any simplifying assumptions on the volumetric equation of state, a subtle interplay between the mass continuity equations and boundary conditions arises in the transient setting. We identify and address this issue for the first time. Altogether, these extensions enable the simulation of electrolyte mixtures used in lithium-ion batteries, with material properties and multicomponent transport coefficients that are obtained entirely from experimental measurements, without making any idealisations.

Finally, chapter 4 extends further on chapter 3 by allowing for anisothermal flow. As a result, we ultimately obtain a large class of finite element algorithms that are capable of solving eqs. (1.50), (1.74), and (1.75) in full generality. We also show, for the first time, that it is possible to construct algorithms in this setting that are structure preserving in the sense of exact energy conservation and entropy dissipation.

Chapter 2

High-order finite element methods for three-dimensional multicomponent convection-diffusion

This chapter is based on the paper [6].

2.1 Introduction

In this chapter we derive and analyse finite element methods for capturing two important physical phenomena in concentrated mixtures: bulk momentum transport and cross-diffusion. There is much existing numerical literature that considers these phenomena separately, but as we will presently discuss, very little numerical literature studies their coupling. We consider low Reynolds number flow and model bulk momentum transport using the Stokes equations; these are well-studied and we refer to [18, 49, 65] for expositions on finite element methods for these equations. The discretisations we introduce in this chapter allow for any conforming inf-sup stable finite element pair for the velocity-pressure formulation of the Stokes equations to be used. Examples include the Taylor–Hood [109] or Scott–Vogelius [102] pairs, on suitable meshes.

Finite element methods for the Onsager–Stefan–Maxwell (OSM) equations are proposed and analysed in [21, 29, 70, 83, 112], but these works assume an isobaric ideal gaseous mixture. The methods proposed in this chapter are similar to that of [83], as we discretise the species mass fluxes in $H(\mathrm{div})$. However, the formulation herein is more general than [83], as we allow for the mixture to be non-ideal, in a gaseous or condensed phase, non-isobaric, and we consider the coupling to the Stokes

equations. In fact, the finite element literature that studies the coupling of the OSM and Stokes (or Navier–Stokes) equations is sparse. The only works we know of are [4, 24, 26, 80], but apart from [4, 24] these papers assume an ideal mixture, with [26] considering gases, [4, 80] considering both gases and condensed phases, and [24] considering mixtures satisfying a generalised incompressibility constraint. Notably, in [4] the OSM equations are formulated and discretised in terms of the species chemical potentials. This enables [4] to handle non-ideal mixtures, and we follow the same approach in this chapter.

This chapter represents a substantial extension of [4]. We devise finite element methods for the coupled Stokes and OSM (SOSM) equations, applicable to non-ideal gases and condensed phases. To facilitate coupling of the Stokes and OSM equations, the methods in [4] require divergence-conforming symmetric stress elements, i.e. elements discretizing $H(\mathrm{div}, \mathbb{S})$. Such elements are difficult to implement [3], limiting [4] to two-dimensional low-order simulations. We circumvent this challenge and derive a large class of high-order methods in two and three spatial dimensions. We do this by reformulating the SOSM equations: in [4] the *species velocities* are discretised in L^2, while we instead discretise the *species mass fluxes* in $H(\mathrm{div})$. The $H(\mathrm{div})$-regularity of the mass fluxes enables coupling of the OSM and Stokes equations without having to discretise the stress. This choice of variables also means that the chemical potentials act as Lagrange multipliers for enforcing the species molar continuity equations, which leads to the requirement that the discretised mass flux and chemical potential spaces form stable $H(\mathrm{div})$–L^2 pairs. Such pairs are standard in finite element software for mixed formulations of the Poisson problem; examples include the $\mathbb{BDM}_k$–$\mathbb{DG}_{k-1}$ [22, 85] and $\mathbb{RT}_k$–$\mathbb{DG}_{k-1}$ [96] pairs. Another benefit of our reformulation is that we seek the chemical potentials and pressure in L^2, whereas [4] seeks these unknowns in a solution-dependent Sobolev space. This leads to a complicated requirement on the discretisation (see [4, Assumption 4.2]) and it is not clear how to satisfy this requirement when using high-order spaces. Our formulation circumvents this challenge.

At a theoretical level, we analyse a Picard linearisation of the SOSM equations, which adopts a Gauß–Seidel approach by segregating the solution of the concentrations from the chemical potentials and other variables. This linearisation, which remarkably leads to a symmetric system, was introduced in [4], but the variational formulation and discretisation studied here is different. We establish well-posedness of our formulation of the linearised SOSM problem in the continuous and discrete setting. We also show that, in this linearised setting, our finite element schemes are quasi-optimal.

The Picard iteration is convenient for analysis, but it can be slow to converge to a root and for challenging problems may diverge altogether. Newton's method [35] provides an alternative, but it requires the solution of larger systems, as the Gauß–Seidel staggering is no longer possible. Newton's method can converge to roots quickly and robustly, but it brings several major challenges. Firstly, it is necessary to preserve invariance of the discretisation with respect to additive constants in the pressure space; doing so requires extra terms in the discretisation. We refer to these as density consistency terms and we find that neglecting them prevents Newton's method from converging. Secondly, for well-posedness of the stationary nonlinear SOSM problem it is necessary to impose constraints on the total number of moles of the species. Constraints of this form have a clear physical interpretation and can be found in the literature on stationary multicomponent flows (see e.g. [25, 57] and also [50, 67]). Each constraint introduces a dense row in the Jacobian matrix; we solve this efficiently using the Woodbury formula [62] on an auxiliary sparse Jacobian. Together, these adaptations enable the efficient solution of the nonlinear SOSM equations with Newton's method for the first time. A disadvantage of our methods is that, for the nonlinear SOSM problem, we empirically observe that the methods converge sub-optimally in space by one order in the mesh size h. This seems to be due to terms that arise from the coupling of the Stokes and OSM equations, and it is unclear how to circumvent this behaviour.

The rest of this chapter is organised as follows. In section 2.2 we derive the variational formulation of the Picard linearised SOSM problem and establish well-posedness at the continuous level. In section 2.3 we derive the finite element methods and establish (linearised) discrete well-posedness and quasi-optimality. In section 2.4 we outline how the discretisations can be used in conjunction with Newton's method to solve the nonlinear SOSM problem. Numerical experiments are given in section 2.5 and conclusions are drawn in section 2.6.

2.2 Continuous problem and Picard linearisation

Consider a stationary isothermal mixture of $n \geq 2$ distinct species in a common thermodynamic phase. We assume the spatial domain $\Omega \subset \mathbb{R}^d$ ($d \in \{2, 3\}$) is bounded, connected, and Lipschitz.

2.2.1 Notation and governing equations

Associated to species $i \in \{1:n\}$ is its molar concentration $c_i : \Omega \to \mathbb{R}^+$ and velocity $v_i : \Omega \to \mathbb{R}^d$. The molar mass of species i is denoted by $m_i > 0$ and is a known constant. The molar flux of species i is $c_i v_i$. For symmetry of our forthcoming variational formulation it shall be convenient to work with mass fluxes, which we denote by $J_i := m_i c_i v_i$. The stationary molar continuity equation for species i reads

$$\nabla \cdot (v_i c_i) = r_i \quad \text{in } \Omega, \tag{2.1}$$

with $r_i : \Omega \to \mathbb{R}$ a prescribed reaction term[1].

The total concentration of the mixture is $c_T := \sum_{j=1}^n c_j$ and the density is $\rho := \sum_{j=1}^n m_j c_j$. The mass fraction of species i is $\omega_i := m_i c_i / \rho$ and the mass-average (or barycentric) velocity of the mixture is

$$v := \sum_{j=1}^n \omega_j v_j = \sum_{j=1}^n J_j / \rho. \tag{2.2}$$

Recall that we refer to eq. (2.2) as the *mass-average constraint* (see eq. (1.44)).

Recall that momentum balance is captured by eq. (1.50b). In this chapter, we consider the stationary, low Reynolds number regime, so that eq. (1.50b) (together with eq. (1.66)) reduces to the steady Stokes momentum equation

$$-\nabla \cdot \tau + \nabla p = \rho f \quad \text{in } \Omega, \tag{2.3}$$

where $\tau : \Omega \to \mathbb{R}^{d\times d}_{\text{sym}}$ is the viscous stress, $p : \Omega \to \mathbb{R}$ the pressure, and $f : \Omega \to \mathbb{R}^d$ a prescribed body force[2]. Recall from eq. (1.74) that τ and v are related through the Newtonian constitutive law

$$\tau = 2\eta\epsilon(v) + \big(\zeta - 2\eta/d\big)\,\mathrm{tr}(\epsilon(v))\mathbb{I} = \mathscr{A}^{-1}\epsilon(v), \tag{2.4}$$

where $\epsilon(v)$ denotes the symmetric gradient of v, $\eta > 0$ is the shear viscosity, $\zeta > 0$ the bulk viscosity, $\mathbb{I}$ the $d \times d$ identity and $\mathscr{A} : \mathbb{R}^{d\times d}_{\text{sym}} \to \mathbb{R}^{d\times d}_{\text{sym}}$ the compliance tensor. In this chapter we assume that η and ζ are constants, to simplify the presentation

[1]Note that we previously omitted reaction terms in eq. (1.50a), since we are not concerned with modelling chemical reactions in this thesis. However, so long as r_i is treated as being *fixed prescribed data*, its presence in eq. (2.1) does not lead to any difficulties. Hence we have opted to include it as a source term for the sake of generality. However, if one were interested in modelling chemical reactions, in most situations it would be necessary to allow for r_i to depend on problem unknowns; here, we are explicitly forbidding this.

[2]Similar to r_i in eq. (2.1), the presence of f in eq. (2.3) leads to no difficulties if it is treated as a prescribed source term.

of our forthcoming numerical analysis[3]. We postpone the consideration of mixtures with non-constant viscosities to chapter 3.

We denote the chemical potential of species i by $\mu_i : \Omega \to \mathbb{R}$. The isothermal, non-isobaric OSM equations are given by (see e.g. [14])

$$-c_i \nabla \mu_i + \omega_i \nabla p = \sum_{j=1}^{n} \boldsymbol{M}_{ij} v_j \quad \text{in } \Omega \quad \forall i \in \{1:n\}. \tag{2.5}$$

The matrix $\boldsymbol{M}$ is called the *isothermal Onsager transport matrix*, with entries

$$\boldsymbol{M}_{ij} := \begin{cases} -\frac{RTc_i c_j}{\mathscr{D}_{ij} c_T} & \text{if } i \neq j, \\ \sum_{k=1, k\neq i}^{n} \frac{RTc_i c_k}{\mathscr{D}_{ik} c_T} & \text{if } i = j, \end{cases} \tag{2.6}$$

where $R > 0$ is the ideal gas constant, $T > 0$ the temperature and $\mathscr{D}_{ij}$ the Stefan–Maxwell diffusivities. Note that $\mathscr{D}_{ii}$ is undefined and $\mathscr{D}_{ij} = \mathscr{D}_{ji}$ $\forall i \neq j$ [14]. It follows that $\boldsymbol{M}$ is symmetric with $\sum_{j=1}^{n} \boldsymbol{M}_{ij} = 0$ $\forall i$. One can verify that the generalised Stefan–Maxwell equations previously introduced in eq. (1.77) reduce to eq. (2.5) when T is constant. The relationship between the isothermal transport matrix $\boldsymbol{M}$ and the thermodiffusion transport matrix $\mathfrak{M}$ from eq. (1.75) is shown in [113, eq. (3.5)].

Following [4], to simplify the presentation of our forthcoming numerical analysis, in this chapter we shall assume that each $\mathscr{D}_{ij}$ is a strictly positive constant. This implies that $\boldsymbol{M}$ is positive-semidefinite, and it has exactly one zero eigenvalue (provided that all species concentrations are strictly positive). However, in a general mixture, $\mathscr{D}_{ij}$ can depend on the temperature, pressure, and species concentrations [75]. Under certain physically reasonable assumptions, our Picard linearised analysis does still hold in this more general setting[4]. We postpone the consideration of mixtures with non-constant diffusivities to chapter 3.

2.2.2 Thermodynamic constitutive law

Fully describing the mixture requires a thermodynamic constitutive law that expresses the concentrations in terms of the pressure and chemical potentials. In other words, we require a relationship between $c_1, \dots, c_n$ and $\mu_1, \dots, \mu_n, p$. Such relationships are determined by the equilibrium thermodynamic properties of the mixture (recall

[3]More generally, all of our Picard linearised analysis in section 2.2.6 and section 2.3 still holds if $\eta, \zeta \in L^\infty(\Omega)$ are fixed prescribed data with $\operatorname{ess\,inf}_\Omega \eta, \operatorname{ess\,inf}_\Omega \zeta > 0$.

[4]More generally, all of our Picard linearised analysis in section 2.2.6 and section 2.3 still holds provided that the $\mathscr{D}_{ij}$ do not depend on pressure and depend continuously on the concentrations, in such a way that $\boldsymbol{M}$ remains positive-semidefinite with exactly one zero eigenvalue. This assumption on $\boldsymbol{M}$ was originally made by Onsager [90] through consideration of the entropy production (cf. eq. (1.72)).

section 1.2). In this chapter, it will be convenient to denote this relationship by a map $\mathcal{C}$ which takes $n+1$ functions $\mu_1, \ldots, \mu_n, p : \Omega \to \mathbb{R}$ and produces n functions $c_1, \ldots, c_n : \Omega \to \mathbb{R}^+$. Hence

$$(c_1, \ldots, c_n) = \mathcal{C}(\mu_1, \ldots, \mu_n, p). \tag{2.7}$$

Importantly, the pressure and chemical potentials only appear in the SOSM equations through their gradients (see eq. (2.19) below), and they do not appear in any of our boundary conditions. Hence these fields are only determined up to additive constants[5]. For $\mathcal{C}$ to be well-defined we require therefore that, for all constants $C_1, \ldots, C_n, C_{n+1}$,

$$\mathcal{C}(\mu_1, \ldots, \mu_n, p) = \mathcal{C}(\mu_1 + C_1, \ldots, \mu_n + C_n, p + C_{n+1}). \tag{2.8}$$

For an isothermal ideal gaseous mixture [60, 61], it holds that (see eq. (1.24))

$$c_i = \frac{p^\ominus}{RT} \exp\Big(\frac{\mu_i - \mu_i^\ominus(T, p^\ominus)}{RT}\Big) \quad \text{in } \Omega \quad \forall i \in \{1 : n\}, \tag{2.9}$$

where $\mu_1^\ominus(T, p^\ominus), \ldots, \mu_n^\ominus(T, p^\ominus)$ are reference chemical potentials and $p^\ominus$ a reference pressure. Both $p^\ominus$ and $\mu_i^\ominus(T, p^\ominus)$ can be eliminated from eq. (2.9). Indeed, since μ_i is undetermined up to additive constants, eq. (2.9) leaves c_i undetermined up to positive multiplicative constants. We can remove this indeterminacy by enforcing that the total number of moles of species i is a prescribed value $\mathscr{N}_i > 0$,

$$\int_\Omega c_i \, \mathrm{d}\Omega = \mathscr{N}_i \quad \forall i \in \{1 : n\}. \tag{2.10}$$

With this indeterminacy removed, there is no loss of generality in expressing eq. (2.9) as

$$c_i = c^\ominus \exp\Big(\frac{\mu_i - \mu_i^{\mathrm{aux}}}{RT}\Big) \quad \text{in } \Omega \quad \forall i \in \{1 : n\}, \tag{2.11}$$

where $\mu_i^{\mathrm{aux}} \in \mathbb{R}$ is an auxiliary constant that is chosen so that eq. (2.10) holds, and $c^\ominus > 0$ is any fixed constant with units of concentration[6]. Defining $\mathcal{C}$ through eqs. (2.10) and (2.11), we observe that eq. (2.8) is satisfied. To motivate eq. (2.10), note that in the transient setting, prescription of $\int_\Omega c_i \, \mathrm{d}\Omega$ is unnecessary since its value is determined by the transient molar continuity equation $\partial_t c_i + \nabla \cdot (v_i c_i) = r_i$.

[5]These constants are undetermined in the present model, but in some settings (e.g. if one is interested in formation energies or entropies, or modelling chemical reactions) they are fully determined and have physical importance.

[6]The actual value of $c^\ominus$ is irrelevant, since scaling $c^\ominus$ is equivalent to shifting μ_i^{aux}. We are being pedantic and include it in eq. (2.11) for dimensional consistency, so that the right-hand side has units of concentration.

Indeed, integration yields $\frac{\mathrm{d}}{\mathrm{d}t}\int_\Omega c_i \,\mathrm{d}\Omega = \int_\Omega [r_i - \nabla\cdot(v_i c_i)]\,\mathrm{d}\Omega$, so that time evolution of $\int_\Omega c_i\,\mathrm{d}\Omega$ is determined by the flux $c_i v_i$, reaction term r_i and initial condition on c_i. However, in the steady case the molar continuity equation eq. (2.1) no longer determines the total number of moles of species i and it is natural to instead impose eq. (2.10) as an additional constraint.

In the completely general setting, where the mixture can be in a gaseous or condensed phase and possibly non-ideal, one must consider the mole fractions $x_i := c_i/c_T$. A general constitutive law can be expressed using n partial molar Gibbs functions $\overline{G_i} : \mathbb{R}^{n+2} \to \mathbb{R}$ and partial molar volume functions $\overline{V_i} : \mathbb{R}^{n+2} \to \mathbb{R}$, whose arguments are the state variables $T, p, x_1, \ldots, x_n$. These functions are derived from partial derivatives of the Gibbs free energy of the mixture (recall eqs. (1.9) and (1.10)) and we assume that they are known. The constitutive law is then an algebraic system of equations (cf. eqs. (1.9) and (1.13)):

$$\mu_i - \mu_i^{\mathrm{aux}} = \overline{G_i}(T, p - p^{\mathrm{aux}}, x_1, \ldots, x_n) \qquad \text{in } \Omega \quad \forall i \in \{1:n\}, \tag{2.12a}$$

$$\frac{1}{c_T} = \sum_{j=1}^{n} x_j \overline{V_j}(T, p - p^{\mathrm{aux}}, x_1, \ldots, x_n) \quad \text{in } \Omega, \tag{2.12b}$$

where $\mu_i^{\mathrm{aux}}, p^{\mathrm{aux}} \in \mathbb{R}$ are auxiliary constants reflecting the indeterminacy of μ_i, p up to additive constants. These auxiliary constants play an analogous role to the μ_i^{aux} in eq. (2.11), but now in the setting of a general constitutive relation formulated using mole fractions. The system in eq. (2.12a) determines $x_1, \ldots, x_n$, which can then be used in eq. (2.12b) to determine c_T. The concentrations are then given by $c_i = c_T x_i$.

By the Gibbs–Duhem relation eq. (1.18), only $n-1$ of the equations in eq. (2.12a) are independent [61]. Likewise, only $n-1$ of the mole fractions are independent as $\sum_{j=1}^n x_j = 1$. Therefore, although the system in eq. (2.12) constitutes $n+1$ equations in the $n+1$ unknowns $c_T, x_1, \ldots, x_n$, only n of these equations and n of these unknowns are independent. In particular, to remove the indeterminacy caused by the $n+1$ auxiliary constants $\mu_1^{\mathrm{aux}}, \ldots, \mu_n^{\mathrm{aux}}, p^{\mathrm{aux}}$, it suffices to prescribe at most n constraints. A reasonable choice of constraints are those in eq. (2.10); however, depending on the form of $\overline{G_i}$ and $\overline{V_i}$ it may not always be possible to satisfy these. For example, if $\overline{V_1}, \ldots, \overline{V_n}$ are bounded below by a constant $V' > 0$ (this is the case in section 2.5.2), then multiplying eq. (2.12b) by c_T and integrating over Ω reveals that $\int_\Omega 1\,\mathrm{d}\Omega \geq V' \sum_{j=1}^n \int_\Omega c_j\,\mathrm{d}\Omega$. Clearly, in this case $\int_\Omega c_i\,\mathrm{d}\Omega$ cannot be prescribed arbitrarily. A related complication is that sometimes it is only possible for $k < n$ constraints to be imposed without overdetermining the system in eq. (2.12) (again, see section 2.5.2). Attempting to analyse exactly what constraints (and how many)

can legitimately be imposed in general is outside the scope of this thesis. In what follows, we assume that an appropriate set of constraints have been suitably chosen so that $\mathcal{C}$ is well-defined and satisfies eq. (2.8).

2.2.3 Augmentation and change of variables

An important property of the isothermal Onsager transport matrix $\boldsymbol{M}$ (recall eq. (2.6)) is that, assuming the concentrations are strictly positive, $\boldsymbol{M}$ is positive-semidefinite with nullspace spanned by $(1,\dots,1)^T$ [90, 112]. Positive-semidefiniteness of $\boldsymbol{M}$ ensures that entropy generation is non-negative[7], while the nullspace of $\boldsymbol{M}$ ensures that bulk convection is nondissipative [4, eqs. (1.15-1.16)]. These properties of $\boldsymbol{M}$ are not only of physical importance; they have crucial implications in our numerics, as we now describe.

In our forthcoming variational formulation, positive-semidefiniteness of $\boldsymbol{M}$ ensures that a certain bilinear form is positive-semidefinite. However, for establishing well-posedness we would prefer this bilinear form to be coercive. We accomplish this using the augmentation strategy of [4, sect. 1.3] (see also [45, 64, 112]), in which multiples of the mass-average constraint eq. (2.2) are added to the Stokes and OSM equations eqs. (2.3) and (2.5). As in [4], we also only strongly enforce the divergence of the mass-average constraint, as this balances the number of equations and unknowns in the SOSM problem. This leads to the augmented equations [4, sect. 1.5]

$$-c_i\nabla\mu_i + \omega_i\nabla p + \gamma\omega_i v = \sum_{j=1}^{n} \boldsymbol{M}^{\gamma}_{ij} v_j \qquad \text{in } \Omega \quad \forall i, \tag{2.13a}$$

$$-\nabla\cdot\tau + \nabla p + \gamma v - \gamma\sum_{j=1}^{n}\omega_j v_j = \rho f \qquad \text{in } \Omega, \tag{2.13b}$$

$$\nabla\cdot v = \nabla\cdot\left(\sum_{j=1}^{n}\omega_j v_j\right) \qquad \text{in } \Omega, \tag{2.13c}$$

where $\gamma > 0$ is a constant user-chosen augmentation parameter, and

$$\boldsymbol{M}^{\gamma}_{ij} := \boldsymbol{M}_{ij} + \gamma\omega_i\omega_j \tag{2.14}$$

is an augmented transport matrix, which turns out to be positive-definite [4, 112].

As discussed in section 2.1, the formulation in [4] discretises the species velocities v_i in L^2 which, in turn, requires the stress to be discretised in $H(\mathrm{div},\mathbb{S})$. This limits

[7] Entropy production from thermodiffusion (recall eq. (1.72)) is $T^{-1}\sum_{i,j=0}^{n} v_i\cdot\boldsymbol{\mathfrak{M}}_{ij}v_j$. In the isothermal setting this reduces to $T^{-1}\sum_{i,j=0}^{n} v_i\cdot\boldsymbol{\mathfrak{M}}_{ij}v_j = T^{-1}\sum_{i,j=1}^{n} v_i\cdot\boldsymbol{M}_{ij}v_j$ [113].

[4] to two-dimensional low-order simulations. We circumvent this by reformulating the SOSM equations in terms of the mass fluxes and we solve for these instead of the velocities; this will allow us to eliminate the stress altogether. It will be convenient to introduce the density reciprocal (or specific volume) $\Psi := 1/\rho$. We divide the augmented OSM equations in eq. (2.13a) by $m_i c_i$ as this will lead to our forthcoming linearisation to be symmetric; written in terms of the mass fluxes, the augmented OSM equations are

$$-m_i^{-1}\nabla\mu_i + \Psi\nabla p + \gamma\Psi v = \sum_{j=1}^{n} \hat{\boldsymbol{M}}_{ij}^{\gamma} J_j \quad \text{in } \Omega \quad \forall i \in \{1:n\}, \tag{2.15}$$

where $\hat{\boldsymbol{M}}_{ij}^{\gamma}$ is a scaling of the augmented transport matrix in eq. (2.14),

$$\hat{\boldsymbol{M}}_{ij}^{\gamma} := \frac{\boldsymbol{M}_{ij}^{\gamma}}{m_i m_j c_i c_j} = \frac{\boldsymbol{M}_{ij}}{m_i m_j c_i c_j} + \gamma\Psi^2. \tag{2.16}$$

Occasional use will be made of $\hat{\boldsymbol{M}}$, the non-augmented analogue of $\hat{\boldsymbol{M}}^{\gamma}$, which is:

$$\hat{\boldsymbol{M}}_{ij} := \frac{\boldsymbol{M}_{ij}}{m_i m_j c_i c_j}. \tag{2.17}$$

Moreover, rewriting the augmented Stokes momentum equation in eq. (2.13b) in terms of the mass fluxes, and eliminating the stress via eq. (2.4), we obtain

$$-\nabla\cdot\left(\mathscr{A}^{-1}\epsilon(v)\right) + \nabla p + \gamma v - \gamma\Psi\sum_{j=1}^{n} J_j = \rho f \quad \text{in } \Omega. \tag{2.18}$$

2.2.4 Full SOSM problem statement

It shall be expedient to employ boldface notation for quantities indexed by $i \in \{1:n\}$. Hence, for example, we write $\boldsymbol{J} = [J_1, \ldots, J_n]^\top$ and $\boldsymbol{\mu} = [\mu_1, \ldots, \mu_n]^\top$. We view these as column vectors (or $n \times 1$ matrices). In this chapter we consider the following formulation of the SOSM problem. Given data $f, \boldsymbol{r}$, find a barycentric velocity v, pressure p, mass fluxes $\boldsymbol{J}$ and chemical potentials $\boldsymbol{\mu}$ such that

$$-m_i^{-1}\nabla\mu_i + \Psi\nabla p + \gamma\Psi v = \sum_{j=1}^{n} \hat{\boldsymbol{M}}_{ij}^{\gamma} J_j \qquad \text{in } \Omega \quad \forall i, \tag{2.19a}$$

$$-\nabla\cdot\left(\mathscr{A}^{-1}\epsilon(v)\right) + \nabla p + \gamma v - \gamma\Psi\sum_{j=1}^{n} J_j = \rho f \qquad \text{in } \Omega, \tag{2.19b}$$

$$m_i^{-1}\nabla\cdot J_i = r_i \qquad \text{in } \Omega \quad \forall i, \tag{2.19c}$$

$$\nabla \cdot v = \nabla \cdot \left(\Psi \sum_{j=1}^{n} J_j \right) \quad \text{in } \Omega, \tag{2.19d}$$

subject to the constitutive law in eq. (2.7), and Dirichlet boundary conditions[8]

$$v = v_D, \quad J_i \cdot \hat{n}_\Gamma = J_{D,i} \quad \text{on } \partial\Omega \quad \forall i \in \{1:n\}, \tag{2.20}$$

where $\hat{n}_\Gamma$ is the unit outward normal on $\Gamma := \partial\Omega$. The Dirichlet data must satisfy compatibility conditions $m_i^{-1} \int_{\partial\Omega} J_{D,i} \cdot \hat{n}_\Gamma \, \mathrm{d}\Gamma = \int_\Omega r_i \, \mathrm{d}\Omega$.

Recall that ρ is the density, $\Psi = 1/\rho$ the density reciprocal, $m_1, \ldots, m_n$ the molar masses, $\gamma > 0$ the augmentation parameter, $\mathscr{A}$ the compliance tensor defined through eq. (2.4) and $\hat{\boldsymbol{M}}_{ij}^{\gamma}$ is a modified isothermal Onsager transport matrix defined through eqs. (2.6) and (2.16). As in [4], we make the following regularity assumptions on the data.

Assumption 2.2.1 (Data regularity)**.** We assume the data regularity $f, r_1, \ldots, r_n \in L^2(\Omega)$, $v_D \in H^{1/2}(\partial\Omega)^d$ and $J_{D,i} \in H^{-1/2}(\partial\Omega)$ for all $i \in \{1:n\}$.

2.2.5 Picard linearisation

We first study a Picard linearisation of the SOSM problem which follows a Gauß–Seidel approach in which the concentrations $\boldsymbol{c}$ are frozen and treated as fixed fields. In practice this can be done at every step of a fixed point iteration, in which one uses the concentrations from the previous step (computed via the constitutive law in eq. (2.7)) to linearise the problem at the current step. Fixing the concentrations also allows for ρ, Ψ and $\hat{\boldsymbol{M}}_{ij}^{\gamma}$ to be fixed, since they can be expressed in terms of the concentrations through simple algebraic formulae. Consequently the SOSM equations in eq. (2.19) become linear in the unknown fields $v, p, \boldsymbol{J}, \boldsymbol{\mu}$. It is these $2 + 2n$ fields that we treat as unknowns in our formulation of the Picard linearisation.

We cast the Picard linearisation of eqs. (2.19) and (2.20) as a variational problem. For the integrals in the variational formulation to be well-defined, as in [4] we require the following physically reasonable assumptions on the density and concentration fields.

Assumption 2.2.2 (Concentration and density regularity)**.** We assume that $\rho \in W^{1,\infty}(\Omega)$, and that $c_i \in L^\infty(\Omega)$ and $c_i \geq c_{\min}$ a.e. in Ω for all $i \in \{1:n\}$ where $c_{\min} > 0$ is a constant. Since $\rho = \sum_{j=1}^{n} m_j c_j$ it also follows that $\Psi = 1/\rho \in W^{1,\infty}(\Omega)$.

[8] Boundary conditions on the total mass flux ρv can also be considered (see [4] and section 2.5.2).

Let $(\cdot,\cdot)_\Omega$ denote the L^2-inner-product on Ω with corresponding norm $\|\cdot\|_{L^2(\Omega)}$. We use standard notation (see e.g. [48]) for the Sobolev spaces $H^1(\Omega), H(\mathrm{div};\Omega)$ and norms $\|\cdot\|_{H^1(\Omega)}, \|\cdot\|_{H(\mathrm{div};\Omega)}$. Their counterparts with vanishing traces are denoted by

$$H_0^1(\Omega) = \{u \in H^1(\Omega) : u|_{\partial\Omega} = 0\}, \quad H_0(\mathrm{div};\Omega) = \{K \in H(\mathrm{div};\Omega) : K \cdot \hat{n}_\Gamma|_{\partial\Omega} = 0\}. \tag{2.21}$$

We also consider the space $L_0^2(\Omega) = \{q \in L^2(\Omega) : (q,1)_\Omega = 0\}$.

Proceeding formally, we multiply eq. (2.19a) by a test function $K_i \in H_0(\mathrm{div};\Omega)$, integrate over Ω, and integrate the terms with gradients by parts, yielding

$$(m_i^{-1}\mu_i, \nabla\cdot K_i)_\Omega - (p, \nabla\cdot(\Psi K_i))_\Omega + (\gamma\Psi v, K_i)_\Omega = \sum_{j=1}^n \left(\hat{\boldsymbol{M}}_{ij}^\gamma J_j, K_i\right)_\Omega. \tag{2.22}$$

Next, we multiply eq. (2.19b) by a test function $u \in H_0^1(\Omega)^d$ and integrate the viscous and pressure terms by parts. This yields

$$(\mathscr{A}^{-1}\epsilon(v), \nabla u)_\Omega - (p, \nabla\cdot u)_\Omega + \left(\gamma v - \gamma\Psi\sum_{j=1}^n J_j, u\right)_\Omega = (\rho f, u)_\Omega. \tag{2.23}$$

Moreover, since $\mathscr{A}$ is defined by eq. (2.4), the viscous terms simplify to

$$(\mathscr{A}^{-1}\epsilon(v), \nabla u)_\Omega = 2\eta(\epsilon(v), \epsilon(u))_\Omega + \lambda(\nabla\cdot v, \nabla\cdot u)_\Omega, \tag{2.24}$$

where $\lambda := \zeta - 2\eta/d$ is a Lamé coefficient. Finally, the variational analogues of eqs. (2.19c) and (2.19d) are simply: for all test functions $w_1,\ldots,w_n, q \in L_0^2(\Omega)$,

$$\sum_{i=1}^n (m_i^{-1}\nabla\cdot J_i, w_i)_\Omega = \sum_{i=1}^n (r_i, w_i)_\Omega, \tag{2.25}$$

$$(\nabla\cdot v, q)_\Omega = \left(\nabla\cdot\left(\Psi\sum_{j=1}^n J_j\right), q\right)_\Omega. \tag{2.26}$$

Assumptions 2.2.1 and 2.2.2 imply that the integrals in eqs. (2.22) to (2.26) are well-defined if $(v,p) \in H^1(\Omega)^d \times L_0^2(\Omega)$ and $(J_i,\mu_i) \in H(\mathrm{div};\Omega)\times L_0^2(\Omega)$ for all i. These are the spaces we will employ in our variational formulation. Note that we seek the pressure and chemical potentials in $L_0^2(\Omega)$ as opposed to $L^2(\Omega)$ to address the fact that they are only determined up to additive constants. We also introduce the product spaces

$$\mathcal{V} = H^1(\Omega)^d \times H(\mathrm{div};\Omega)^n,\ \mathcal{V}_0 = H_0^1(\Omega)^d \times H_0(\mathrm{div};\Omega)^n,\ \mathcal{Q} = L_0^2(\Omega)\times L_0^2(\Omega)^n. \tag{2.27}$$

Note that $\mathcal{V}_0 \subset \mathcal{V}$ consists of the traceless functions in $\mathcal{V}$. Consider the bilinear forms

$$\begin{cases} a_v : H^1(\Omega)^d \times H^1_0(\Omega)^d \to \mathbb{R}, \\ a_v(v,u) := 2\eta(\epsilon(v),\epsilon(u))_\Omega + \lambda(\nabla\cdot v, \nabla\cdot u)_\Omega, \end{cases} \tag{2.28a}$$

$$\begin{cases} a_o : \mathcal{V}\times\mathcal{V}_0 \to \mathbb{R}, \\ a_o((v,\boldsymbol{J}),(u,\boldsymbol{K})) := \gamma\left(v - \Psi\sum_{j=1}^n J_j, u - \Psi\sum_{i=1}^n K_i\right)_\Omega \\ \qquad\qquad + \sum_{i,j=1}^n \left(\hat{\boldsymbol{M}}_{ij}J_j, K_i\right)_\Omega, \\ \text{where } \hat{\boldsymbol{M}}_{ij} := \boldsymbol{M}_{ij}/(m_i m_j c_i c_j) \text{ and } \boldsymbol{M}_{ij} \text{ is defined in eq. (2.6)}, \end{cases} \tag{2.28b}$$

$$\begin{cases} a : \mathcal{V}\times\mathcal{V}_0 \to \mathbb{R}, \\ a((v,\boldsymbol{J}),(u,\boldsymbol{K})) := a_v(v,u) + a_o((v,\boldsymbol{J}),(u,\boldsymbol{K})), \end{cases} \tag{2.28c}$$

$$\begin{cases} b : \mathcal{V}\times\mathcal{Q} \to \mathbb{R}, \\ b((u,\boldsymbol{K}),(p,\boldsymbol{\mu})) := -(p,\nabla\cdot u)_\Omega + \sum_{i=1}^n (p,\nabla\cdot(\Psi K_i))_\Omega \\ \qquad\qquad - \sum_{i=1}^n (m_i^{-1}\mu_i, \nabla\cdot K_i)_\Omega. \end{cases} \tag{2.28d}$$

The conditions in eqs. (2.22) to (2.26) are equivalent to the following problem: find $((v,\boldsymbol{J}),(p,\boldsymbol{\mu})) \in \mathcal{V}\times\mathcal{Q}$ such that $(v,\boldsymbol{J})$ satisfy the boundary conditions in eq. (2.20) and

$$a((v,\boldsymbol{J}),(u,\boldsymbol{K})) + b((u,\boldsymbol{K}),(p,\boldsymbol{\mu})) = (\rho f, u)_\Omega \qquad \forall (u,\boldsymbol{K}) \in \mathcal{V}_0, \tag{2.29a}$$

$$b((v,\boldsymbol{J}),(q,\boldsymbol{w})) = -\sum_{i=1}^n (r_i, w_i)_\Omega \quad \forall (q,\boldsymbol{w}) \in \mathcal{Q}. \tag{2.29b}$$

This constitutes our variational formulation of the Picard linearised SOSM problem. Note that a is symmetric on $\mathcal{V}_0\times\mathcal{V}_0$ and therefore eq. (2.29) is a symmetric problem.

2.2.6 Linearised well-posedness

We now establish well-posedness of the problem in eq. (2.29). Without loss of generality we may consider the case of homogeneous Dirichlet boundary data, so that $(v,\boldsymbol{J})$ is sought for in $\mathcal{V}_0$. By linearity the inhomogeneous case can be recovered by decomposing the solution as $(v,\boldsymbol{J}) = (v_0,\boldsymbol{J}_0) + (v_l,\boldsymbol{J}_l)$ where $(v_0,\boldsymbol{J}_0) \in \mathcal{V}_0$ are functions to be sought for and $(v_l,\boldsymbol{J}_l) \in \mathcal{V}$ are fixed liftings which satisfy the inhomogeneous Dirichlet boundary conditions in eq. (2.20).

We equip the product spaces $\mathcal{V}$ and $\mathcal{Q}$ with their Hilbertian product norms

$$\|(u, \boldsymbol{K})\|_{\mathcal{V}}^2 = \|u\|_{H^1(\Omega)^d}^2 + \sum_{j=1}^{n} \|K_j\|_{H(\mathrm{div};\Omega)}^2 , \tag{2.30}$$

$$\|(q, \boldsymbol{w})\|_{\mathcal{Q}}^2 = \|q\|_{L^2(\Omega)}^2 + \sum_{j=1}^{n} \|w_j\|_{L^2(\Omega)}^2 . \tag{2.31}$$

One can verify that a and b are bounded in these norms, with constants of boundedness dependent on the concentrations and density. The linear forms on the right-hand side of eq. (2.29) are also bounded in these norms. Well-posedness of the problem in eq. (2.29) follows from the following two standard conditions on a and b (see e.g. [18, Thm. 4.2.1]).

(i) An inf-sup condition on b: For some constant $\beta > 0$, there holds

$$\sup_{(u,\boldsymbol{K})\in\mathcal{V}_0} \frac{b((u, \boldsymbol{K}), (q, \boldsymbol{w}))}{\|(u, \boldsymbol{K})\|_{\mathcal{V}}} \geq \beta \, \|(q, \boldsymbol{w})\|_{\mathcal{Q}} \quad \forall (q, \boldsymbol{w}) \in \mathcal{Q}. \tag{2.32}$$

(ii) Coercivity of a on $\ker b$: For some constant $\alpha > 0$, there holds

$$a((u, \boldsymbol{K}), (u, \boldsymbol{K})) \geq \alpha \, \|(u, \boldsymbol{K})\|_{\mathcal{V}}^2 \quad \forall (u, \boldsymbol{K}) \in \mathcal{W}, \tag{2.33}$$

where $\mathcal{W} \subset \mathcal{V}_0$ is the kernel of b, i.e.

$$\mathcal{W} := \Big\{ (u, \boldsymbol{K}) \in \mathcal{V}_0 : b((u, \boldsymbol{K}), (q, \boldsymbol{w})) = 0 \ \forall (q, \boldsymbol{w}) \in \mathcal{Q} \Big\}. \tag{2.34}$$

Proof of the inf-sup condition in eq. (2.32). Let $\mathcal{Q}^*$ denote the dual space of $\mathcal{Q}$. Let $B : \mathcal{V}_0 \to \mathcal{Q}^*$ be the linear operator corresponding to b, i.e.

$$[B(u, \boldsymbol{K})](q, \boldsymbol{w}) = b((u, \boldsymbol{K}), (q, \boldsymbol{w})) \quad \forall ((u, \boldsymbol{K}), (q, \boldsymbol{w})) \in \mathcal{V}_0 \times \mathcal{Q}. \tag{2.35}$$

The inf-sup condition in eq. (2.32) is equivalent to the statement that B is a surjection (see e.g. [18, sect. 4.2.2]). To verify surjectivity of B, let $l \in \mathcal{Q}^*$ be given. Since $\mathcal{Q} = L_0^2(\Omega) \times L_0^2(\Omega)^n$, by the Riesz representation theorem there exists functions $l_0, l_1, \ldots, l_n \in L_0^2(\Omega)$ such that $l(q, \boldsymbol{w}) = (l_0, q)_\Omega + \sum_{i=1}^n (l_i, w_i)_\Omega$ for all $(q, \boldsymbol{w}) \in \mathcal{Q}$. Since $\mathrm{div} : H_0(\mathrm{div};\Omega) \to L_0^2(\Omega)$ is surjective [58], we can choose $K_i \in H_0(\mathrm{div};\Omega)$ with $-m_i^{-1} \nabla \cdot K_i = l_i$ for each $i \in \{1 : n\}$. Likewise, since $\mathrm{div} : H_0^1(\Omega)^d \to L_0^2(\Omega)$ is surjective [58], we can choose $u \in H_0^1(\Omega)^d$ with $\nabla \cdot u = -l_0 + \sum_{i=1}^n \nabla \cdot (\Psi K_i)$. The definitions of B and b (see eqs. (2.28d) and (2.35)) reveal that $B(u, \boldsymbol{K}) = l$. □

Proof of the coercivity condition in eq. (2.33). Using the definitions of $\mathcal{W}$ and b (see eqs. (2.28d) and (2.34)) one can check that if $(u, \boldsymbol{K}) \in \mathcal{W}$ then $\nabla \cdot K_i = 0$ for all i. The inequality in eq. (2.33) will therefore follow if we can prove that

$$a((u, \boldsymbol{K}), (u, \boldsymbol{K})) \geq \alpha \left[\|u\|^2_{H^1(\Omega)^d} + \sum_{i=1}^{n} \|K_i\|^2_{L^2(\Omega)^d} \right] \quad \forall (u, \boldsymbol{K}) \in \mathcal{V}_0. \tag{2.36}$$

We emphasise that eq. (2.36) holds for all $(u, \boldsymbol{K}) \in \mathcal{V}_0$ and not just $(u, \boldsymbol{K}) \in \mathcal{W}$. This fact will be important later on for establishing discrete well-posedness.

We now establish eq. (2.36). Recalling the definition of a in eq. (2.28c), we have

$$a((u, \boldsymbol{K}), (u, \boldsymbol{K})) = a_v(u, u) + a_o((u, \boldsymbol{K}), (u, \boldsymbol{K})). \tag{2.37}$$

A lower bound for $a_v(u, u)$ (recall eq. (2.28a)) can be obtained with standard arguments involving a Korn inequality (see e.g. [49, ch. 42]), which yield

$$a_v(u, u) \geq C_1 \delta \, \|u\|^2_{H^1(\Omega)^d} \quad \forall u \in H^1_0(\Omega)^d, \tag{2.38}$$

for some constant $C_1 > 0$ and $\delta = \min\{\eta, \zeta\}$. To bound $a_o((u, \boldsymbol{K}), (u, \boldsymbol{K}))$, let $(u, \boldsymbol{K}) \in \mathcal{V}_0$ and set $u_i = K_i/(m_i c_i) \in L^2(\Omega)$. The definition of a_o (recall eq. (2.28b)) reveals that

$$\begin{aligned} a_o((u, \boldsymbol{K}), (u, \boldsymbol{K})) &= \sum_{i,j=1}^{n} \big(\hat{\boldsymbol{M}}_{ij} K_j, K_i\big)_\Omega \\ &\quad + \gamma \left(u - \Psi \sum_{j=1}^{n} K_j, u - \Psi \sum_{i=1}^{n} K_i \right)_\Omega \\ &= \sum_{i,j=1}^{n} \big(\boldsymbol{M}_{ij} u_j, u_i\big)_\Omega \\ &\quad + \sum_{i,j=1}^{n} \gamma \big(\omega_j (u - u_j), \omega_i (u - u_i)\big)_\Omega. \end{aligned} \tag{2.39}$$

Also, since $\boldsymbol{M}_{ij}$ is symmetric with $\sum_{j=1}^{n} \boldsymbol{M}_{ij} = 0$ for all i, we have

$$\sum_{i,j=1}^{n} \big(\boldsymbol{M}_{ij} u_j, u_i\big)_\Omega = \sum_{i,j=1}^{n} \big(\boldsymbol{M}_{ij} (u - u_j), u - u_i\big)_\Omega. \tag{2.40}$$

But $\boldsymbol{M}^\gamma_{ij} = \boldsymbol{M}_{ij} + \gamma \omega_i \omega_j$ (recall eq. (2.14)) and hence eqs. (2.39) to (2.40) yield

$$a_o((u, \boldsymbol{K}), (u, \boldsymbol{K})) = \sum_{i,j=1}^{n} \big(\boldsymbol{M}^\gamma_{ij} (u - u_j), u - u_i\big)_\Omega. \tag{2.41}$$

As argued in the proof of [4, Lem. 3.3], since $\gamma > 0$ the matrix $\boldsymbol{M}_{ij}^{\gamma}$ is uniformly positive-definite on Ω. Hence, by eq. (2.41), for some constant $C_2 > 0$ there holds

$$a_o((u, \boldsymbol{K}), (u, \boldsymbol{K})) \geq C_2 \sum_{i=1}^{n} \|u - u_i\|_{L^2(\Omega)^d}^2 . \tag{2.42}$$

Note that C_2 depends on the concentrations, as discussed in [112, Rem. 4.4].

Finally, let $C_3 = 1/\max\left\{ \|m_j c_j\|_{L^\infty(\Omega)} \right\}_{j=1}^{n} > 0$. Since $u_i = K_i/(m_i c_i)$ we then have $\|u_i\|_{L^2(\Omega)^d} \geq C_3 \|K_i\|_{L^2(\Omega)^d}$ for all i. Combining eqs. (2.38) and (2.42) we find that

$$\begin{aligned}
a((u, \boldsymbol{K}), (u, \boldsymbol{K})) &\geq \min\{C_1\delta/2, C_2\} \left[\|u\|_{H^1(\Omega)^d}^2 + \|u\|_{L^2(\Omega)^d}^2 + \sum_{i=1}^{n} \|u - u_i\|_{L^2(\Omega)^d}^2 \right] && (2.43)\\
&\geq \min\{C_1\delta/2, C_2\} \left[\|u\|_{H^1(\Omega)^d}^2 + (n+1)^{-1} \sum_{i=1}^{n} \|u_i\|_{L^2(\Omega)^d}^2 \right] && (2.44)\\
&\geq \min\{C_1\delta/2, C_2\} \cdot \min\{1, C_3^2/(n+1)\} && (2.45)\\
&\quad \cdot \left[\|u\|_{H^1(\Omega)^d}^2 + \sum_{i=1}^{n} \|K_i\|_{L^2(\Omega)^d}^2 \right], && (2.46)
\end{aligned}$$

where we used the reverse triangle inequality. This establishes the bound in eq. (2.36). □

2.3 Discretisation of the Picard linearisation

We now derive quasi-optimal finite element methods for solving the Picard linearised SOSM problem eq. (2.29). Let $\mathcal{V}_h^v \subset H^1(\Omega)^d$ denote the discrete barycentric velocity space, $\mathcal{V}_h^J \subset H(\mathrm{div}; \Omega)$ the discrete species mass flux space, $\mathcal{P}_h \subset L_0^2(\Omega)$ the discrete pressure space and $\mathcal{U}_h \subset L_0^2(\Omega)$ the discrete species chemical potential space. Here $h \in (0, \infty)$ is a parameter generating these spaces (e.g. the maximum cell diameter in a mesh of Ω). We also set

$$\mathcal{V}_h := \mathcal{V}_h^v \times (\mathcal{V}_h^J)^n \subset \mathcal{V} \quad \text{and} \quad \mathcal{Q}_h := \mathcal{P}_h \times (\mathcal{U}_h)^n \subset \mathcal{Q}. \tag{2.47}$$

The subspaces with vanishing traces are denoted by $\mathcal{V}_{0h}^v := \mathcal{V}_h^v \cap H_0^1(\Omega)^d$, $\mathcal{V}_{0h}^J := \mathcal{V}_h^J \cap H_0(\mathrm{div}; \Omega)$ and $\mathcal{V}_{0h} := \mathcal{V}_{0h}^v \times (\mathcal{V}_{0h}^J)^n \subset \mathcal{V}_0$. For simplicity we take $\mathcal{V}_h^J$ and $\mathcal{U}_h$ to be independent of the species index $i \in \{1 : n\}$, i.e. for each species we use the same mass flux and chemical potential space. However, the results here can be extended to

the case where different mass flux and chemical potential spaces are used for different species.

A conforming discretisation of eq. (2.29) is obtained by employing Galerkin's method with $\mathcal{V}_{0h} \times \mathcal{Q}_h$ as the discrete subspace of $\mathcal{V}_0 \times \mathcal{Q}$. We assume homogeneous Dirichlet boundary conditions in eq. (2.20); the inhomogeneous case is addressed using discrete lifting functions. The discrete analogue of eq. (2.29) is thus: find $((v_h, \boldsymbol{J}_h), (p_h, \boldsymbol{\mu}_h)) \in \mathcal{V}_{0h} \times \mathcal{Q}_h$ such that for all $((u_h, \boldsymbol{K}_h), (q_h, \boldsymbol{w}_h)) \in \mathcal{V}_{0h} \times \mathcal{Q}_h$ there holds

$$a((v_h, \boldsymbol{J}_h), (u_h, \boldsymbol{K}_h)) + b((u_h, \boldsymbol{K}_h), (p_h, \boldsymbol{\mu}_h)) = (\rho f, u_h)_\Omega, \tag{2.48a}$$

$$b((v_h, \boldsymbol{J}_h), (q_h, \boldsymbol{w}_h)) = -\sum_{i=1}^{n} (w_{h,i}, r_i)_\Omega. \tag{2.48b}$$

Since eq. (2.29) is a saddle-point problem, well-posedness at the continuous level is not automatically inherited at the discrete level. The following theorem (see e.g. [18, ch. 5]) outlines conditions that ensure discrete well-posedness and quasi-optimality.

Theorem 2.3.1 (Discrete well-posedness)**.** *Assume that there exists constants $\tilde{\beta}, \tilde{\alpha} > 0$ independent of h such that we have (i) the discrete inf-sup condition*

$$\sup_{(u_h, \boldsymbol{K}_h) \in \mathcal{V}_{0h}} \frac{b((u_h, \boldsymbol{K}_h), (q_h, \boldsymbol{w}_h))}{\|(u_h, \boldsymbol{K}_h)\|_{\mathcal{V}}} \geq \tilde{\beta} \, \|(q_h, \boldsymbol{w}_h)\|_{\mathcal{Q}} \quad \forall (q_h, \boldsymbol{w}_h) \in \mathcal{Q}_h, \tag{2.49}$$

and (ii) on the discrete kernel of b

$$\mathcal{W}_h := \big\{ (u_h, \boldsymbol{K}_h) \in \mathcal{V}_{0h} : b((u_h, \boldsymbol{K}_h), (q_h, \boldsymbol{w}_h)) = 0 \ \forall (q_h, \boldsymbol{w}_h) \in \mathcal{Q}_h \big\}, \tag{2.50}$$

there holds the coercivity condition

$$a((u_h, \boldsymbol{K}_h), (u_h, \boldsymbol{K}_h)) \geq \tilde{\alpha} \, \|(u_h, \boldsymbol{K}_h)\|_{\mathcal{V}}^2 \quad \forall (u_h, \boldsymbol{K}_h) \in \mathcal{W}_h. \tag{2.51}$$

Then the discrete problem in eq. (2.48) is well-posed. Also, let $((v, \boldsymbol{J}), (p, \boldsymbol{\mu})) \in \mathcal{V}_0 \times \mathcal{Q}$ denote the solution of eq. (2.29) and $((v_h, \boldsymbol{J}_h), (p_h, \boldsymbol{\mu}_h)) \in \mathcal{V}_{0h} \times \mathcal{Q}_h$ the solution of eq. (2.48). Then we have the quasi-optimal a priori error estimate

$$\|(v - v_h, \boldsymbol{J} - \boldsymbol{J}_h)\|_{\mathcal{V}} + \|(p - p_h, \boldsymbol{\mu} - \boldsymbol{\mu}_h)\|_{\mathcal{Q}} \leq C \cdot \mathcal{E}_h, \tag{2.52}$$

with $C > 0$ independent of h, and $\mathcal{E}_h$ the best approximation error, i.e.

$$\mathcal{E}_h := \inf_{(u_h, \boldsymbol{K}_h) \in \mathcal{V}_{0h}} \|(v - u_h, \boldsymbol{J} - \boldsymbol{K}_h)\|_{\mathcal{V}} + \inf_{(q_h, \boldsymbol{w}_h) \in \mathcal{Q}_h} \|(p - q_h, \boldsymbol{\mu} - \boldsymbol{w}_h)\|_{\mathcal{Q}}. \tag{2.53}$$

The next two lemmas give conditions which ensure that eqs. (2.49) and (2.51) hold.

Lemma 2.3.2 (Inf-sup stability)**.** *Condition eq.* (2.49) *will hold provided that, for some constants* $\beta_1, \beta_2 > 0$ *independent of* h, $(\mathcal{V}_h^v, \mathcal{P}_h)$ *and* $(\mathcal{V}_h^J, \mathcal{U}_h)$ *satisfy inf-sup conditions*

$$\sup_{u_h \in \mathcal{V}_{0h}^v} \frac{(\nabla \cdot u_h, q_h)_\Omega}{\|u_h\|_{H^1(\Omega)^d}} \geq \beta_1 \|q_h\|_{L^2(\Omega)} \quad \forall q_h \in \mathcal{P}_h, \tag{2.54a}$$

$$\sup_{K_h \in \mathcal{V}_{0h}^J} \frac{(\nabla \cdot K_h, w_h)_\Omega}{\|K_h\|_{H(\mathrm{div};\Omega)}} \geq \beta_2 \|w_h\|_{L^2(\Omega)} \quad \forall w_h \in \mathcal{U}_h. \tag{2.54b}$$

Proof. The proof is analogous to that of the continuous inf-sup condition eq. (2.32), but with the need to use β_1 and β_2 to obtain an h-independent lower bound for $\tilde{\beta}$. □

Lemma 2.3.3 (Discrete coercivity)**.** *Condition eq.* (2.51) *will hold provided there exists a constant* $c > 0$ *independent of* h *such that*

$$\|K_h\|_{L^2(\Omega)^d} \geq c \|K_h\|_{H(\mathrm{div};\Omega)} \tag{2.55}$$

for all $K_h \in \mathcal{V}_{0h}^J$ *satisfying* $(\nabla \cdot K_h, w_h)_\Omega = 0 \ \forall w_h \in \mathcal{U}_h$. *Note that the condition in eq.* (2.55) *holds with* $c = 1$ *for divergence-free pairs, i.e. pairs such that if* $K_h \in \mathcal{V}_{0h}^J$ *satisfies* $(\nabla \cdot K_h, w_h)_\Omega = 0 \ \forall w_h \in \mathcal{U}_h$ *then* $\nabla \cdot K_h = 0$.

Proof. Using the definition of $\mathcal{W}_h$ and b (see eqs. (2.28d) and (2.50)) one verifies that for all $(u_h, \boldsymbol{K}_h) \in \mathcal{W}_h$, there holds $(\nabla \cdot K_{h,i}, w_h)_\Omega = 0 \ \forall w_h \in \mathcal{U}_h \ \forall i$. The bounds in eq. (2.36) and eq. (2.55) then immediately yield that eq. (2.51) holds with $\tilde{\alpha} = \alpha \cdot \min\{1, c^2\}$. □

Many standard finite element spaces satisfy the hypotheses of lemmas 2.3.2 and 2.3.3. The barycentric velocity and pressure pair $(\mathcal{V}_h^v, \mathcal{P}_h)$ needs to satisfy the inf-sup condition in eq. (2.54a), which can be accomplished by employing any conforming inf-sup stable Stokes pair. Examples include the Taylor–Hood [109] or Scott–Vogelius [102] pairs. The mass flux and chemical potential pair $(\mathcal{V}_h^J, \mathcal{U}_h)$ must satisfy the conditions in eqs. (2.54b) and (2.55), which can be accomplished by employing, for example, $\mathbb{BDM}_k$–$\mathbb{DG}_{k-1}$ [22, 85] or $\mathbb{RT}_k$–$\mathbb{DG}_{k-1}$ [96] pairs (these pairs are divergence-free). Optimal, high-order spatial convergence rates can be achieved when using the Taylor–Hood pair with degree $k \geq 2$ [17] or Scott–Vogelius on suitable meshes (e.g. $k \geq d$ on barycentrically-refined meshes [126]) for $(\mathcal{V}_h^v, \mathcal{P}_h)$, and $\mathbb{BDM}_k$–$\mathbb{DG}_{k-1}$ or $\mathbb{RT}_k$–$\mathbb{DG}_{k-1}$

pairs for $(\mathcal{V}_h^J, \mathcal{U}_h)$. For sufficiently smooth solutions, the bound in eq. (2.52) then predicts an optimal rate of

$$\|(v - v_h, \boldsymbol{J} - \boldsymbol{J}_h)\|_{\mathcal{V}} + \|(p - p_h, \boldsymbol{\mu} - \boldsymbol{\mu}_h)\|_{\mathcal{Q}} = \mathcal{O}(h^k), \tag{2.56}$$

where h is the maximum cell diameter of a shape-regular triangulation of Ω. We emphasise, however, that we have only proven these spatial rates of convergence for the Picard linearisation of the SOSM problem.

In single-component incompressible flow it can be advantageous to use divergence-free Stokes elements, as these yield velocity approximations that are independent of the pressure (i.e. *pressure-robust*) [66]. For this reason Scott–Vogelius may be preferable to Taylor–Hood in the single-component incompressible setting, as the former is divergence-free whereas the latter is not. However, in the multicomponent setting there does not seem to be an analogue of the pressure-robustness phenomenon, since the mass-average constraint couples the barycentric velocity to the density and mass fluxes, which in turn are coupled to the pressure through the OSM equations. Hence, we do not expect a pressure-robust velocity approximation even with divergence-free Stokes elements. For this reason we prefer to use Taylor–Hood in our simulations, as it has no apparent disadvantage relative to Scott–Vogelius but does not require special meshes. It is less clear whether to use $\mathbb{BDM}_k$ or $\mathbb{RT}_k$ for the mass fluxes, since both lead to the same convergence rates in eq. (2.56). Note that the $\mathbb{BDM}_k$ finite element space includes all polynomials of degree k whereas the $\mathbb{RT}_k$ space is a strict subspace of these [18]. Hence, for a given mesh and polynomial degree k, a $\mathbb{BDM}_k$ discretisation may be slightly more accurate but also slightly more expensive than that of $\mathbb{RT}_k$. In practice the value of this (fairly minor) trade-off will be problem- and user-dependent.

2.4 Nonlinear monolithic discretisation and Newton's method

When combined with fixed point iteration, the Picard linearisation can be used to solve the nonlinear SOSM problem. However, for challenging problems this iteration often does not converge to a root, or does so at a prohibitively slow rate. A more robust approach is to use Newton's method [35]; this requires a monolithic discretisation of the nonlinear SOSM problem, which we now outline.

In the monolithic setting, the Gauß–Seidel staggering employed in the Picard linearisation is no longer possible. We still seek $((v_h, \boldsymbol{J}_h), (p_h, \boldsymbol{\mu}_h))$ in $\mathcal{V}_h \times \mathcal{Q}_h$ (recall

eq. (2.47)), but we must introduce additional unknowns to discretise the constitutive law in eq. (2.7). It is natural to seek the mole fractions in a finite element space $\mathcal{X}_h \subset L^2(\Omega)$ and enforce the L^2-projection of eq. (2.12a) into $\mathcal{X}_h$. Hence the discrete analogue of eq. (2.12a) is to find $\boldsymbol{x}_h \in (\mathcal{X}_h)^n$ such that for all $\boldsymbol{y}_h \in (\mathcal{X}_h)^n$,

$$(\mu_{h,i} - \mu_i^{\mathrm{aux}}, y_{h,i})_\Omega = (\overline{G_i}(T, p_h - p^{\mathrm{aux}}, x_{h,1}, \ldots, x_{h,n}), y_{h,i})_\Omega \quad \forall i \in \{1:n\}. \tag{2.57}$$

As discussed in section 2.2.2, the constants $\mu_1^{\mathrm{aux}}, \ldots, \mu_n^{\mathrm{aux}}, p^{\mathrm{aux}} \in \mathbb{R}$ reflect the indeterminacy of the pressure and chemical potentials up to additive constants. To avoid solving for these constants we use the following trick. Recall that in section 2.3 we employed discrete chemical potential and pressure spaces $\mathcal{P}_h, \mathcal{U}_h \subset L_0^2(\Omega)$. Using $L_0^2(\Omega)$ instead of $L^2(\Omega)$ is convenient for the analysis, but at an implementation level it is easier to work with the analogues of these spaces containing all constant functions,

$$\mathcal{P}_h' := \mathcal{P}_h \oplus \mathrm{span}\{1\},\ \mathcal{U}_h' := \mathcal{U}_h \oplus \mathrm{span}\{1\} \text{ and } \mathcal{Q}_h' := \mathcal{P}_h' \times (\mathcal{U}_h')^n. \tag{2.58}$$

If we seek $(p_h, \boldsymbol{\mu}_h) \in \mathcal{Q}_h'$ then there is no need for $\mu_1^{\mathrm{aux}}, \ldots, \mu_n^{\mathrm{aux}}, p^{\mathrm{aux}}$ to appear in eq. (2.57) as they can be absorbed into $(p_h, \boldsymbol{\mu}_h)$. This is a simple trick, but using $\mathcal{Q}_h'$ instead of $\mathcal{Q}_h$ requires the introduction of *density consistency* terms, as discussed further below.

Satisfaction of eq. (2.57) does not ensure that the discrete mole fractions exactly sum to unity, i.e. $\sum_{j=1}^n x_{h,j} = 1$ will only hold approximately. One can instead solve for the $n-1$ discrete mole fractions $x_{h,2}, \ldots, x_{h,n}$ and express $x_{h,1} = 1 - \sum_{j=2}^n x_{h,j}$. However, this breaks permutational symmetry of the species and it does not ensure that all n equations in eq. (2.12a) hold in an approximate sense (e.g. as in eq. (2.57)). We therefore prefer to enforce eq. (2.57) and in the computations we verify that $\sum_{j=1}^n x_{h,j} = 1$ holds to a satisfactory extent. Of course, we can still introduce normalised discrete mole fractions $x_{h,i}^{\mathrm{nm}} := x_{h,i} / \sum_{j=1}^n x_{h,j}$. Using eq. (2.12b) and since $c_i = c_T x_i$, a discrete expression for the concentrations (as a function of $p_h, \boldsymbol{x}_h$ only) is

$$c_{h,i} := \left[\sum_{j=1}^n x_{h,j}^{\mathrm{nm}} \overline{V_j}(T, p_h, x_{h,1}^{\mathrm{nm}}, \ldots, x_{h,n}^{\mathrm{nm}}) \right]^{-1} x_{h,i}^{\mathrm{nm}} \quad \forall i \in \{1:n\}. \tag{2.59}$$

Analogously to eq. (2.28d) our discretisation will contain terms involving $\nabla \cdot (\Psi_h K_{h,i})$ where $K_{h,i} \in \mathcal{V}_{0h}^J \subset H_0(\mathrm{div}; \Omega)$ and Ψ_h is a discrete density reciprocal. To ensure that $\Psi_h K_{h,i}$ admits a weak divergence we introduce a finite element space $\mathcal{R}_h \subset W^{1,\infty}(\Omega)$ and seek $\Psi_h \in \mathcal{R}_h$ (cf. assumption 2.2.2). The regularity $\Psi_h \in W^{1,\infty}(\Omega)$ implies that $\nabla \cdot (\Psi_h K_{h,i}) \in L^2(\Omega)$. The equation used to determine Ψ_h is given below in eq. (2.65d).

Recall from section 2.2.2 that constraints must be introduced to fix the degrees of freedom $\mu_1^{\text{aux}}, \ldots, \mu_n^{\text{aux}}, p^{\text{aux}}$, which were absorbed into the enlarged space $\mathcal{P}_h' \times (\mathcal{U}_h')^n$. These $n+1$ degrees of freedom require $n+1$ constraints, denoted very generally by $F(p_h, \boldsymbol{\mu}_h, \boldsymbol{x}_h) = 0$ where $F : \mathcal{P}_h' \times (\mathcal{U}_h')^n \times (\mathcal{X}_h)^n \to \mathbb{R}^{n+1}$ is a user-chosen function. For example, integral constraints on the concentrations (cf. eq. (2.10)) can be imposed using integrals of $c_{h,i}$ in eq. (2.59). The Gibbs–Duhem relation implies that only n constraints are required; we need $n+1$ constraints here since we are solving for all n mole fractions despite only $n-1$ of them being independent. Hence, one of our constraints is not physical. Instead, it reflects our desire for the discrete mole fractions to sum to unity. In particular, satisfaction of eq. (2.57) does not ensure that $\sum_{j=1}^n x_{h,j} = 1$ holds exactly in Ω, but we can still enforce that this equality holds on average over Ω, i.e. we consider

$$\int_\Omega \left(1 - \sum_{j=1}^n x_{h,j}\right) \mathrm{d}\Omega = 0. \tag{2.60}$$

In this thesis we shall take F to impose eq. (2.60) along with n physical constraints.

In section 2.3 we assumed homogeneous Dirichlet boundary data. We do not make this assumption here, as the inhomogeneous case has non-trivial consequences in our monolithic discretisation, discussed further below. The discrete solution $(v_h, \boldsymbol{J}_h) \in \mathcal{V}_h$ generally cannot satisfy the boundary conditions eq. (2.20) exactly. Instead, we consider

$$v_h = v_{h,D} \quad \text{and} \quad J_{h,i} \cdot \hat{n}_\Gamma = J_{h,D,i} \cdot \hat{n}_\Gamma \quad \text{on } \partial\Omega \quad \forall i \in \{1 : n\}, \tag{2.61}$$

where $(v_{h,D}, \boldsymbol{J}_{h,D}) \in \mathcal{V}_h$ are fixed discrete lifting functions, which, by a method such as interpolation, are chosen to approximately satisfy the boundary conditions in eq. (2.20), and satisfy the compatibility conditions $m_i^{-1} \int_{\partial\Omega} J_{h,D,i} \cdot \hat{n}_\Gamma \, \mathrm{d}\Gamma = \int_\Omega r_i \, \mathrm{d}\Omega$.

Finally, to state the full monolithic discrete SOSM problem, we introduce a discrete transport matrix $\boldsymbol{M}_{ij}^{[\boldsymbol{c}_h]}$ which is computed using the formula eq. (2.6) but with the discrete concentrations $\boldsymbol{c}_h$ (recall eq. (2.59)). Since $\boldsymbol{c}_h$ is a function of $p_h, \boldsymbol{x}_h$, so too is $\boldsymbol{M}_{ij}^{[\boldsymbol{c}_h]}$. We consider discrete analogues of eqs. (2.28b) to (2.28d) which employ

$\boldsymbol{c}_h$ and Ψ_h:

$$\begin{cases} a_o^{[\boldsymbol{c}_h,\Psi_h]} : \mathcal{V}_h \times \mathcal{V}_{0h} \to \mathbb{R}, \\ a_o^{[\boldsymbol{c}_h,\Psi_h]}((v_h,\boldsymbol{J}_h),(u_h,\boldsymbol{K}_h)) := \gamma\left(v_h - \Psi_h \sum_{j=1}^n J_{h,j}, u_h - \Psi_h \sum_{i=1}^n K_{h,i}\right)_\Omega \\ \qquad\qquad + \sum_{i,j=1}^n \left(\hat{\boldsymbol{M}}_{ij}^{[\boldsymbol{c}_h]} J_{h,j}, K_{h,i}\right)_\Omega, \\ \text{where } \hat{\boldsymbol{M}}_{ij}^{[\boldsymbol{c}_h]} := \boldsymbol{M}_{ij}^{[\boldsymbol{c}_h]}/(m_i m_j c_{h,i} c_{h,j}), \end{cases} \tag{2.62}$$

$$\begin{cases} a^{[\boldsymbol{c}_h,\Psi_h]} : \mathcal{V}_h \times \mathcal{V}_{0h} \to \mathbb{R}, \\ a^{[\boldsymbol{c}_h,\Psi_h]}((v_h,\boldsymbol{J}_h),(u_h,\boldsymbol{K}_h)) := a_v(v_h,u_h) + a_o^{[\boldsymbol{c}_h,\Psi_h]}((v_h,\boldsymbol{J}_h),(u_h,\boldsymbol{K}_h)), \\ \text{where } a_v \text{ is defined in eq. (2.28a)}, \end{cases} \tag{2.63}$$

$$\begin{cases} b^{[\Psi_h]} : \mathcal{V}_h \times \mathcal{Q}_h' \to \mathbb{R}, \\ b^{[\Psi_h]}((u_h,\boldsymbol{K}_h),(p_h,\boldsymbol{\mu}_h)) := -(p_h, \nabla\cdot u_h)_\Omega + \sum_{i=1}^n (p_h, \nabla\cdot(\Psi_h K_{h,i}))_\Omega \\ \qquad\qquad - \sum_{i=1}^n (m_i^{-1}\mu_{h,i}, \nabla\cdot K_{h,i})_\Omega. \end{cases} \tag{2.64}$$

The monolithic problem is: find $((v_h,\boldsymbol{J}_h),(p_h,\boldsymbol{\mu}_h),\boldsymbol{x}_h,\Psi_h) \in \mathcal{V}_h \times \mathcal{Q}_h' \times (\mathcal{X}_h)^n \times \mathcal{R}_h$ such that $(v_h,\boldsymbol{J}_h)$ satisfies the boundary conditions in eq. (2.61) and for all test functions $((u_h,\boldsymbol{K}_h),(q_h,\boldsymbol{w}_h),\boldsymbol{y}_h,r_h) \in \mathcal{V}_{0h} \times \mathcal{Q}_h' \times (\mathcal{X}_h)^n \times \mathcal{R}_h$ there holds

$$a^{[\boldsymbol{c}_h,\Psi_h]}((v_h,\boldsymbol{J}_h),(u_h,\boldsymbol{K}_h)) + b^{[\Psi_h]}((u_h,\boldsymbol{K}_h),(p_h,\boldsymbol{\mu}_h)) = \sum_{i=1}^n (m_i c_{h,i} f, u_h)_\Omega, \tag{2.65a}$$

$$b^{[\Psi_h]}((v_h,\boldsymbol{J}_h),(q_h,\boldsymbol{w}_h)) + b_{dc}^{[\Psi_h]}((v_h,\boldsymbol{J}_h),(q_h,\boldsymbol{w}_h)) = -\sum_{i=1}^n (w_{h,i}, r_i)_\Omega, \tag{2.65b}$$

$$(\mu_{h,i} - \overline{G_i}(T, p_h, x_{h,1}, \ldots, x_{h,n}), y_{h,i})_\Omega = 0 \quad \forall i \in \{1:n\}, \tag{2.65c}$$

$$(1/\Psi_h - \sum_{i=1}^n m_i c_{h,i}, r_h)_\Omega = 0, \tag{2.65d}$$

$$F(p_h, \boldsymbol{\mu}_h, \boldsymbol{x}_h) = 0. \tag{2.65e}$$

Here $b_{dc}^{[\Psi_h]}((v_h,\boldsymbol{J}_h),(q_h,\boldsymbol{w}_h))$ are *density consistency terms*, described below. As in section 2.3, for $\mathcal{V}_h \times \mathcal{Q}_h'$ we employ spaces satisfying lemmas 2.3.2 and 2.3.3. In practice this leads to spaces of degree $k \geq 1$ being employed for $\mathcal{V}_h$ and $k-1$ for $\mathcal{Q}_h'$. In this case we also employ degree $k-1$ spaces for $\mathcal{X}_h$ and $\mathcal{R}_h$. This is because $\boldsymbol{x}_h, \Psi_h$ are related to $(p_h,\boldsymbol{\mu}_h) \in \mathcal{Q}_h'$ through L^2-projections of algebraic equations; we do not expect to gain approximation power by using higher degree spaces for these unknowns.

To motivate the density consistency terms, recall that we enriched the discrete pressure and chemical potential spaces to contain all constant functions (see eq. (2.58)).

This may have seemed harmless, since at the continuous level the SOSM equations eq. (2.19) are invariant under shifts in the pressure and chemical potential by additive constants. One can also verify that, at the discrete level, shifting $(p_h, \boldsymbol{\mu}_h)$ by constants leaves eq. (2.65a) unchanged (integrate by parts and observe $(u_h, \boldsymbol{K}_h)$ have vanishing normal components on $\partial\Omega$). However, we must also ensure that using $\mathcal{Q}_h'$ instead of $\mathcal{Q}_h$ does not affect eq. (2.65b), i.e. that shifting $(q_h, \boldsymbol{w}_h)$ by constants leaves eq. (2.65b) unchanged. Since $(v_h, \boldsymbol{J}_h)$ do not have vanishing normal components on $\partial\Omega$ and instead satisfy the boundary conditions in eq. (2.61), this invariance property will hold provided we take

$$b_{dc}^{[\Psi_h]}((v_h, \boldsymbol{J}_h), (q_h, \boldsymbol{w}_h)) := \int_{\partial\Omega} q_h \left(v_h - \sum_{i=1}^{n} \Psi_h J_{h,i} \right) \cdot \hat{n}_\Gamma \, \mathrm{d}\Gamma \,. \tag{2.66}$$

We call these density consistency terms, since in general $v_h \cdot \hat{n}_\Gamma = \sum_{i=1}^n \Psi_h J_{h,i} \cdot \hat{n}_\Gamma$ holds only approximately on $\partial\Omega$, whereas at the continuous level $v \cdot \hat{n}_\Gamma = \sum_{i=1}^n \Psi J_i \cdot \hat{n}_\Gamma$ holds exactly due to the mass-average constraint eq. (2.2). We find empirically in section 2.5.1 that these terms are crucial for ensuring that Newton's method converges. We prefer to use a discrete density reciprocal Ψ_h instead of a discrete density ρ_h, as this enables the terms in eq. (2.66) to be integrated exactly with quadrature rules of a sufficiently high degree. However, in our experience discretizing ρ instead of Ψ has no tangible impact on the performance of our numerical schemes; both choices seem viable in practice.

Let $D = \dim(\mathcal{V}_{0h} \times \mathcal{Q}_h' \times (\mathcal{X}_h)^n \times \mathcal{R}_h)$. Once a basis has been chosen, the discrete problem in eq. (2.65) constitutes $D + n + 1$ equations in D unknowns. However, $n+1$ of the equations obtained from eq. (2.65b) can be eliminated, since the compatibility conditions on $J_{h,D,i}$ and our construction of $b_{dc}^{[\Psi_h]}$ ensures that eq. (2.65b) holds automatically when $(q_h, \boldsymbol{w}_h)$ are constants. We solve the resulting system of D equations in D unknowns using Newton's method. The constraints in eq. (2.65e) will typically (e.g. when imposing integral constraints) lead to dense rows in the Jacobian at each Newton iteration; these could be undesirable when using direct linear solvers. We avoid these dense rows by employing an auxiliary sparse Jacobian that is obtained by replacing the constraints in eq. (2.65e) with $n + 1$ auxiliary constraints that fix the values of $p_h, \boldsymbol{\mu}_h$ at a mesh node. The true Jacobian is then a rank $n + 1$ update of the auxiliary Jacobian and we compute the action of its inverse using the Woodbury formula [62].

2.5 Numerical examples

In this section we test our methods. The experiments were implemented using Firedrake [63] and PETSc [9, 33]. We solved the linear systems using the LU solver MUMPS [1]. Code is available at https://bitbucket.org/abaierr/multicomponent_code and software versions are archived on Zenodo [5].

2.5.1 Manufactured solution

To study the spatial errors of the discretisation, we consider a manufactured solution with $n = 2$ species. We conduct tests in two and three spatial dimensions on the domain $\Omega = (0,1)^d$. The thermodynamic constitutive law is taken to be that of an ideal gaseous mixture (recall eq. (1.21)) [60, 61]; hence in eq. (2.12) we employ $\overline{G_i}(T,p,x_1,x_2) = RT\ln(x_i p)$ and $\overline{V_i}(T,p,x_1,x_2) = RT/p$.

We employ the manufactured solution introduced in [4, sect. 4.4], which requires that $RT = 1$. If the diffusion coefficients are parametrised by $\mathscr{D}_{ij} = D_i D_j$ for $D_j > 0$, and $g : \mathbb{R}^d \to \mathbb{R}$ is a smooth function, this solution is given by $c_i = \exp(g/D_i)$ and $v_i = D_i \nabla g$. Specification of c_i and v_i implicitly defines all other unknowns. We use $D_1 = 1/2, D_2 = 2$. For $d = 2$ we set $g(x,y) = \sin(\pi x)\sin(\pi y)$ and for $d = 3$ we set $g(x,y,z) = \sin(\pi x)\sin(\pi y)\sin(\pi z)$. For the molar masses we use $m_1 = m_2 = 1$, for the viscosities $\eta = \zeta = 0.1$ and for the augmentation parameter $\gamma = 10$.

We conduct tests for the Picard linearised problem eq. (2.48) and the nonlinear problem eq. (2.65). In the Picard linearised setting, we use the concentrations (and quantities ρ, Ψ and $\hat{\boldsymbol{M}}_{ij}^{\gamma}$) of the exact solution. We employ a uniform structured mesh consisting of triangles when $d = 2$ and hexahedra when $d = 3$. For the barycentric velocity and pressure we use the degree $k = 4$ generalised Taylor–Hood pair [49, sect. 54.4.1]. For the mass flux and chemical potentials we use the $\mathbb{RT}_k$–$\mathbb{DG}_{k-1}$ pair [96] when $d = 2$ and its hexahedral analogue [84] when $d = 3$. In the nonlinear setting, we discretise the mole fractions (resp. density reciprocal) using discontinuous (resp. continuous) degree $k - 1 = 3$ polynomial spaces. As constraints in eq. (2.65e) we impose $\int_\Omega c_{h,i}\,\mathrm{d}\Omega = \int_\Omega c_i\,\mathrm{d}\Omega \ \ \forall i$ and eq. (2.60). We use Newton's method with an absolute tolerance on the residual of 10^{-10} in the Euclidean norm. The initial guess we supply to Newton's method is the L^2-projection of the exact solution, since our purpose here is to study the spatial errors of the discretisation, not the root-finding ability of Newton's method from a poor initial guess. Depending on the mesh size this led to Newton's method terminating in 1 to 3 iterations.

Table 2.1: Computed spatial errors and associated rates for the Picard linearised test case in section 2.5.1.

h	E_v (rate)	$E_{\nabla v}$ (rate)	E_p (rate)	$E_{\boldsymbol{J}}$ (rate)	$E_{\boldsymbol{\mu}}$ (rate)	E_{MA} (rate)
Spatial dimension $d = 2$						
2^{-3}	1.8e-05	1.9e-3	4.4e-4	5.0e-4	1.0e-4	1.5e-4
2^{-4}	5.2e-07 (5.1)	1.1e-4 (4.2)	2.6e-5 (4.1)	3.0e-5 (4.1)	5.5e-6 (4.2)	9.1e-6 (4.1)
2^{-5}	1.6e-08 (5.0)	6.3e-6 (4.1)	1.6e-6 (4.0)	1.8e-6 (4.0)	3.2e-7 (4.1)	5.6e-7 (4.0)
2^{-6}	5.0e-10 (5.0)	3.9e-7 (4.0)	9.8e-8 (4.0)	1.1e-7 (4.0)	1.9e-8 (4.0)	3.5e-8 (4.0)
2^{-7}	1.6e-11 (4.9)	2.6e-8 (3.9)	1.0e-8 (3.3)	7.1e-9 (4.0)	5.9e-9 (1.7)	2.2e-9 (4.0)
Spatial dimension $d = 3$						
2^{-1}	4.6e-03	1.1e-1	3.6e-2	5.7e-2	9.8e-3	1.8e-2
2^{-2}	1.1e-04 (5.4)	5.2e-3 (4.3)	1.7e-3 (4.4)	2.4e-3 (4.6)	3.4e-4 (4.9)	9.2e-4 (4.3)
2^{-3}	3.3e-06 (5.0)	3.9e-4 (3.7)	1.4e-4 (3.6)	2.1e-4 (3.5)	1.7e-5 (4.4)	6.1e-5 (3.9)
2^{-4}	9.5e-08 (5.1)	2.0e-5 (4.3)	7.9e-6 (4.1)	1.3e-5 (4.1)	6.2e-7 (4.7)	3.7e-6 (4.0)

We uniformly refine the mesh starting from an initial mesh size of $h = 2^{-3}$ in two dimensions and $h = 2^{-1}$ in three dimensions. We measure the following errors:

$$E_v := \|v - v_h\|_{L^2(\Omega)^d}, \quad E_{\nabla v} := \|\nabla v - \nabla v_h\|_{L^2(\Omega)^{d\times d}}, \quad E_p := \|p - p_h\|_{L^2(\Omega)},$$
$$E_{\boldsymbol{J}} := \sqrt{\sum_{i=1}^{n} \|J_i - J_{h,i}\|^2_{L^2(\Omega)^d}}, \quad E_{\boldsymbol{\mu}} := \sqrt{\sum_{i=1}^{n} \|\mu_i - \mu_{h,i}\|^2_{L^2(\Omega)}}.$$

We also measure the error in the mass-average constraint (recall eq. (2.2)) by means of $E_{\mathrm{MA}} := \|v_h - \Psi \sum_{i=1}^n J_{h,i}\|_{L^2(\Omega)^d}$ for the Picard linearised problem and $E_{\mathrm{MA}} := \|v_h - \Psi_h \sum_{i=1}^n J_{h,i}\|_{L^2(\Omega)^d}$ for the nonlinear problem. For the nonlinear problem we also measure the mole fraction error $E_{\boldsymbol{x}} := \sqrt{\sum_{i=1}^n \|x_i - x_{h,i}\|^2_{L^2(\Omega)}}$.

The numerical results for the Picard linearised problem are shown in table 2.1. Our chosen finite element spaces satisfy the hypotheses of lemmas 2.3.2 and 2.3.3, and the quasi-optimal error bound in eq. (2.52) therefore predicts that $E_v, E_{\nabla v}, E_p, E_{\boldsymbol{J}}, E_{\boldsymbol{\mu}}$ and E_{MA} go to zero as $\mathcal{O}(h^k) = \mathcal{O}(h^4)$. This theoretical prediction is consistent with the empirical convergence rates shown in table 2.1. When $d = 2$ and $h = 2^{-7}$ the rates for E_p and $E_{\boldsymbol{\mu}}$ appear to decay below $\mathcal{O}(h^4)$, but we believe this is due to rounding error and solver tolerances. Moreover, it appears that E_v converges as $\mathcal{O}(h^{k+1}) = \mathcal{O}(h^5)$, and we hypothesise that it may be possible to prove this rigorously using an Aubin–Nitsche technique.

The results for the nonlinear problem are shown in table 2.2. When $d = 2$ it appears that $E_v, E_{\nabla v}, E_p, E_{\boldsymbol{J}}, E_{\boldsymbol{\mu}}$ and E_{MA} converge suboptimally by a factor of h, i.e. they converge as $\mathcal{O}(h^{k-1}) = \mathcal{O}(h^3)$ ($\mathcal{O}(h^4)$ for E_v). When $d = 3$ these quantities

Table 2.2: Computed spatial errors and associated rates for the nonlinear test case in section 2.5.1.

h	E_v (rate)	$E_{\nabla v}$ (rate)	E_p (rate)	$E_{\boldsymbol{J}}$ (rate)	$E_{\boldsymbol{\mu}}$ (rate)	E_{MA} (rate)	$E_{\boldsymbol{x}}$ (rate)
Spatial dimension $d = 2$							
2^{-3}	2.0e-05	2.0e-3	4.6e-4	5.3e-4	1.0e-4	2.1e-4	9.4e-06
2^{-4}	6.5e-07 (5.0)	1.3e-4 (4.0)	3.0e-5 (3.9)	3.5e-5 (3.9)	8.3e-6 (3.6)	1.6e-5 (3.8)	5.7e-07 (4.0)
2^{-5}	2.7e-08 (4.6)	1.1e-5 (3.5)	2.5e-6 (3.6)	3.0e-6 (3.5)	9.2e-7 (3.2)	1.5e-6 (3.4)	3.6e-08 (4.0)
2^{-6}	1.4e-09 (4.3)	1.2e-6 (3.2)	2.6e-7 (3.3)	3.3e-7 (3.2)	1.1e-7 (3.0)	1.7e-7 (3.2)	2.2e-09 (4.0)
2^{-7}	8.2e-11 (4.1)	1.5e-7 (3.1)	3.1e-8 (3.1)	3.9e-8 (3.1)	1.4e-8 (3.0)	2.0e-8 (3.0)	1.4e-10 (4.0)
Spatial dimension $d = 3$							
2^{-1}	5.9e-03	8.4e-2	2.5e-2	6.0e-2	7.1e-3	1.4e-2	1.3e-03
2^{-2}	1.4e-04 (5.4)	6.1e-3 (3.8)	1.7e-3 (3.9)	2.5e-3 (4.6)	3.3e-4 (4.5)	1.2e-3 (3.6)	6.8e-05 (4.2)
2^{-3}	3.7e-06 (5.3)	4.1e-4 (3.9)	1.4e-4 (3.6)	2.1e-4 (3.6)	1.7e-5 (4.3)	7.5e-5 (4.0)	3.5e-06 (4.3)
2^{-4}	1.1e-07 (5.1)	2.0e-5 (4.3)	7.9e-6 (4.1)	1.3e-5 (4.1)	6.3e-7 (4.7)	4.7e-6 (4.0)	2.1e-07 (4.0)

appear to instead converge as $\mathcal{O}(h^4)$ ($\mathcal{O}(h^5)$ for E_v), but we anticipate that if the mesh were to be refined further, they would also begin to converge suboptimally by a factor of h. Interestingly, the mole fraction error $E_{\boldsymbol{x}}$ seems to converge optimally as $\mathcal{O}(h^4)$ for $d = 2, 3$ despite the other quantities converging suboptimally when $d = 2$.

We hypothesise that the suboptimal rates in $E_v, E_{\nabla v}, E_p, E_{\boldsymbol{J}}, E_{\boldsymbol{\mu}}$ and E_{MA}, which only appear when solving the nonlinear problem, are due to the presence of $\nabla\Psi_h$ in our discretisation. More precisely, the form $b^{[\Psi_h]}$ in eq. (2.64) contains the terms

$$\big(p_h, \nabla\cdot(\Psi_h K_{h,i})\big)_\Omega = \big(p_h, (\nabla\Psi_h)\cdot K_{h,i}\big)_\Omega + \big(p_h, \Psi_h \nabla\cdot K_{h,i}\big)_\Omega. \tag{2.67}$$

The culprit seems to be the term $\big(p_h, (\nabla\Psi_h)\cdot K_{h,i}\big)_\Omega$. In additional experiments (not shown here), we find that if $\nabla\Psi_h$ is replaced by $\nabla\Psi$ in this term, we recover optimal rates of convergence for the nonlinear problem. Of course, this is useless in practice; we only know what $\nabla\Psi$ is here because we are using a manufactured solution. However, this does provide a heuristic explanation for these suboptimal rates. We expect that $\nabla\Psi_h$ converges to $\nabla\Psi$ slower by a factor of h than Ψ_h converges to Ψ, which "pollutes" $b^{[\Psi_h]}$. Also, we expect that Ψ_h can, at best, converge at the same rate that $p_h, \boldsymbol{\mu}_h$ converge, since the concentrations (hence also Ψ) are related to $p, \boldsymbol{\mu}$ through algebraic equations eq. (2.12). The "pollution" in $b^{[\Psi_h]}$ caused by $\nabla\Psi_h$ therefore, at best, exceeds the optimal approximation error for $p, \boldsymbol{\mu}$ by a factor of h, leading to suboptimal rates. Discretizing the density ρ instead of its reciprocal Ψ does not appear to alleviate these suboptimal rates, and more broadly it does not seem straightforward to devise a numerical scheme that circumvents this difficulty.

The terms in eq. (2.67) arise due to coupling of the Stokes and OSM equations; they would not appear in a formulation of the isobaric OSM problem alone.

The density consistency terms in eq. (2.65b) are crucial in this example. Without them, we find that Newton's method diverges for the values of d and h from table 2.2.

2.5.2 Benzene-cyclohexane

We consider the three-dimensional mixing of liquid flows of benzene and cyclohexane in a microfluidic container. This example is analogous to the two-dimensional benzene-cyclohexane simulation in [4, sect. 4.5], but here we consider the more challenging three-dimensional case. We refer to benzene and cyclohexane as species 1 and 2, respectively. Following [4] we use parameter values $T = 298.15\,\mathrm{K}$, $\mathscr{D}_{12} = 2.1 \times 10^{-9}\,\mathrm{m^2\,s^{-1}}$, $\eta = 6 \times 10^{-4}\,\mathrm{Pa\,s}$ and $\zeta = 10^{-7}\,\mathrm{Pa\,s}$. As molar masses we take $m_1 = 0.078\,\mathrm{kg\,mol^{-1}}$ and $m_2 = 0.084\,\mathrm{kg\,mol^{-1}}$.

We take the ambient pressure to be $p^{\mathrm{ref}} = 10^5\,\mathrm{Pa}$ and assume that the dependence of the partial molar volumes on pressure variations and composition can be neglected. Hence each $\overline{V_i}(T, p, x_1, x_2)$ is treated as being a constant (recall the discussion following eq. (1.30); see also [41] and references therein). It follows that $\overline{V_i}(T, p, x_1, x_2) = 1/c_i^{\mathrm{ref}}$ where c_i^{ref} is the concentration of pure species i at temperature T and pressure p^{ref}. Moreover, benzene and cyclohexane form a non-ideal solution, and we capture this using a Margules model [60] (recall eq. (1.33)) of the form

$$\overline{G_1}(T, p, x_1, x_2) = p/c_1^{\mathrm{ref}} + RT \ln x_1 + RT x_2^2 (A_{12} + 2(A_{21} - A_{12})x_1), \tag{2.68}$$

$$\overline{G_2}(T, p, x_1, x_2) = p/c_2^{\mathrm{ref}} + RT \ln x_2 + RT x_1^2 (A_{21} + 2(A_{12} - A_{21})x_2). \tag{2.69}$$

As in [4] we set $A_{12} = 0.4498$, $A_{21} = 0.4952$, $m_1 c_1^{\mathrm{ref}} = 876\,\mathrm{kg\,m^{-3}}$ and $m_2 c_2^{\mathrm{ref}} = 773\,\mathrm{kg\,m^{-3}}$. Since each $\overline{G_i}$ is linear in p, and $\overline{V_i}$ is independent of p, the value of p^{aux} plays no role in the constitutive relation eq. (2.12) as it can be absorbed into each of the μ_i^{aux}. The auxiliary constants in eq. (2.12) therefore only allow us to prescribe $n - 1 = 1$ physical constraint. To demonstrate the flexibility of our method we take this to be that $m_1 c_{h,1} - m_2 c_{h,2}$ integrates to zero on the outflow boundary of the container; physically this states that the species have equal average densities on the outflow. The non-physical constraints that we employ are $\int_\Omega p \,\mathrm{d}\Omega = 0$ and eq. (2.60).

The domain Ω, shown in fig. 2.1, is a chamber with two inflow pipes and an outflow pipe. The length scale of the domain is on the order of millimetres. Benzene flows in from the back pipe (at $x = -0.5$), cyclohexane from the side pipe (at roughly $x = 1$), and both flow out of the front pipe (at $x = 5.5$). As boundary conditions, we enforce

parabolic profiles on $J_i \cdot \hat{n}_\Gamma$ at inflow i and on the outflow, and $J_i \cdot \hat{n}_\Gamma = 0$ elsewhere on the boundary. Instead of specifying the value of the barycentric velocity on the inflows and outflow, we enforce $\rho v \cdot \hat{n}_\Gamma = (J_1 + J_2) \cdot \hat{n}_\Gamma$ and $\rho v \times \hat{n}_\Gamma = 0$ in these regions. Elsewhere on the boundary we enforce $v = 0$. The magnitude of the parabolic profile enforced on $J_i \cdot \hat{n}_\Gamma$ is $m_i c_i^{\mathrm{ref}} v_i^{\mathrm{ref}}$ where, as in [4], we symmetrise the molar fluxes so that $c_1^{\mathrm{ref}} v_1^{\mathrm{ref}} = c_2^{\mathrm{ref}} v_2^{\mathrm{ref}}$. We choose $v_1^{\mathrm{ref}} = 10\,\mu\mathrm{m\,s}^{-1}$, which results in a Reynolds number for the problem of $\mathrm{Re} = 3 \times 10^{-2}$ and a Péclet number of $\mathrm{Pe} = 1 \times 10^{1}$.

Figure 2.1: The domain and mesh used in section 2.5.2. A unit of length on the axes corresponds to a physical length of 2 mm. The volume is coloured by the nondimensionalised pressure solution p.

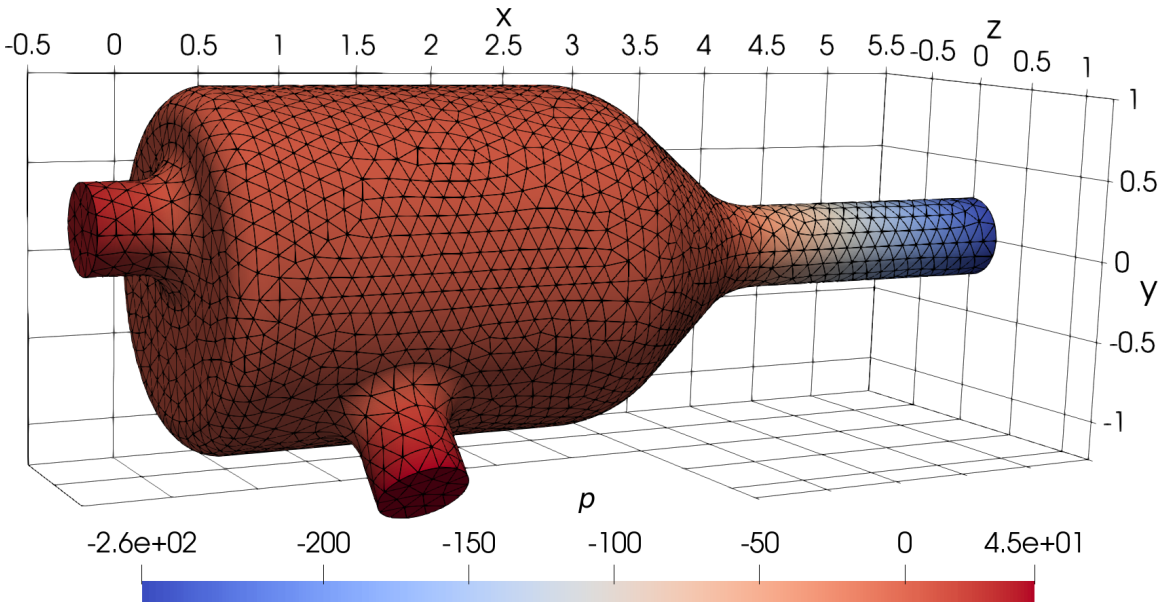

We employ a curved tetrahedral mesh of order 5, shown in fig. 2.1. The mesh was generated using ngsPETSc [12, 101] and OpenCASCADE Technology. For the barycentric velocity and pressure we use the degree $k = 5$ generalised Taylor–Hood pair [49, sect. 54.4.1]. For the mass flux and chemical potentials we use the $\mathbb{BDM}_k$–$\mathbb{DG}_{k-1}$ pair [22, 85]. For the mole fractions (resp. density reciprocal) we use discontinuous (resp. continuous) degree $k-1 = 4$ polynomial spaces. We solve a nondimensionalised SOSM system with augmentation parameter $\gamma = 0.1$.

We solve the discretised nonlinear problem using Newton's method with an absolute tolerance on the residual of 10^{-11} in the Euclidean norm. We first solve the problem with a low-order $k = 2$ discretisation (on the same curved mesh), and we use the resulting solution as the initial guess to Newton's method in the high-order $k = 5$

case. With this low-order initial guess, Newton's method in the $k = 5$ case converges in 5 iterations. We also solve the $k = 2$ problem using Newton's method with the same absolute tolerance, but we employ continuation [35] to aid convergence. We take five continuation steps by gradually increasing v_1^{ref}. In particular we use values of $v_1^{\mathrm{ref}} = 10^{\theta_{\mathrm{cont}}/4} \cdot 1\,\mu\mathrm{m\,s}^{-1}$ for $\theta_{\mathrm{cont}} = 0, 1, 2, 3, 4$. For our initial guess at the first step $\theta_{\mathrm{cont}} = 0$, we set the velocity and mass fluxes to be zero, and assume an equimolar isobaric mixture wherein $x_{h,1} = x_{h,2} = 0.5$ and $p_h = 0$, which together with eq. (2.12) determines the $\mu_{h,i}$ and Ψ_h. The five continuation steps $\theta_{\mathrm{cont}} = 0, 1, 2, 3, 4$ respectively required $5, 5, 6, 6, 7$ Newton iterations.

Figure 2.2: A cross-sectional view of the domain in section 2.5.2. The volume is coloured by the mole fraction x_1 of benzene. Isosurfaces of x_1 and streamlines of the nondimensionalised benzene velocity field v_1 are also shown. The streamlines are coloured by the magnitude of v_1.

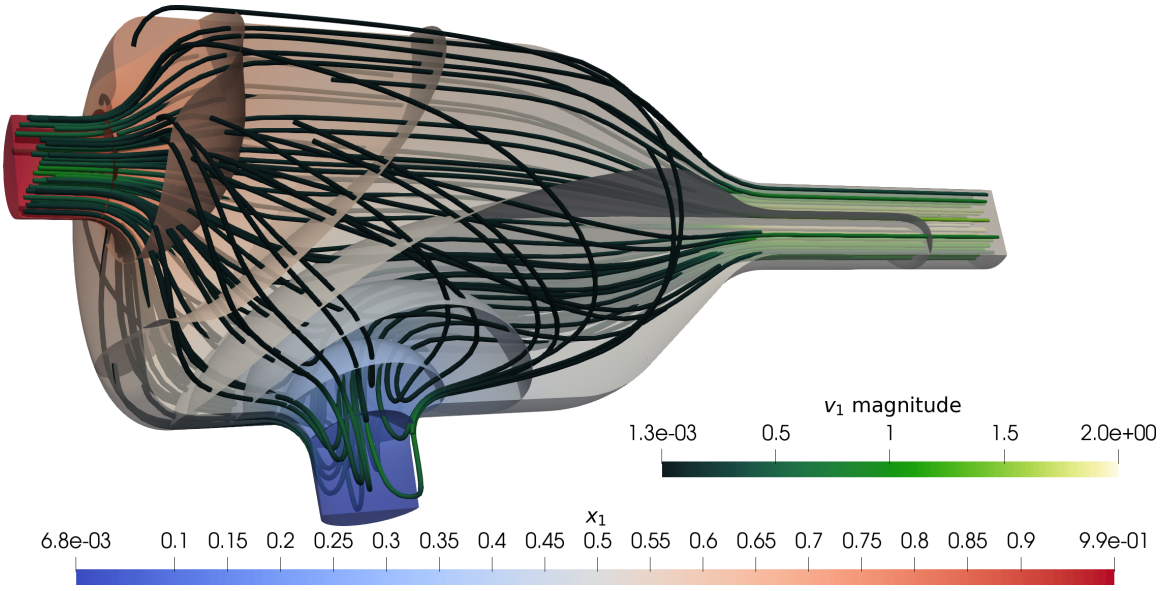

The pressure solution, shown in fig. 2.1, is largest at the inlets and at a minimum on the outlet. The benzene mole fraction and velocity are visualised in fig. 2.2. The benzene mole fraction approaches 1 at the benzene inlet and a value close to 0.5 at the outlet. The benzene velocity field is laminar but exhibits complicated behaviour near the cyclohexane inlet; our high-order scheme captures this effectively despite the coarse mesh (the cell diameter is roughly 1/4 the inlet diameter). Finally, we compute errors in the (nondimensionalised) mass-average constraint and in the requirement that the mole fractions sum to unity, yielding reassuringly small values of $\|v_h - \Psi_h \sum_{i=1}^n J_{h,i}\|_{L^2(\Omega)^d} = 1.1 \times 10^{-4}$ and $\|1 - \sum_{i=1}^n x_{h,i}\|_{L^2(\Omega)} = 1.6 \times 10^{-6}$.

2.5.3 High-order versus low-order discretisation

To study the advantages of using a high-order discretisation, we repeat the benzene-cyclohexane simulation in section 2.5.2, but we vary the polynomial degree k of the finite element spaces. In particular we vary $k \in \{2, \dots, 5\}$, and we compare this to fixing the degree at $k = 2$ and once uniformly refining the mesh (starting with the same mesh from section 2.5.2). In all cases we employ a curved mesh of order 5, so that the effect of curving the mesh with different orders does not play a role in our experiment.

Figure 2.3: Plots of the L^2-errors in the mole fraction and (nondimensionalised) mass-average constraints for the experiment of section 2.5.3. The blue plot with square markers is obtained by holding the mesh fixed and varying $k \in \{2, \dots, 5\}$. The red plot with circle markers is obtained by holding $k = 2$ fixed and once uniformly refining the mesh.

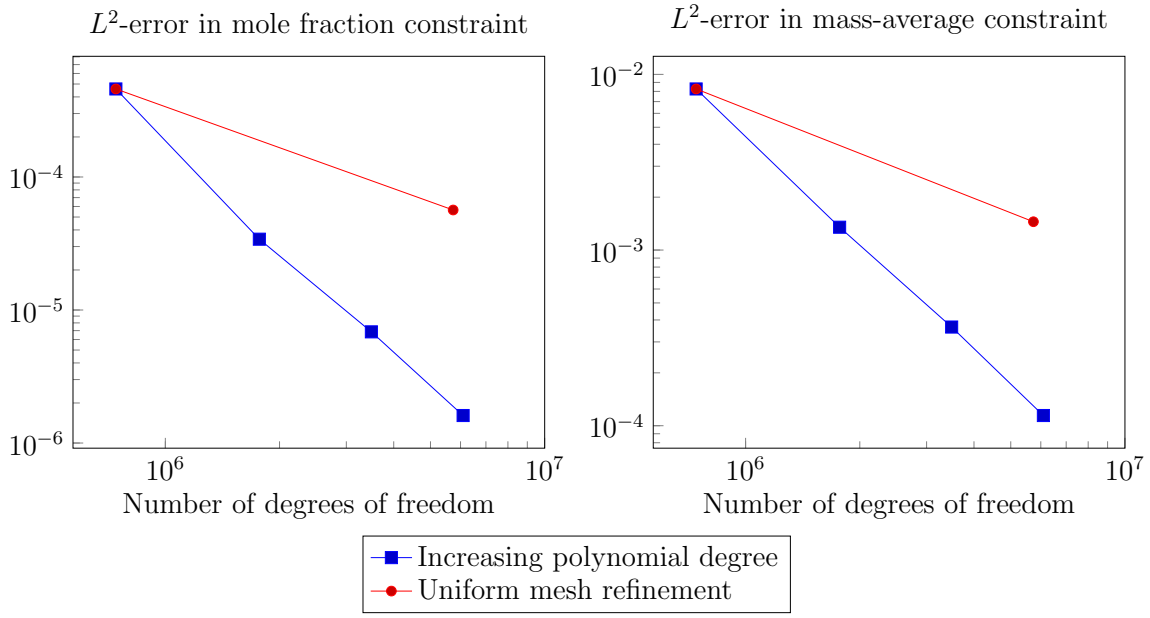

To quantify the accuracy of our numerical solutions, we measure L^2-errors in the mole fraction constraint $\|1 - \sum_{i=1}^{n} x_{h,i}\|_{L^2(\Omega)}$ and (nondimensionalised) mass-average constraint $\|v_h - \Psi_h \sum_{i=1}^{n} J_{h,i}\|_{L^2(\Omega)^d}$. In fig. 2.3 we plot these errors against the number of degrees of freedom (DOFs) of the finite element spaces. In blue we plot the approach of holding the mesh fixed and varying $k \in \{2, \dots, 5\}$, and in red the approach of holding $k = 2$ fixed and uniformly refining the mesh.

When $k = 2$ on the coarse mesh, the finite element space has 7.4×10^5 DOFs, while on the fine mesh for $k = 2$ there are 5.7×10^6 DOFs. When $k = 5$ on the

coarse mesh there are 6.1×10^6 DOFs, which is comparable to that of $k = 2$ on the fine mesh. However, we see from fig. 2.3 that the $k = 5$ discretisation achieves significantly lower L^2-errors than the $k = 2$ discretisation on the fine mesh. In fact, even taking $k \in \{3, 4\}$ leads to a greater accuracy than the $k = 2$ discretisation on the fine mesh, and for a much lower DOF count. These findings are corroborated in fig. 2.4 where, taking the $k = 5$ solution as a reference solution, the errors in all fields (against this reference solution) are again lower for $k \in \{3, 4\}$ on the coarse mesh than for $k = 2$ on the refined mesh. These findings indicate that a high-order discretisation may be a more efficient choice for a given DOF count, and motivate the study of preconditioners for this case [72].

Figure 2.4: Plots of the errors in (nondimensionalised) fields for the experiment of section 2.5.3. Errors are computed with respect to the $k = 5$ solution on the coarse mesh. The blue plots with square markers are obtained by holding the mesh fixed and varying $k \in \{2, \ldots, 4\}$. The red plots with circle markers are obtained by holding $k = 2$ fixed and once uniformly refining the mesh.

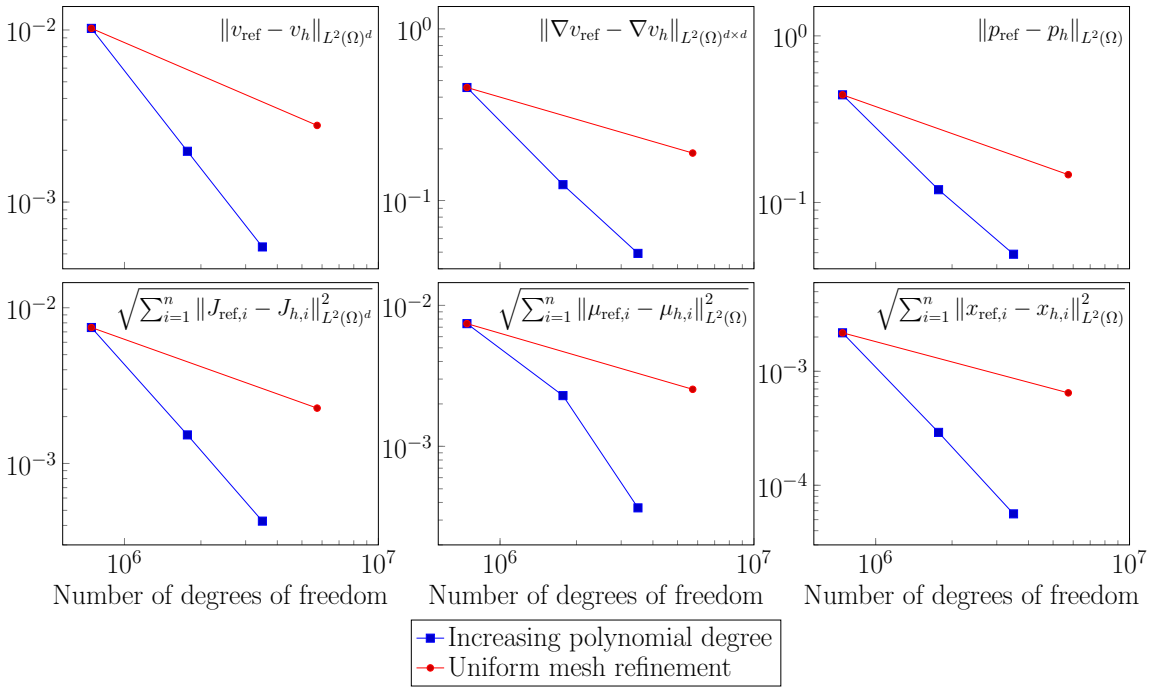

2.5.4 Comparison to a previous method

We next compare our method to that of [4], which, to the best of our knowledge, is the only other finite element method in the literature for the SOSM equations in

the non-ideal setting. Since the discretisation of [4] is limited to two-dimensional low-order simulations, we use as a basis for comparison the two-dimensional benzene-cyclohexane simulation from [4]. The physical setup is similar to that of section 2.5.2 and we refer to [4, sect. 4.5] for the details.

For the low-order method of [4] we employ a non-curved mesh consisting of 10503 triangles. For our method we employ a curved mesh of order 4 with 3164 triangles and we employ a discretisation of order $k = 4$. We have chosen the resolution of these meshes so that when we compare the two methods they result in linear systems of approximately the same size; see below. In both cases we use ngsPETSc [12, 101] to mesh the domain. The method of [4] employs Picard iteration, which, due to our choice of mesh, requires that a linear system with 3.49×10^5 DOFs be solved at each iteration. For our method we employ the monolithic Newton scheme (without continuation) as described in section 2.4, for which the resulting Newton linearised systems to be solved at each iteration have 3.51×10^5 DOFs. In both cases we choose an equimolar mixture as an initial guess in the iterative schemes.

The two discretisations that we consider result in different nonlinear systems of equations to be solved. The nonlinear equations are solved using Picard iteration in [4] and Newton iteration for our method. To quantify how well these iterative schemes converge, we measure the L^2-norm of the update in the (nondimensionalised) concentration fields at each iteration, and we terminate once this falls below 10^{-10}. We have chosen to measure this quantity because it is readily computable for both of the methods, despite the fact that they are based on different formulations and choices of unknowns in the SOSM equations. We also measure L^2-errors in the (nondimensionalised) mass-average constraint at each iteration.

We first carry out this experiment with a benzene reference inflow velocity of $v_1^{\mathrm{ref}} = 0.4\,\mu\mathrm{m\,s}^{-1}$. The results of this experiment are plotted in fig. 2.5. The concentration update plot indicates that both methods successfully converge, with our method doing so quadratically (as expected of Newton's method), and the method of [4] linearly (as expected of Picard iteration). The quadratic convergence of Newton's method means that our scheme converges much faster than that of [4]; we converge in 6 iterations whereas [4] converges in 15. Moreover, our high-order discretisation achieves a significantly lower L^2-error in the mass-average constraint, despite the fact that both schemes result in linear systems with roughly the same number of DOFs. We ran the experiment of this subsection in parallel on 8 cores with an Intel Core i9-10920X processor, and we solved the linear systems with MUMPS [1]. The linear solve runtime was similar for both methods. For our method the average runtime was

Figure 2.5: Plot of the concentration updates and mass-average constraint errors in the L^2-norm, versus the number of iterations, for the experiment of section 2.5.4 with $v_1^{\text{ref}} = 0.4\,\mu\text{m}\,\text{s}^{-1}$. We compare our method with the previous method of [4]. The dashed grey line represents the termination condition of 10^{-10} for the concentration updates in the L^2-norm.

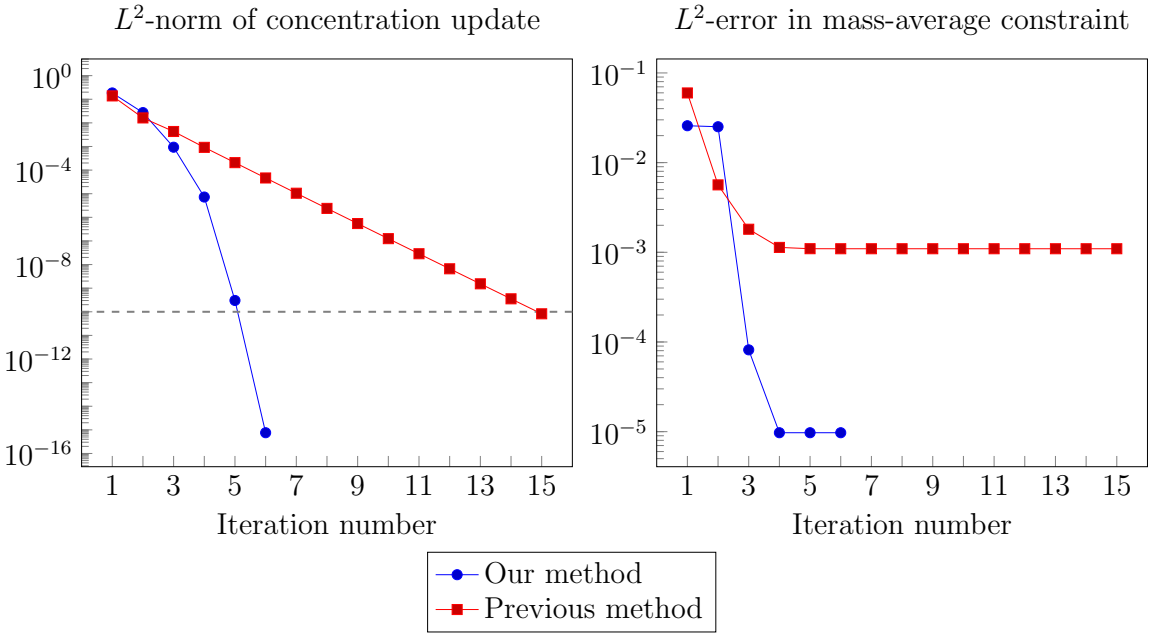

2.0 seconds, where we have accounted for the additional computational time resulting from applying the Woodbury formula (recall section 2.4). For the method of [4] the average runtime was 2.4 seconds.

Finally, we repeat this experiment with a larger benzene reference inflow velocity of $v_1^{\text{ref}} = 4.0\,\mu\text{m}\,\text{s}^{-1}$. This results in a nonlinear system that is appreciably more difficult to solve, as demonstrated in fig. 2.6. Indeed, our method converges but now requires 8 iterations to do so. Moreover, for the method of [4] we employ the under-relaxation strategy outlined in [4, sect. 4.5] to aid with nonlinear convergence, but we find that for both small and moderate under-relaxation parameters $\epsilon \in \{0.1, 0.5\}$ the method fails to converge and the mass-average error does not decrease with the iteration count. These findings indicate that our Newton scheme is more robust than Picard iteration when solving more challenging problems. In this case the linear solve runtimes were again similar for both methods; we recorded an average runtime of 1.9 seconds for our method and 2.4 seconds for that of [4].

Figure 2.6: Plot of the concentration updates and mass-average constraint errors in the L^2-norm, versus the number of iterations, for the experiment of section 2.5.4 with $v_1^{\text{ref}} = 4.0\,\mu\text{m}\,\text{s}^{-1}$. We compare our method with the previous method of [4] using an under-relaxation parameter ϵ. The dashed grey line represents the termination condition of 10^{-10} for the concentration updates in the L^2-norm.

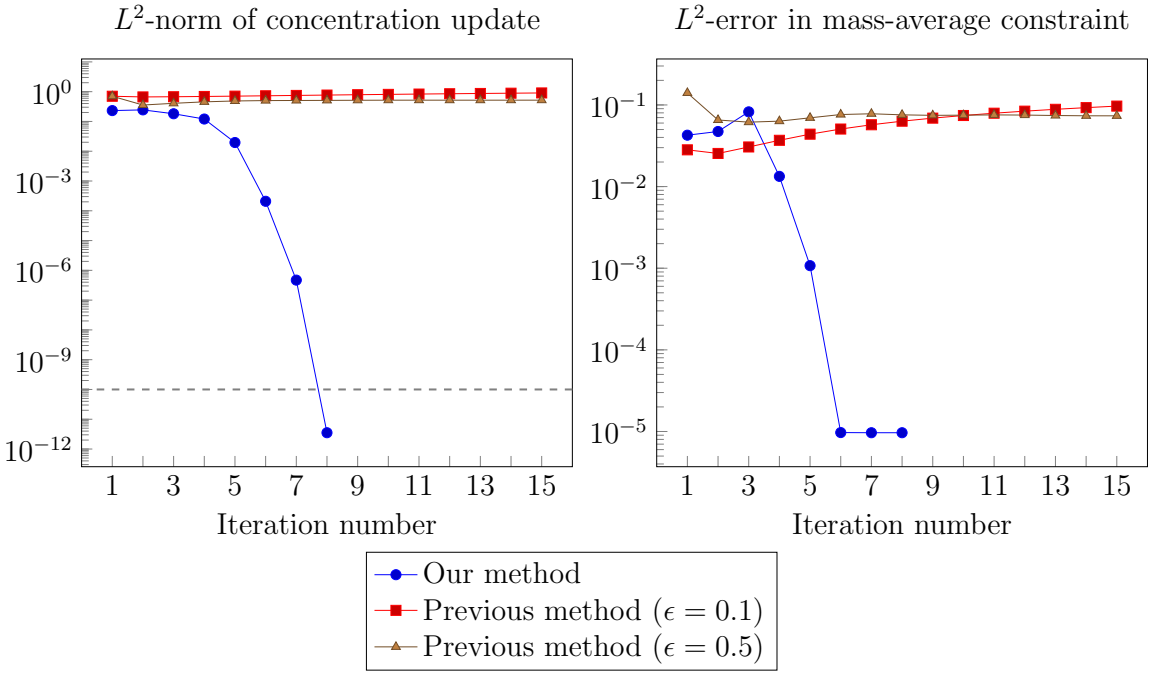

2.6 Conclusions

In this chapter we have introduced and analysed a large family of finite element methods for solving the SOSM equations, which model bulk momentum transport and multicomponent diffusion in concentrated mixtures. To the best of our knowledge, this chapter represents the first work in the finite element literature that introduces a discretisation for these equations that is applicable to non-ideal mixtures and is straightforward to implement in two and three spatial dimensions. At a theoretical level, we studied a Picard linearisation of the SOSM problem and we proved that our discretisations are convergent and quasi-optimal in this linearised setting. We also showed how the methods can be extended to the full nonlinear SOSM problem and how the resulting monolithic system can be solved using Newton's method. Numerical experiments substantiated our theory and demonstrate that the methods achieve high-order spatial convergence rates. Our numerical experiments also suggest that, for a given computational cost, our high-order discretisations in conjunction with Newton's

method outperform previous low-order approaches in both accuracy and robustness.

Chapter 3

Finite element methods for electroneutral multicomponent electrolyte flows

This chapter is based on the manuscript [7].

3.1 Introduction

This chapter addresses the numerical simulation of liquid electrolytes, which are fluids that transport electrical charge by the motion of ions. Electrolytes are *multicomponent fluids* (or *mixtures*), since they consist of multiple distinct chemical species [56, 123]. While a general mixture may consist entirely of uncharged species, in an electrolyte at least two of the species must be ions of opposite charge. For example, dissolving table salt in water yields an electrolyte with three species: H_2O, Na^+ and Cl^-. Prominent applications of electrolytic flows include energy storage (e.g. batteries and fuel cells), chemical processes (e.g. electrodialysis and electroplating) and biological systems (e.g. biological membranes) [11, 86, 123].

We assume that the electrolyte is *electroneutral*, which means that its local charge density is everywhere zero[1]. This is a common and accurate assumption for most electrochemical systems at length scales much larger than the Debye length (which is typically on the order of nanometers) [86, 123]. For example, in lithium-ion batteries, electroneutrality holds throughout the bulk of the electrolyte and is only violated in sub-nanometer-wide layers near the electrolyte-electrode interfaces. Consequentially, physics-based microscale lithium-ion battery models typically use differential equations that assume electroneutrality throughout the domain and incorporate interfacial

[1]Note that electroneutrality does not prevent the transport of charge within the mixture.

charge layers through boundary conditions [23, 97]. In this chapter, electroneutrality allows us to follow work done earlier by Van-Brunt et al. [114] and employ a change of basis that transforms the governing equations into a form that is structurally similar to that of an uncharged mixture, simplifying both the model and numerics.

A constitutive relation for the species mass fluxes must be chosen to model mass transport in multicomponent flows. For electrolytic flows, the popular Nernst–Planck model accounts for mass transport by convection, Fickian diffusion and electromigration [10, 40]. Several finite element methods exist for the electroneutral Nernst–Planck model [19, 43, 98], and literature for its non-electroneutral analogue, the Poisson–Nernst–Planck model, is especially abundant (see e.g. [32, 95, 124]). However, because the Nernst–Planck model assumes that every species in isolation obeys Fick's law of diffusion [53], it has the drawback of being unable to capture *cross-diffusion*, a physical phenomenon that arises when different species exert diffusional forces on each other [69, 108, 116]. For *dilute mixtures*, i.e., mixtures with only one species present in non-trace amounts, it is usually assumed appropriate to neglect cross-diffusion, and doing so greatly simplifies the model. However, many practical problems involve non-dilute mixtures for which Fick's law is inadequate. For example, in lithium-ion battery electrolyte modelling, cation-anion cross-diffusion must be accounted for to match experimentally observed conductivity, salt diffusivity and transference numbers [15]. For detailed discussions on the limitations of Fick's law, we refer to [76, 77, 78] for generic mixtures and [86, ch. 11-12] for electrolytes. Drawbacks of the Nernst–Planck model from a thermodynamical perspective are also given in [40].

To avoid the limitations of Nernst–Planck theory, we treat mass transport using the Onsager–Stefan–Maxwell[2] (OSM) constitutive laws [14, 78, 99, 123], which were introduced in section 1.6. Due to its flexibility in treating complicated transport phenomena and nonideal thermodynamics, the OSM framework has received much attention in electrochemistry as a tool for modelling electrolytic flows [86]. In the context of electrochemistry, the OSM framework is sometimes known as *concentrated solution theory*. For example, the framework has been applied to lithium-ion batteries [97], fuel cells [121, 122], electrodialysis [74] and electrolysis [104]. Nonetheless, the OSM equations have received limited attention in the scientific computing literature, especially for the coupling of OSM diffusion to Stokes or Navier–Stokes flow. We

[2]Nomenclature varies depending on the source; sometimes the name *Maxwell–Stefan* or even *generalised Maxwell–Stefan* is used instead.

refer to the coupled Stokes (resp. Navier–Stokes) and OSM equations as the SOSM (resp. NSOSM) equations.

Most numerics papers on the OSM equations assume a thermodynamically ideal gaseous mixture, such as the finite element methods in [21, 29, 70, 83, 112]. For numerics papers on the SOSM or NSOSM equations, we are aware of [46] for a finite difference scheme, [8, 13, 38, 37, 39, 92, 106] for a series of Cartesian-grid finite volume schemes under various physical assumptions in the setting of fluctuating hydrodynamics, and [4, 24, 26, 80] for finite element schemes (in addition to chapter 2). Among these works, only chapter 2 considers spatially high-order methods, and only [39, 92] consider charged species (although [39, 92] make the Boussinesq approximation to simplify the numerics). We are not aware of existing finite element algorithms for the electroneutral NSOSM equations, a gap the present chapter addresses.

A major novelty of this chapter lies in our treatment of the electroneutrality condition, which in mathematical terms places an algebraic constraint on the species concentrations. Previous works have used this constraint to obtain an elliptic equation for the electrical potential, which is then coupled to the relevant equations that govern mass and momentum transport [39, 43, 98]. The structure of these coupled transport equations does not resemble that afforded by an uncharged mixture, requiring the development of new solution techniques: temporal splitting schemes are introduced in [39, 43] and a monolithic approach is considered in [98]. By contrast, in this chapter we use the so-called *salt-charge transformation*, introduced in [114] and inspired by Newman's work on binary electrolytes [87], to transform the electroneutral NSOSM equations into a form that structurally resembles the NSOSM equations for an uncharged mixture. We then apply the method of lines, whereby we spatially discretise the transformed problem using a steady NSOSM solver and then solve the resulting spatially discrete system of differential-algebraic equations by timestepping. Hence, our approach has the advantage of allowing uncharged NSOSM spatial discretisations and solvers to be employed for electroneutral electrolytic mixtures.

The steady NSOSM discretisation we employ modifies the SOSM scheme introduced in chapter 2 to include the nonlinear convective terms in the momentum balance. These are trivial to include because we assume a low Reynolds number flow, so the convective terms do not require stabilization. We also apply a second modification that is straightforward but has consequences regarding the set of material parameters one must specify to implement the model. Namely, instead of discretizing the OSM equations using chemical potentials (as is done in [4, 24] and chapter 2), we express the OSM diffusional driving forces in terms of mole fraction gradients and we only

discretise the mole fractions. Because we do not discretise the chemical potentials, we do not require experimental knowledge of species activity coefficients in the mixture. Only the *thermodynamic factors* (i.e. partial derivatives of activity coefficients with respect to mole fractions) are required, which allows us to straightforwardly draw on experimental data from [117, 118] in our numerical experiments.

When modelling mixtures, the interplay between the volumetric equation of state (EOS), given by eq. (1.13), and boundary conditions (BCs), is subtle. The EOS and BCs can both impose restrictions on the species concentrations, and these restrictions must be compatible. Investigating this interplay is mathematically challenging even for a two-species Fickian mixture [52]. Here, this challenge is exacerbated by the fact that our steady NSOSM solver requires user-chosen integral constraints to be imposed on the mathematical solution[3], as was the case in chapter 2. These constraints arise naturally in the steady case, because the steady mass continuity equations do not dictate how many moles of each species are present in the domain; this must be prescribed by additional integral constraints. However, in the transient case, the constraints must be chosen carefully, such that they are compatible with the choice of EOS and BCs. We discuss several physically relevant choices of EOS and BCs along with appropriate corresponding constraints. We also discuss a seemingly physical combination of EOS and BCs that appears to yield an ill-posed problem. We are not aware of discussions regarding this interplay in the multicomponent numerics literature and believe these findings may be of independent interest. Incidentally, we mention that a discussion about the challenges of discretizing the multicomponent mass continuity equations, in a way that is compatible with the EOS, is given in [38] in the case of a low-order finite volume scheme[4].

The remainder of this chapter is organised as follows. In section 3.2 we introduce the electroneutral NSOSM equations, and show how the salt-charge transformation can be applied to obtain an equivalent system amenable to a steady NSOSM solver. In section 3.3 we first consider the transformed steady problem, which we discretise using the (modified) scheme from chapter 2. In section 3.4 we apply the method of lines to the transformed transient problem, discretizing in space using the steady scheme from section 3.3 and taking special care to identify what constraints must be

[3]Henceforth we shall always use "solution" in the mathematical, rather than the physical, sense.

[4]The challenges encountered in [38] are different from those encountered in this chapter, presumably because they discretise the species partial densities whereas we discretise mole fractions, and also because they attempt to enforce the EOS pointwise, whereas we enforce the EOS intrinsically due to our choice of variables.

imposed depending on the EOS and BCs. In section 3.5 we demonstrate our algorithm with a variety of numerical examples, and conclusions are drawn in section 3.6.

3.2 Governing equations and salt-charge transformation

We consider an isothermal, chemically nonreacting mixture of $n \geq 3$ species indexed by $i \in \{1 : n\}$. Let z_i denote the equivalent charge of species i and $n_c \geq 2$ the number of charged species. Note that $n_c = n$ is possible, e.g. for a molten salt. We list the species so that the first $(n - n_c)$ species are uncharged and the last two species are oppositely charged. This means that $z_1, \ldots, z_{n-n_c} = 0$ and $z_{n-n_c+1}, \ldots, z_n \neq 0$ with $z_n/z_{n-1} < 0$.

We next state the governing partial differential equations, which are posed on a bounded and connected Lipschitz spatial domain $\Omega \subset \mathbb{R}^d$ with $d \in \{2, 3\}$.

3.2.1 Electroneutral NSOSM equations

The thermodynamic state variables that we consider are the temperature T, the pressure p and the species molar concentrations c_i for $i \in \{1 : n\}$. Since the mixture is isothermal T is a fixed parameter, but p and $c_1, \ldots, c_n$ may vary with space and time. The total concentration is $c_T = \sum_{j=1}^n c_j$ and the density is $\rho = \sum_{j=1}^n m_j c_j$ where m_i is the molar mass of species i. Composition can be described using the species mole fractions $x_i = c_i/c_T$. Note that by definition $\sum_{j=1}^n x_j = 1$. The charge density is $\rho_e = F \sum_{j=1}^n z_j c_j$ where F is Faraday's constant. Electroneutrality requires that $\rho_e = 0$, or equivalently

$$\sum_{j=1}^{n} z_j c_j = 0 \quad \text{in } \Omega, \tag{3.1}$$

which restricts the space of permissible compositions.

To model momentum and mass transport we employ the Cauchy momentum equation (recall eqs. (1.50b) and (1.66)) and nonreacting species mass continuity equations (recall eq. (1.50a)), written in the following form:

$$\frac{\partial(\rho v)}{\partial t} + \nabla \cdot (\rho v \otimes v) + \nabla p - \nabla \cdot \tau = \rho f \quad \text{in } \Omega, \tag{3.2}$$

$$\frac{\partial c_i}{\partial t} + \nabla \cdot N_i = 0 \qquad \text{in } \Omega \quad \forall i \in \{1 : n\}. \tag{3.3}$$

Here v is the barycentric velocity, τ is the viscous stress, f is a prescribed body force which is typically zero, and $N_i = c_i v_i$ is the molar flux of species $i \in \{1 : n\}$. Note

that in this chapter, it is convenient to use molar fluxes N_i (and not mass fluxes J_i, as in chapter 2), due to the interplay between the salt-charge transformation and stoichiometry.

The barycentric velocity is related to the molar fluxes through the *mass-average constraint* (recall eq. (1.44)),

$$\rho v = \sum_{j=1}^{n} m_j N_j \quad \text{in } \Omega. \tag{3.4}$$

Since $\rho = \sum_{j=1}^{n} m_j c_j$ one can multiply eq. (3.3) by m_i and sum over i while using eq. (3.4) to obtain the equation for total mass continuity $\partial_t \rho + \nabla \cdot (\rho v) = 0$. However, as in chapter 2, we never explicitly discretise this equation since it is a consequence of eq. (3.3) and eq. (3.4).

The balance laws eqs. (3.2) and (3.3) must be closed with constitutive laws for the viscous stress and molar fluxes (recall section 1.6) For the former we apply the Newtonian fluid law (recall eq. (1.74))

$$\tau = 2\eta\epsilon(v) + (\zeta - 2\eta/d)(\nabla \cdot v)\mathbb{I}, \tag{3.5}$$

where $\epsilon(v)$ is the symmetric gradient of v, $\mathbb{I}$ is the $d \times d$ identity matrix, $\eta > 0$ is the shear viscosity and $\zeta > 0$ is the bulk viscosity. In contrast to chapter 2, we now allow the viscosities η and ζ to depend on the thermodynamic state variables T, p and $x_1, \ldots, x_n$.

We model the molar fluxes using the isothermal, non-isobaric Onsager–Stefan–Maxwell (OSM) equations, as was done in eq. (2.5) of chapter 2. When written using molar fluxes, eq. (2.5) takes the form

$$-\nabla \mu_i + \frac{m_i}{\rho} \nabla p = \sum_{j=1}^{n} \mathbf{M}_{ij} N_j \quad \text{in } \Omega \quad \forall i \in \{1 : n\}, \tag{3.6}$$

where μ_i is the *electrochemical potential* of species $i \in \{1 : n\}$ and $\mathbf{M}$ is an *isothermal Onsager transport matrix*.

Three immediate remarks on eq. (3.6) are in order. The first is a matter of bookkeeping. Note that $\mathbf{M}$ is related to the transport matrices $\boldsymbol{M}$ (recall eq. (2.6)) and $\hat{\boldsymbol{M}}$ (recall eq. (2.17)) from chapter 2 by the formula

$$\mathbf{M}_{ij} = \hat{\boldsymbol{M}}_{ij} m_i m_j = \frac{\boldsymbol{M}_{ij}}{c_i c_j}. \tag{3.7}$$

In this chapter, it is natural to use $\mathbf{M}$, since we are using molar fluxes.

The second remark concerns the spectral properties of $\mathbf{M}$, which are analogous to our considerations regarding $\boldsymbol{M}$ in chapter 2. The two crucial properties of $\mathbf{M}$ are that it is symmetric positive-semidefinite, and its nullspace is spanned by $[c_1, \ldots, c_n]^\top$. Moreover, the Gibbs–Duhem relation implies that $\sum_{j=1}^n c_j(-\nabla\mu_j + [m_j/\rho]\nabla p) = 0$ (recall eq. (1.18)). The left side of eq. (3.6) therefore lies in the orthogonal complement of $\operatorname{span}\{[c_1, \ldots, c_n]^\top\}$, which is the range of $\mathbf{M}$. Hence eq. (3.6) is non-uniquely solvable for $N_1, \ldots, N_n$. Uniqueness of the fluxes comes from imposing the mass-average constraint eq. (3.4) in addition to eq. (3.6). Often $\mathbf{M}$ is written in terms of so-called *Stefan–Maxwell diffusivities* $\mathscr{D}_{ij}$ as

$$\mathbf{M}_{ij} = \begin{cases} -\frac{RT}{\mathscr{D}_{ij} c_T} & \text{if } i \neq j, \\ \sum_{k=1, k\neq i}^n \frac{RT c_k}{\mathscr{D}_{ik} c_T c_j} & \text{if } i = j, \end{cases} \tag{3.8}$$

with R the gas constant. The diffusivities satisfy $\mathscr{D}_{ij} = \mathscr{D}_{ji}$ for $i \neq j$ [14], while $\mathscr{D}_{ii}$ is undefined. In contrast to chapter 2, we now allow the $\mathscr{D}_{ij}$ to be functions of T, p and $x_1, \ldots, x_n$ (see e.g. [75]). For the purposes of this chapter[5], this functional dependence can be arbitrary, so long as $\mathbf{M}$ remains positive-semidefinite with its nullspace spanned by $[c_1, \ldots, c_n]^\top$.

The third remark is that μ_i in eq. (3.6) is now the *electrochemical potential* [86], and no longer the *chemical potential*, as was the case in chapters 1 and 2. For uncharged species in locally electroneutral mixtures, these two notions coincide. However, for charged species, the electrochemical potential differs from the chemical potential, since it depends on the so-called *electrical state* of the system. We shall discuss what this means in more detail imminently. Fortunately, the subtleties that arise due to the electrical state are elegantly handled by the salt-charge transformation.

Equations (3.1) to (3.6) comprise the electroneutral NSOSM equations. In addition to needing suitable boundary and initial conditions, the equations as written are still not closed. One must additionally supply a volumetric equation of state (EOS), which gives the total concentration c_T (or equivalently, mass density ρ) as a function of T, p and $x_1, \ldots, x_n$. This is done using either eq. (1.13) or eq. (1.39). A constitutive law giving the electrochemical potentials μ_i as a function of $T, p, x_1, \ldots, x_n$ and the *electrical state* of the system must also be given. However, in multicomponent systems, formulating the notion of electrical state is delicate, and requires a foray into technicalities of electrochemical thermodynamics.

[5] In this chapter we do not pursue a rigorous well-posedness analysis, as was the case in sections 2.2.6 and 2.3.

Intuitively, the electrical state should quantify how much electrical potential energy is locally available in the system. A reasonable model may be to introduce an "electrostatic potential" ϕ which acts as a Lagrange multiplier for enforcing electroneutrality, and to then decompose the electrochemical potentials as $\mu_i = \mu_i^{\text{chem}} + Fz_i\phi$, where μ_i^{chem} encodes the "chemical" or "non-electrical" part of μ_i and depends on T, p and $x_1, \ldots, x_n$ only. However, Guggenheim and Newman have criticised such decompositions as being ambiguous [61, 86], with Newman noting that several inequivalent notions of "electrostatic potential" exist in concentrated mixtures (see also [16, 93]). Fortunately, we do not need to contend with this thermodynamical technicality in the present chapter. Indeed, owing to electroneutrality, the salt-charge transformation will eliminate any need to model the dependence of electrochemical potentials on the electrical state [114]. In what follows, it will only be necessary to model the dependence of *chemical potentials* of hypothetical *uncharged salts* on T, p and $x_1, \ldots, x_n$[6].

3.2.2 Salt-charge transformation

It will be helpful to use boldface notation for vectors and matrices that are indexed by $i \in \{1 : n\}$. For example, we shall write $\boldsymbol{z} = [z_1, \ldots, z_n]^\top$, $\boldsymbol{c} = [c_1, \ldots, c_n]^\top$, $\boldsymbol{m} = [m_1, \ldots, m_n]^\top$ and so on. These should be interpreted as column vectors (or $n \times 1$ matrices). Taking their gradient yields $n \times d$ matrices, hence for example $(\nabla \boldsymbol{\mu})_{ij} = (\nabla \mu_i)_j$. For the fluxes and other $\mathbb{R}^d$-valued quantities we write $\boldsymbol{N} = [N_1, \ldots, N_n]^\top$ which is understood to be an $n \times d$ matrix, and the divergence acts on its rows so that $\nabla \cdot \boldsymbol{N}$ is a column vector (or $n \times 1$ matrix). With this notation, the governing equations in eqs. (3.1), (3.3), (3.4), and (3.6) become

$$\boldsymbol{z}^\top \boldsymbol{c} = 0 \qquad \text{in } \Omega, \tag{3.9}$$

$$\frac{\partial \boldsymbol{c}}{\partial t} + \nabla \cdot \boldsymbol{N} = 0 \qquad \text{in } \Omega, \tag{3.10}$$

$$v = \boldsymbol{\psi}^\top \boldsymbol{N} \quad \text{in } \Omega, \tag{3.11}$$

$$-\nabla \boldsymbol{\mu} + \boldsymbol{\psi} \nabla p = \mathbf{M}\boldsymbol{N} \quad \text{in } \Omega, \tag{3.12}$$

where $\boldsymbol{\psi} := \boldsymbol{m}/\rho$ and ∇p is viewed as being a $1 \times d$ row vector.

We now carry out the salt-charge transformation. While a detailed presentation is given in [114], we briefly outline it here for completeness, and because [114] assumes

[6] In the non-electroneutral setting this strategy does not work. One must instead choose how to quantify the electrical state and model how the electrochemical potentials depend on it.

an isobaric mixture and hence does not keep track of pressure gradient terms in the OSM equations. The starting point is an $n \times n$ transformation matrix $\boldsymbol{Z}$ given by

$$\boldsymbol{Z} = \begin{bmatrix} \boldsymbol{\nu}_1^\top \\ \vdots \\ \boldsymbol{\nu}_{n-1}^\top \\ \boldsymbol{z}^\top / \|\boldsymbol{z}\| \end{bmatrix}. \tag{3.13}$$

Here $\|\boldsymbol{z}\| = \sqrt{\boldsymbol{z}^\top \boldsymbol{z}}$ and $\boldsymbol{\nu}_1, \ldots \boldsymbol{\nu}_{n-1}$ are $n \times 1$ column vectors whose entries contain the stoichiometric coefficients of $n-1$ independent hypothetical chemical reactions that neutralise the species. An example from [114] is an $n = 5$ species mixture consisting of H_2O, Na^+, Cl^-, Mg^{2+} and SO_4^{2-}. Therefore $\boldsymbol{z}^\top = [0, 1, -1, 2, -2]$, and a choice of neutralizing reactions with corresponding stoichiometric coefficient vectors is

$$\begin{aligned} \mathrm{H_2O} &\rightleftharpoons \mathrm{H_2O} && \longrightarrow && \boldsymbol{\nu}_1^\top = [1,0,0,0,0], \\ \mathrm{Na^+ + Cl^-} &\rightleftharpoons \mathrm{NaCl} && \longrightarrow && \boldsymbol{\nu}_2^\top = [0,1,1,0,0], \\ \mathrm{Mg^{2+} + 2\,Cl^-} &\rightleftharpoons \mathrm{MgCl_2} && \longrightarrow && \boldsymbol{\nu}_3^\top = [0,0,2,1,0], \\ \mathrm{2\,Na^+ + SO_4^{2-}} &\rightleftharpoons \mathrm{Na_2SO_4} && \longrightarrow && \boldsymbol{\nu}_4^\top = [0,2,0,0,1]. \end{aligned}$$

Note that the choice of reactions may not be unique. Following [114] we make the convention that $\boldsymbol{\nu}_1, \ldots \boldsymbol{\nu}_{n-1}$ have the following properties. First, for the uncharged species $i \in \{1 : n-n_c\}$ we have $(\boldsymbol{\nu}_i)_j = \delta_{ij}$, corresponding to a trivial identity reaction. Second, for $i \in \{n - n_c + 1 : n-1\}$ the first $n - n_c$ entries of $\boldsymbol{\nu}_i$ are zero, and exactly two of the remaining entries of $\boldsymbol{\nu}_i$ are nonzero, and must be coprime positive integers such that $\boldsymbol{\nu}_i$ is orthogonal to $\boldsymbol{z}$. Third, the $\boldsymbol{\nu}_i$ for $i \in \{n - n_c + 1 : n-1\}$ must be linearly independent. The last two properties state that the non-trivial reactions form simple neutral salts (i.e. salts formed from two ions) and are independent. These three properties imply that $\{\boldsymbol{\nu}_1, \ldots, \boldsymbol{\nu}_n, \boldsymbol{z}\}$ is a basis for $\mathbb{R}^n$ and therefore $\boldsymbol{Z}$ is invertible.

Through $\boldsymbol{Z}$ the electrochemical potentials transform by $\boldsymbol{\mu}_Z := \boldsymbol{Z}\boldsymbol{\mu}$. Under electroneutrality, entries $(\boldsymbol{\mu}_Z)_i$ for $i \in \{1 : n-1\}$ are independent of the electrical state of the system and represent chemical potentials. Indeed, for $i \in \{1 : n-n_c\}$, $(\boldsymbol{\mu}_Z)_i = \mu_i$ is the electrochemical potential of species i, but because species i is uncharged, its electrochemical potential does not depend on the electrical state and is just a chemical potential. For $i \in \{n-n_c+1 : n-1\}$, $(\boldsymbol{\mu}_Z)_i = \boldsymbol{\nu}_i^\top \boldsymbol{\mu}$ does not depend on the electrical state because it is the chemical potential of the neutral salt formed in the reaction corresponding to $\boldsymbol{\nu}_i$ [87, 114]. Following [114], we decompose $\boldsymbol{\mu}_Z$ as (recall that F is the Faraday constant) $\boldsymbol{\mu}_Z^\top = [\boldsymbol{\mu}_\nu^\top, (F\,\|\boldsymbol{z}\|\,\Phi_Z)]$ where $\boldsymbol{\mu}_\nu$ is an $(n-1) \times 1$ column vector of the chemical potentials and Φ_Z is a scalar-valued *salt-charge potential*. The

potential Φ_Z can be related to the potential of a hypothetical probe reference electrode immersed in the mixture, and serves to quantify the electrical state. However, no material parameters in the model depend on Φ_Z.

The concentrations and fluxes transform by $\boldsymbol{c}_Z := \boldsymbol{Z}^{-\top}\boldsymbol{c}$ and $\boldsymbol{N}_Z := \boldsymbol{Z}^{-\top}\boldsymbol{N}$. Since $\boldsymbol{\mu}_Z := \boldsymbol{Z}\boldsymbol{\mu}$ these transformations preserve the structure of the volumetric Gibbs free energy $\tilde{G} = \boldsymbol{c}^\top\boldsymbol{\mu} = \boldsymbol{c}_Z^\top\boldsymbol{\mu}_Z$ (cf. eq. (1.20)). Under isobaric and isothermal circumstances the entropy production due to diffusion is given by $-T^{-1}\operatorname{tr}(\boldsymbol{N}^\top\nabla\boldsymbol{\mu}) = -T^{-1}\operatorname{tr}(\boldsymbol{N}_Z^\top\nabla\boldsymbol{\mu}_Z)$ (cf. eq. (1.65)), which is also preserved by this transformation. As in [114] we decompose

$$\boldsymbol{c}_Z = \begin{bmatrix}\boldsymbol{c}_\nu \\ 0\end{bmatrix}, \qquad \boldsymbol{N}_Z = \begin{bmatrix}\boldsymbol{N}_\nu \\ I^\top/(F\,\|\boldsymbol{z}\|)\end{bmatrix}. \tag{3.14}$$

The condition $(\boldsymbol{c}_Z)_n = 0$ is equivalent to the electroneutrality condition eq. (3.9), and $I = F\boldsymbol{N}^\top\boldsymbol{z}$ is the current density. The variables $\boldsymbol{c}_\nu$ can be thought of as the molar concentrations of the salts formed in the neutralizing reactions, and $\boldsymbol{N}_\nu$ can be thought of as their molar fluxes. Following [114], we refer to these hypothetical salts as *components* as opposed to *species*. Using the equivalent electroneutrality condition $(\boldsymbol{c}_Z)_n = 0$, one verifies that the governing equations eqs. (3.10) to (3.12) transform as

$$\frac{\partial}{\partial t}\begin{bmatrix}\boldsymbol{c}_\nu \\ 0\end{bmatrix} + \begin{bmatrix}\nabla\cdot\boldsymbol{N}_\nu \\ \nabla\cdot I\end{bmatrix} = 0 \qquad \text{in } \Omega, \tag{3.15}$$

$$v = \boldsymbol{\psi}_Z^\top\boldsymbol{N}_Z \quad \text{in } \Omega, \tag{3.16}$$

$$-\nabla\boldsymbol{\mu}_Z + \boldsymbol{\psi}_Z\nabla p = \mathbf{M}_Z\boldsymbol{N}_Z \quad \text{in } \Omega, \tag{3.17}$$

where $\boldsymbol{\psi}_Z := \boldsymbol{Z}\boldsymbol{\psi}$ and $\mathbf{M}_Z := \boldsymbol{Z}\mathbf{M}\boldsymbol{Z}^\top$. Since the *transformed isothermal Onsager transport matrix* $\mathbf{M}_Z$ is congruent to $\mathbf{M}$, it retains the crucial structural properties of symmetry and positive-semidefiniteness (with a nullspace of dimension one).

Equations (3.15) to (3.17) structurally resemble the uncharged OSM equations. In particular, the stationary version of eqs. (3.15) to (3.17) (removing the time derivative term in eq. (3.15)) may be coupled to the stationary Stokes equations for v and p, and the resulting problem can be solved using the stationary SOSM solver from chapter 2. The Picard linearised analysis of chapter 2 is also applicable in such a setting. However, instead of working with this formulation we will instead further develop eq. (3.17) by expressing the chemical potential gradients in terms of mole fraction gradients. Consequently we will not need a constitutive formula for the chemical potentials (or equivalently, activities) and will only need a constitutive formula for the thermodynamic factors. The mole fractions transform as $\boldsymbol{x}_Z := \boldsymbol{Z}^{-\top}\boldsymbol{x}$ and electroneutrality implies $(\boldsymbol{x}_Z)_n = 0$, hence we write $\boldsymbol{x}_Z^\top = [\boldsymbol{x}_\nu^\top, 0]$ with $\boldsymbol{x}_\nu$ an $(n-1)\times 1$

column vector that parametrises composition of the electroneutral mixture. The normalization constraint $\sum_{i=1}^{n} x_i = 1$ transforms to

$$\boldsymbol{\nu}_Z^\top \boldsymbol{x}_\nu = 1 \tag{3.18}$$

where $(\boldsymbol{\nu}_Z)_i = \sum_{j=1}^{n} \boldsymbol{Z}_{ij}$ for $i \in \{1 : n-1\}$. Generalizing [114, eq. (8.22)] to the non-isobaric case, we have

$$\nabla \boldsymbol{\mu}_\nu = RT \boldsymbol{X}_\nu^0 \nabla \boldsymbol{x}_\nu + \overline{\boldsymbol{V}_\nu} \nabla p \tag{3.19}$$

where the $(n-1) \times (n-1)$ matrix $\boldsymbol{X}_\nu^0$ encodes the thermodynamic factors under electroneutrality, and $\overline{\boldsymbol{V}_\nu}$ is an $(n-1) \times 1$ column vector of partial molar volumes:

$$\overline{\boldsymbol{V}_\nu} := \Big(\frac{\partial \boldsymbol{\mu}_\nu}{\partial p}\Big)_{T, \boldsymbol{x}_\nu = \text{constant.}} \tag{3.20}$$

Equation (3.20) is analogous to the Maxwell relation eq. (1.11a), now expressed in the salt-charge basis. Partial molar volumes can be recovered from mass-density measurements using Newman's formula [86, appendix A]. Both $\boldsymbol{X}_\nu^0$ and $\overline{\boldsymbol{V}_\nu}$ are functions of $(T, p, \boldsymbol{x}_\nu)$ only.

3.2.3 Augmentation strategy

As mentioned previously, the isothermal Onsager transport matrix $\mathbf{M}$ has a nullspace of dimension one, and only $n-1$ of the OSM equations in eq. (3.6) are linearly independent. It is the mass-average constraint eq. (3.4), in conjunction with the OSM equations eq. (3.6), that allows for the molar fluxes to be uniquely determined. To weakly enforce the mass-average constraint at the discrete level and simultaneously address the fact that $\mathbf{M}$ is singular, we employ the augmentation strategy introduced in [45, 64] and used in [4, 112] and chapter 2. In the present transformed setting, we introduce a user-chosen augmentation parameter $\gamma > 0$ and add a multiple of the mass-average constraint eq. (3.16) to the OSM equation eq. (3.17) in the following way:

$$-\nabla \boldsymbol{\mu}_Z + \boldsymbol{\psi}_Z \nabla p + \gamma \boldsymbol{\psi}_Z v = \gamma \boldsymbol{\psi}_Z \boldsymbol{\psi}_Z^\top \boldsymbol{N}_Z + \mathbf{M}_Z \boldsymbol{N}_Z = \mathbf{M}_Z^\gamma \boldsymbol{N}_Z \quad \text{in } \Omega, \tag{3.21}$$

where $\mathbf{M}_Z^\gamma := \gamma \boldsymbol{\psi}_Z \boldsymbol{\psi}_Z^\top + \mathbf{M}_Z$ is a nonsingular augmented transport matrix. Following [4] and chapter 2, for symmetry we also incorporate the mass-average constraint in eq. (3.2) through

$$\frac{\partial(\rho v)}{\partial t} + \nabla \cdot (\rho v \otimes v) + \nabla p + \gamma(v - \boldsymbol{\psi}_Z^\top \boldsymbol{N}_Z) - \nabla \cdot \tau = \rho f \quad \text{in } \Omega. \tag{3.22}$$

We also only explicitly enforce the divergence of the mass-average constraint, i.e.

$$\nabla \cdot v = \nabla \cdot (\boldsymbol{\psi}_Z^\top \boldsymbol{N}_Z) \quad \text{in } \Omega. \tag{3.23}$$

We shall employ the augmented equations eqs. (3.21) to (3.23) because they yield a system with the same number of equations as unknowns, and, in an appropriate Picard linearised setting, yield a well-posed symmetric saddle point problem (as shown in [4] and chapter 2).

3.2.4 Full problem formulation

Our final formulation of the electroneutral NSOSM problem comprises the following set of equations, taken from eq. (3.15), eq. (3.22), eq. (3.23) and combining eq. (3.19) with eq. (3.21). The unknown functions of space and time to be solved for are the velocity v, transformed fluxes $\boldsymbol{N}_\nu$, current density I, pressure p, transformed mole fractions $\boldsymbol{x}_\nu$ and salt-charge potential Φ_Z, such that:

$$\frac{\partial(\rho v)}{\partial t} + \nabla \cdot (\rho v \otimes v) + \nabla p + \gamma(v - \boldsymbol{\psi}_Z^\top \boldsymbol{N}_Z) - \nabla \cdot \tau = \rho f \qquad \text{in } \Omega, \tag{3.24a}$$

$$- \begin{bmatrix} RT\boldsymbol{X}_\nu^0 & 0 \\ 0 & F\,\|\boldsymbol{z}\| \end{bmatrix} \begin{bmatrix} \nabla \boldsymbol{x}_\nu \\ \nabla \Phi_Z \end{bmatrix} + \left\{ \boldsymbol{\psi}_Z - \begin{bmatrix} \overline{\boldsymbol{V}_\nu} \\ 0 \end{bmatrix} \right\} \nabla p + \gamma \boldsymbol{\psi}_Z v = \mathbf{M}_Z^\gamma \boldsymbol{N}_Z \quad \text{in } \Omega, \tag{3.24b}$$

$$\nabla \cdot (v - \boldsymbol{\psi}_Z^\top \boldsymbol{N}_Z) = 0 \qquad \text{in } \Omega, \tag{3.24c}$$

$$\frac{\partial}{\partial t} \begin{bmatrix} \boldsymbol{c}_\nu \\ 0 \end{bmatrix} + \begin{bmatrix} \nabla \cdot \boldsymbol{N}_\nu \\ \nabla \cdot I \end{bmatrix} = 0 \qquad \text{in } \Omega. \tag{3.24d}$$

This problem must be supplemented with suitable initial and boundary conditions, which we discuss in forthcoming sections.

We recall how all quantities appearing in eq. (3.24) depend on the unknowns. The viscous stress τ in eq. (3.24a) is given by eq. (3.5) and the viscosities in eq. (3.5) are assumed to be known functions of $(T, p, \boldsymbol{x}_\nu)$. The vector $\boldsymbol{N}_Z$ was defined in eq. (3.14) and is simply a concatenation of the fluxes $\boldsymbol{N}_\nu$ and scaled current density I. The constant $\gamma > 0$ is a user-chosen augmentation parameter and f is a known forcing term. All remaining quantities in eq. (3.24) are assumed to be known Lipschitz continuous functions of $(T, p, \boldsymbol{x}_\nu)$. The density ρ, concentrations $\boldsymbol{c}_\nu$ and partial molar volumes $\overline{\boldsymbol{V}_\nu}$ can be determined as functions of $(T, p, \boldsymbol{x}_\nu)$ using the volumetric EOS. The vector $\boldsymbol{\psi}_Z = \boldsymbol{Z}\boldsymbol{m}/\rho$ depends on ρ only. The matrix $\boldsymbol{X}_\nu^0$ of thermodynamic factors can be expressed in terms of $(n-1)(n-2)/2$ independent Darken factors, while the transport matrix $\mathbf{M}_Z^\gamma$ can be expressed in terms of $n(n-1)/2$ independent Stefan–Maxwell diffusivities [114]. The dependence of these material parameters on $(T, p, \boldsymbol{x}_\nu)$ is typically modelled by fitting experimental data.

3.3 Spatial discretisation

In this section, we introduce finite element methods to spatially discretise the electroneutral NSOSM equations eq. (3.24) in steady form:

$$\nabla \cdot (\rho v \otimes v) + \nabla p + \gamma(v - \boldsymbol{\psi}_Z^\top \boldsymbol{N}_Z) - \nabla \cdot \tau = \rho f \qquad \text{in } \Omega, \quad (3.25a)$$

$$-\begin{bmatrix} RT\boldsymbol{X}_\nu^0 & 0 \\ 0 & F\,\|\boldsymbol{z}\| \end{bmatrix} \begin{bmatrix} \nabla \boldsymbol{x}_\nu \\ \nabla \Phi_Z \end{bmatrix} + \left\{ \boldsymbol{\psi}_Z - \begin{bmatrix} \overline{\boldsymbol{V}_\nu} \\ 0 \end{bmatrix} \right\} \nabla p + \gamma \boldsymbol{\psi}_Z v = \mathbf{M}_Z^\gamma \boldsymbol{N}_Z \quad \text{in } \Omega, \quad (3.25b)$$

$$\nabla \cdot (v - \boldsymbol{\psi}_Z^\top \boldsymbol{N}_Z) = 0 \qquad \text{in } \Omega, \quad (3.25c)$$

$$\nabla \cdot \boldsymbol{N}_\nu = 0 \qquad \text{in } \Omega, \quad (3.25d)$$

$$\nabla \cdot I = 0 \qquad \text{in } \Omega. \quad (3.25e)$$

The steady problem eq. (3.25) must be supplemented with suitable boundary conditions and integral constraints, which we now describe.

3.3.1 Boundary conditions

Let $\Gamma := \partial\Omega$ denote the boundary of Ω and $\hat{n}_\Gamma$ the unit outward normal on Γ. We consider the following flux[7] boundary conditions:

$$v = [(\boldsymbol{\psi}_Z^\top \boldsymbol{N}_Z) \cdot \hat{n}_\Gamma]\hat{n}_\Gamma + g_{v_\parallel} \quad \text{on } \Gamma, \qquad (3.26a)$$

$$(\boldsymbol{N}_\nu)_i \cdot \hat{n}_\Gamma = g_i \quad \text{on } \Gamma \quad \forall i \in \{1 : n-1\}, \qquad (3.26b)$$

$$I \cdot \hat{n}_\Gamma = g_I \quad \text{on } \Gamma. \qquad (3.26c)$$

The functions $g_{v_\parallel} : \Gamma \to \mathbb{R}^d$, $g_i : \Gamma \to \mathbb{R}$ and $g_I : \Gamma \to \mathbb{R}$ are prescribed data. We assume $g_{v_\parallel} \cdot \hat{n}_\Gamma = 0$ on Γ, so that eq. (3.26a) enforces the mass-average constraint eq. (3.16) in the normal direction and $v = g_{v_\parallel}$ in the tangential directions.

In practical applications the prescribed normal fluxes g_i and g_I may be known algebraic functions of the state variables $(T, p, \boldsymbol{x}_\nu)$ and Φ_Z. We shall allow for such dependencies. An example is that of a Butler–Volmer boundary condition [27, 36, 44, 86], which on an electrode interface $\Gamma_\mathrm{e} \subset \Gamma$ relates the normal component of current density to the *overpotential*. The overpotential quantifies the electrical potential difference across the interface. Butler–Volmer BCs generally depend on $(T, p, \boldsymbol{x}_\nu)$ and Φ_Z nonlinearly, and we consider this case in section 3.5. However, if the overpotential

[7] We do not consider Dirichlet BCs in this section, but see section 3.5.2 for an example of how they can be implemented.

is sufficiently small and its dependence on electrolyte composition is negligible, it is worth noting that Butler–Volmer BCs may be approximated by a linear relation [86]

$$g_I = -i_0 \frac{n_e F}{RT}(V_\mathrm{e} - \Phi_Z) \quad \text{on } \Gamma_\mathrm{e}. \tag{3.27}$$

Here i_0 denotes the *exchange-current density*, which generally depends on $(T, p, \boldsymbol{x}_\nu)$. Furthermore, V_e denotes the electrode voltage, and n_e is a stoichiometric coefficient representing the number of electrons transferred in the electrode reaction.

3.3.2 Integral constraints

In general, the steady problem eq. (3.25) with boundary conditions eq. (3.26) is not uniquely solvable, and $1 \leq k \leq n+1$ additional constraints must be imposed for uniqueness. The necessity of such constraints in the uncharged, steady SOSM setting was pointed out in chapter 2. However, the present situation is more complicated than that of chapter 2 because we allow for the boundary data in eqs. (3.26b) to (3.26c) to depend on the local state of the mixture. Further complications will arise in section 3.4 when we consider the transient problem, but for now we focus on the steady case.

The need for constraints can be motivated as follows. Integrate the solenoidal condition eq. (3.25e) on I over Ω and use the divergence theorem together with the BC eq. (3.26c) to obtain a fundamental *compatibility condition* on the problem data:

$$\int_\Gamma g_I \,\mathrm{d}\Gamma = 0, \tag{3.28}$$

which states that the total charge flux into the electroneutral mixture is zero. By contrast, in a general electrolytic cell the total component molar fluxes need not be zero, unless the mixture is at a steady state. In the steady case, however, the continuity equations eq. (3.25d) and BCs eq. (3.26b) yield $n-1$ additional compatibility conditions:

$$\int_\Gamma g_i \,\mathrm{d}\Gamma = 0 \quad \forall i \in \{1 : n-1\}. \tag{3.29}$$

For the steady problem eq. (3.25) with BCs eq. (3.26) to admit a solution, the conditions in eqs. (3.28) and (3.29) must be satisfiable. Assuming this is so, let $l \leq n$ denote the number of independent constraints that eqs. (3.28) and (3.29) impose on the unknowns $(p, \boldsymbol{x}_\nu, \Phi_Z)$ due to their (possible) appearance in g_I and g_i. Finally, similarly integrate eq. (3.25c) over Ω and use the BC eq. (3.26a) to obtain an $(n+1)$-th compatibility condition

$$\int_\Gamma g_{v_\parallel} \cdot \hat{n}_\Gamma \,\mathrm{d}\Gamma = 0, \tag{3.30}$$

which holds automatically since $g_{v_\parallel} \cdot \hat{n}_\Gamma = 0$. Hence, we have shown that integrating the $n+1$ equations in eqs. (3.25c) to (3.25e) over Ω leads to only $l \leq n$ independent constraints on the solution. An additional $k = n + 1 - l$ constraints must therefore be imposed for uniqueness. The same argument will apply at the discrete level. Namely, if D denotes the number of discrete degrees of freedom, then discretisation of eqs. (3.25) to (3.26) will result in a system of D equations, but only $D - k$ of these will be independent. This motivates why k additional constraints are needed for uniqueness. We will give examples of choices of constraints in section 3.3.6. Note that these constraints do not need to be integral constraints, but they usually are in practice.

3.3.3 Finite element spaces

We use the standard notation for Lebesgue and Sobolev spaces $L^2(\Omega)$, $W^{1,\infty}(\Omega)$, $H^1(\Omega)$, $H(\mathrm{div};\Omega)$ and their norms [48]. We use $(\cdot,\cdot)_\Omega$ and $\langle\cdot,\cdot\rangle_\Gamma$ to denote the L^2-inner products on Ω and Γ respectively. Moreover, we write $L^2_0(\Omega) := \{q \in L^2(\Omega) : (q,1)_\Omega = 0\}$ for the subspace of functions in $L^2(\Omega)$ with vanishing mean. We write $H^1_0(\Omega) := \{u \in H^1(\Omega) : u|_\Gamma = 0\}$ and $H_0(\mathrm{div};\Omega) := \{u \in H(\mathrm{div};\Omega) : (u \cdot \hat{n}_\Gamma)|_\Gamma = 0\}$ for subspaces with vanishing traces.

To discretise eq. (3.25) we introduce finite dimensional finite element subspaces that may depend on a parameter $h \in (0,\infty)$ representing, for example, the mesh size:

$$\mathcal{V}_h \subset H^1(\Omega)^d, \qquad \mathcal{V}_{0h} := \mathcal{V}_h \cap H^1_0(\Omega)^d, \tag{3.31a}$$

$$\mathcal{P}_h \subset L^2(\Omega), \qquad \mathcal{P}_{0h} := \mathcal{P}_h \cap L^2_0(\Omega), \tag{3.31b}$$

$$\mathcal{N}_h \subset H(\mathrm{div};\Omega), \qquad \mathcal{N}_{0h} := \mathcal{N}_h \cap H_0(\mathrm{div};\Omega), \tag{3.31c}$$

$$\mathcal{X}_h \subset L^2(\Omega), \qquad \mathcal{X}_{0h} := \mathcal{X}_h \cap L^2_0(\Omega). \tag{3.31d}$$

Importantly, we assume $\mathcal{P}_h$ and $\mathcal{X}_h$ contain the constant functions, i.e. $1 \in \mathcal{P}_h \cap \mathcal{X}_h$.

We shall seek the discrete velocity $v_h \in \mathcal{V}_h$ and pressure $p_h \in \mathcal{P}_h$. We assume that $(\mathcal{V}_h, \mathcal{P}_h)$ forms an inf-sup stable Stokes pair [49], in the sense that:

$$\beta \left\|q_h\right\|_{L^2(\Omega)} \leq \sup_{u_h \in \mathcal{V}_{0h}} \frac{(q_h, \nabla \cdot u_h)_\Omega}{\left\|u_h\right\|_{H^1(\Omega)^d}} \qquad \forall q_h \in \mathcal{P}_{0h}, \tag{3.32}$$

for some $\beta > 0$ independent of h. We shall seek the discrete fluxes $(\boldsymbol{N}_{\nu,h})_i \in \mathcal{N}_h$ for $i \in \{1 : n-1\}$ and current density $I_h \in \mathcal{N}_h$. We seek the discrete mole fractions

$(\boldsymbol{x}_{\nu,h})_i \in \mathcal{X}_h$ for $i \in \{1 : n-1\}$ and salt-charge potential $\Phi_{Z,h} \in \mathcal{X}_h$. We assume that $(\mathcal{N}_h, \mathcal{X}_h)$ forms a divergence-free and inf-sup stable mixed-Poisson pair [49], i.e. that:

$$\operatorname{div} \mathcal{N}_{0h} \subset \mathcal{X}_{0h} \quad \text{and} \quad \beta' \left\| y_h \right\|_{L^2(\Omega)} \leq \sup_{K_h \in \mathcal{N}_{0h}} \frac{(y_h, \nabla \cdot K_h)_\Omega}{\left\| K_h \right\|_{H(\operatorname{div};\Omega)}} \qquad \forall y_h \in \mathcal{X}_{0h}, \tag{3.33}$$

for some $\beta' > 0$ independent of h. Assumptions eqs. (3.32) and (3.33) are motivated by the analysis of chapter 2, where similar assumptions are shown to ensure well-posedness of a Picard linearised SOSM system (recall section 2.3).

Following chapter 2, in our numerical experiments we employ the degree $k \geq 2$ Taylor–Hood pair [17, 109] for $(\mathcal{V}_h, \mathcal{P}_h)$ (but cf. section 2.3 for a discussion of other choices, such as Scott–Vogelius [102]). For $(\mathcal{N}_h, \mathcal{X}_h)$ we employ either the $\mathbb{BDM}_k$–$\mathbb{DG}_{k-1}$ pair [22, 85] or the $\mathbb{RT}_k$–$\mathbb{DG}_{k-1}$ [96] pair. These spaces are standard in finite element software packages, extend to high orders, and are applicable in two or three spatial dimensions on triangular, tetrahedral, quadrilateral or hexahedral (possibly curved) meshes.

3.3.4 Lipschitz continuous reconstruction operators

Our discretisation in section 3.3.5 will involve integration-by-parts of the gradient terms on the left side of eq. (3.25b). This requires the entries of $\boldsymbol{X}_\nu^0$, $\boldsymbol{\psi}_Z$ and $\overline{\boldsymbol{V}_\nu}$ to lie in $W^{1,\infty}(\Omega)$. Discretisation of eq. (3.25c) will likewise require $\boldsymbol{\psi}_Z \in (W^{1,\infty}(\Omega))^n$. Recall that we assume these quantities to be known Lipschitz continuous functions of $(T, p, \boldsymbol{x}_\nu)$. However, at the discrete level, the spaces $\mathcal{P}_h$ or $\mathcal{X}_h$ may be discontinuous. For this reason we shall evaluate thermodynamic properties such as $\boldsymbol{X}_\nu^0$, $\boldsymbol{\psi}_Z$, $\overline{\boldsymbol{V}_\nu}$ using Lipschitz continuous reconstructions of p_h and $\boldsymbol{x}_{\nu,h}$. To be precise, we assume that smoothing operators

$$\pi_{\mathcal{P}_h} : \mathcal{P}_h \to \mathcal{P}_h \cap W^{1,\infty}(\Omega) \quad \text{and} \quad \pi_{\mathcal{X}_h} : \mathcal{X}_h \to \mathcal{X}_h \cap W^{1,\infty}(\Omega) \tag{3.34}$$

are available. In our numerical simulations we take $\pi_{\mathcal{P}_h}$ to be the $L^2(\Omega)$-projection of $\mathcal{P}_h$ into $\mathcal{P}_h \cap W^{1,\infty}(\Omega)$ and likewise for $\mathcal{X}_h$. Nodal averaging operators could alternatively be employed [47]. Given p_h and $\boldsymbol{x}_{\nu,h}$ we introduce their *reconstructions*

$$\widetilde{p_h} := \pi_{\mathcal{P}_h} p_h \quad \text{and} \quad \widetilde{(\boldsymbol{x}_{\nu,h})_i} := \pi_{\mathcal{X}_h}(\boldsymbol{x}_{\nu,h})_i \Big/ \sum_{j=1}^{n-1} (\boldsymbol{\nu}_Z)_j \cdot \pi_{\mathcal{X}_h}(\boldsymbol{x}_{\nu,h})_j. \tag{3.35}$$

Note that the reconstructed mole fractions are normalised to satisfy condition eq. (3.18) exactly. We then write $\widetilde{\boldsymbol{X}_\nu^0}$, $\widetilde{\boldsymbol{\psi}_Z}$, $\widetilde{\overline{\boldsymbol{V}_\nu}}$, $\widetilde{\rho}$, and so on, to denote quantities evaluated with the reconstructed $\widetilde{p_h}$ and $\widetilde{\boldsymbol{x}_{\nu,h}}$ instead of p_h and $\boldsymbol{x}_{\nu,h}$.

3.3.5 Discretised problem

Our discrete variational formulation of eq. (3.25) can be obtained by multiplying the equations with suitable test functions and integrating over Ω. The pressure and viscous terms in eq. (3.25a), as well as the gradient terms on the left side of eq. (3.25b), are integrated by parts, and all boundary terms vanish owing to our BCs in eq. (3.26). Following chapter 2 we also add *density consistency terms* (recall eq. (2.66)) to eq. (3.25c).

The precise discretisation we consider is as follows. We seek discrete functions $v_h \in \mathcal{V}_h$, $p_h \in \mathcal{P}_h$, $\boldsymbol{N}_{\nu,h} \in (\mathcal{N}_h)^{n-1}$, $I_h \in \mathcal{N}_h$, $\boldsymbol{x}_{\nu,h} \in (\mathcal{X}_h)^{n-1}$ and $\Phi_{Z,h} \in \mathcal{X}_h$. Let

$$\boldsymbol{N}_{Z,h} := \begin{bmatrix} \boldsymbol{N}_{\nu,h} \\ I_h^\top / (F\,\|z\|) \end{bmatrix} \in (\mathcal{N}_h)^n, \tag{3.36}$$

which is analogous to $\boldsymbol{N}_Z$ in eq. (3.14). The discrete variational problem reads:

$$\begin{aligned} &\big(\nabla\cdot(\widetilde{\rho}v_h\otimes v_h) + \gamma(v_h - \widetilde{\boldsymbol{\psi}_Z^\top}\boldsymbol{N}_{Z,h}) - \widetilde{\rho}f, u_h\big)_\Omega - \big(p_h, \nabla\cdot u_h\big)_\Omega \\ &+ \big(2\widetilde{\eta}\epsilon(v_h) + (\widetilde{\zeta} - 2\widetilde{\eta}/d)(\nabla\cdot v_h)\mathbb{I}, \epsilon(u_h)\big)_\Omega = 0 \quad \forall u_h \in \mathcal{V}_{0h}, \end{aligned} \tag{3.37a}$$

$$\begin{aligned} &\left(\begin{bmatrix}\boldsymbol{x}_{\nu,h}\\ \Phi_{Z,h}\end{bmatrix}, \nabla\cdot\begin{bmatrix} RT\widetilde{\boldsymbol{X}_\nu^0}\boldsymbol{W}_h \\ F\,\|\boldsymbol{z}\|\,K_h\end{bmatrix}\right)_\Omega - \left(p_h, \nabla\cdot\left\{\widetilde{\boldsymbol{\psi}_Z^\top}\begin{bmatrix}\boldsymbol{W}_h\\ K_h\end{bmatrix} - \widetilde{\overline{\boldsymbol{V}_\nu}^\top}\boldsymbol{W}_h\right\}\right)_\Omega \\ &+ \left(\gamma\widetilde{\boldsymbol{\psi}_Z}v_h, \begin{bmatrix}\boldsymbol{W}_h\\ K_h\end{bmatrix}\right)_\Omega = \left(\widetilde{\mathbf{M}_Z^\gamma}\boldsymbol{N}_{Z,h}, \begin{bmatrix}\boldsymbol{W}_h\\ K_h\end{bmatrix}\right)_\Omega \quad \forall \begin{bmatrix}\boldsymbol{W}_h\\ K_h\end{bmatrix} \in (\mathcal{N}_{0h})^n, \end{aligned} \tag{3.37b}$$

$$\Big(\nabla\cdot(v_h - \widetilde{\boldsymbol{\psi}_Z^\top}\boldsymbol{N}_{Z,h}), q_h\Big)_\Omega - \Big\langle \hat{n}_\Gamma\cdot(v_h - \widetilde{\boldsymbol{\psi}_Z^\top}\boldsymbol{N}_{Z,h}), q_h\Big\rangle_\Gamma = 0 \quad \forall q_h \in \mathcal{P}_h, \tag{3.37c}$$

$$\big(\nabla\cdot\boldsymbol{N}_{Z,h}, \boldsymbol{y}_h\big)_\Omega = 0 \quad \forall \boldsymbol{y}_h \in (\mathcal{X}_h)^n. \tag{3.37d}$$

Moreover, we strongly impose the following discrete analogue of the BCs in eq. (3.26):

$$v_h = \pi_{\mathcal{V}_h}\Big([(\widetilde{\boldsymbol{\psi}_Z^\top}\boldsymbol{N}_{Z,h})\cdot\hat{n}_\Gamma]\hat{n}_\Gamma + g_{v_\parallel}\Big) \quad \text{on } \Gamma, \tag{3.38a}$$

$$(\boldsymbol{N}_{\nu,h})_i\cdot\hat{n}_\Gamma = \pi_{\mathcal{N}_h}(\widetilde{g_i}) \quad \text{on } \Gamma \quad \forall i \in \{1:n-1\}, \tag{3.38b}$$

$$I_h\cdot\hat{n}_\Gamma = \pi_{\mathcal{N}_h}(\widetilde{g_I}) \quad \text{on } \Gamma. \tag{3.38c}$$

Here $\pi_{\mathcal{V}_h}$ and $\pi_{\mathcal{N}_h}$ are $L^2(\Gamma)$-projection operators onto the discrete trace spaces[8]

$$\pi_{\mathcal{V}_h} : [L^2(\Gamma)]^d \to \{u_h|_\Gamma : u_h \in \mathcal{V}_h\} \subset [L^2(\Gamma)]^d, \tag{3.39a}$$

$$\pi_{\mathcal{N}_h} : L^2(\Gamma) \to \{(K_h\cdot\hat{n}_\Gamma)|_\Gamma : K_h \in \mathcal{N}_h\} \subset L^2(\Gamma). \tag{3.39b}$$

Conditions eqs. (3.37) to (3.38) define our discrete scheme.

[8]For eq. (3.39b) to be well-defined, we implicitly assume $(K_h\cdot\hat{n}_\Gamma)|_\Gamma \in L^2(\Gamma)\ \forall K_h \in \mathcal{N}_h$. In practice, the finite element space $\mathcal{N}_h$ will consist of piecewise smooth functions, so that this indeed holds.

3.3.6 Integral constraints in the discrete setting

As already discussed in section 3.3.2, for uniqueness of a solution to the discretised problem eqs. (3.37) to (3.38), additional constraints must be supplied. To see this at the discrete level, let $D := \dim\left(\mathcal{V}_h \times \mathcal{P}_h \times (\mathcal{N}_h)^n \times (\mathcal{X}_h)^n\right)$ and note that, once a finite element basis has been chosen, the problem eqs. (3.37) to (3.38) amounts to a non-linear system of D equations in D unknowns. However, notice that eq. (3.37c) holds automatically when q_h is a constant, as verified from integration by parts (analogous to the way eq. (3.30) holds automatically). This property is one way of motivating density consistency terms (i.e. the boundary terms, as in eq. (2.66)) in eq. (3.37c). Also, taking the entries of $\boldsymbol{y}_h$ to be constants in eq. (3.37d), integrating by parts and using eqs. (3.38b) to (3.38c) yields (in analogy to eqs. (3.28) and (3.29))

$$\int_\Gamma \pi_{\mathcal{N}_h}\left(\widetilde{g}_i\right) \mathrm{d}\Gamma = 0 \quad \forall i \in \{1 : n-1\} \quad \text{and} \quad \int_\Gamma \pi_{\mathcal{N}_h}\left(\widetilde{g}_I\right) \mathrm{d}\Gamma = 0. \tag{3.40}$$

Let $l \leq n$ denote the number of independent constraints that eq. (3.40) imposes on the discrete solution. Problem eqs. (3.37) to (3.38) then consists of only $D - k$ independent equations, where $k = n + 1 - l$. Hence, an additional k constraints must be imposed.

Since $k \geq 1$, at least one constraint is always required. This constraint does not encode physical information, and instead reflects our choice to solve for $n - 1$ transformed mole fractions despite the fact that only $n - 2$ of them are independent. Following chapter 2 (specifically eq. (2.60)) we impose the normalization condition eq. (3.18) on average over Ω:

$$\int_\Omega (\boldsymbol{\nu}_Z^\top \boldsymbol{x}_{\nu,h} - 1) \, \mathrm{d}\Omega = 0. \tag{3.41}$$

Together with eq. (3.41), the remaining $k - 1$ constraints must be chosen on a case-by-case basis. What choices of constraints are appropriate will depend on BCs and the functional dependence of the thermodynamic properties (i.e. the properties in eq. (3.37) with a tilde) on p and $\boldsymbol{x}_\nu$. We now give examples of this for concreteness.

Case (i): The BCs in eqs. (3.26b) *and* (3.26c) *do not depend on* p, $\boldsymbol{x}_\nu$ *or* Φ_Z. In this case, the compatibility conditions eq. (3.40) do not impose any constraints on the solution, so $l = 0$ and n additional constraints are required. Since no thermodynamic properties depend on Φ_Z, this field is then undetermined up to an additive constant, which can be fixed through a constraint such as $\int_\Omega \Phi_{Z,h} \, \mathrm{d}\Omega = 0$. If no thermodynamic properties depend on p then it too is undetermined up to an additive constant, which can be fixed by means of $\int_\Omega p_h \, \mathrm{d}\Omega = 0$. However, if any of thermodynamic properties

depend on p then additive shifts of p_h by a constant affect the physical content of the model. In this case, constraints of the form $\int_\Omega (p_h - \bar{p})\,\mathrm{d}\Omega = 0$ may be used, where $\bar{p} \in \mathbb{R}$ is a user-prescribed mean pressure. If the volumetric EOS depends on p (equivalently if ρ depends on p) then an alternative constraint that is more harmonious with experimentally available information may be $\int_\Omega \widetilde{\rho}\,\mathrm{d}\Omega = M^{\mathrm{tot}}$, where $M^{\mathrm{tot}} \in \mathbb{R}$ is the user-prescribed total mass of fluid in Ω. The final $n-2$ constraints may be chosen to express the relative abundances of the components in Ω. For example, one may use $\int_\Omega \widetilde{(\boldsymbol{c}_\nu)}_i\,\mathrm{d}\Omega = c_i^{\mathrm{tot}}$ for $i \in \mathscr{S}$, where $\mathscr{S} \subset \{1 : n-1\}$ contains $n-2$ indices, and $c_i^{\mathrm{tot}} \in \mathbb{R}$ are user-prescribed total numbers of moles of the components in Ω.

Case (ii): The BCs in eqs. (3.26b) *and* (3.26c) *depend on the local state of the mixture.* To illustrate how solution-dependent BCs fit into this framework, consider the case of an electrolytic cell where g_I follows a Butler–Volmer-type relation in eq. (3.27) or some nonlinear analogue of this, while $g_i = \alpha_i g_I/F$ on Γ for $i \in \{1 : n-1\}$ with $\{\alpha_i\}_{i=1}^{n-1}$ a set of known constants. These BCs model electrode kinetics, and the α_i relate to the stoichiometric coefficients of the electrode reaction[9]. Since each g_i is a multiple of g_I, the compatibility conditions in eq. (3.40) impose exactly one constraint on the solution, so $l = 1$ and $n-1$ additional constraints are required. Since Φ_Z appears in the BC eq. (3.27) it is no longer necessary (or physically reasonable) to fix $\int_\Omega \Phi_{Z,h}\,\mathrm{d}\Omega = 0$. Instead, the $n-1$ constraints should be chosen to determine the pressure and relative component abundances, as in case (i).

3.4 Temporal discretisation

Our spatial discretisation from section 3.3 can be applied in the transient setting using the method of lines. However, special care must be taken to address the subtle interplay between the component mass continuity equations, boundary conditions, volumetric EOS and integral constraints.

3.4.1 Semi-discrete problem

Discretisation in space (but not time) of the transient problem eq. (3.24) yields the following semi-discrete analogue of eq. (3.37). We seek time-dependent discrete functions $v_h \in \mathcal{V}_h$, $p_h \in \mathcal{P}_h$, $\boldsymbol{N}_{\nu,h} \in (\mathcal{N}_h)^{n-1}$, $I_h \in \mathcal{N}_h$, $\boldsymbol{x}_{\nu,h} \in (\mathcal{X}_h)^{n-1}$ and $\Phi_{Z,h} \in \mathcal{X}_h$ such

[9]Generally the value of α_i can differ on the anode and cathode; we assume here it is the same on both (this holds, for example, in symmetric cells and lithium-ion battery cells). The relation $g_i = \alpha_i g_I/F$ is also valid on the insulating walls of the cell since therein both g_i and g_I are zero.

that:

$$\frac{\mathrm{d}}{\mathrm{d}t}\big(\widetilde{\rho}v_h, u_h\big)_\Omega + \ \big(\nabla\cdot(\widetilde{\rho}v_h\otimes v_h) + \gamma(v_h - \widetilde{\boldsymbol{\psi}_Z^\top}\boldsymbol{N}_{Z,h}) - \widetilde{\rho}f, u_h\big)_\Omega$$
$$- \ \big(p_h, \nabla\cdot u_h\big)_\Omega + \ \big(2\widetilde{\eta}\epsilon(v_h) + (\widetilde{\zeta} - 2\widetilde{\eta}/d)(\nabla\cdot v_h)\mathbb{I}, \epsilon(u_h)\big)_\Omega = 0 \quad \forall u_h \in \mathcal{V}_{0h}, \tag{3.42a}$$

$$\left(\begin{bmatrix}\boldsymbol{x}_{\nu,h}\\ \Phi_{Z,h}\end{bmatrix}, \nabla\cdot\begin{bmatrix}RT\widetilde{\boldsymbol{X}_\nu^0}\boldsymbol{W}_h\\ F\,\|\boldsymbol{z}\|\,K_h\end{bmatrix}\right)_\Omega - \left(p_h, \nabla\cdot\left\{\widetilde{\boldsymbol{\psi}_Z^\top}\begin{bmatrix}\boldsymbol{W}_h\\ K_h\end{bmatrix} - \widetilde{\boldsymbol{V}_\nu^\top}\boldsymbol{W}_h\right\}\right)_\Omega$$
$$+ \ \left(\gamma\widetilde{\boldsymbol{\psi}_Z}v_h, \begin{bmatrix}\boldsymbol{W}_h\\ K_h\end{bmatrix}\right)_\Omega = \left(\widetilde{\mathbf{M}_Z^\gamma}\boldsymbol{N}_{Z,h}, \begin{bmatrix}\boldsymbol{W}_h\\ K_h\end{bmatrix}\right)_\Omega \quad \forall\begin{bmatrix}\boldsymbol{W}_h\\ K_h\end{bmatrix} \in (\mathcal{N}_{0h})^n, \tag{3.42b}$$

$$\Big(\nabla\cdot(v_h - \widetilde{\boldsymbol{\psi}_Z^\top}\boldsymbol{N}_{Z,h}), q_h\Big)_\Omega - \Big\langle\hat{n}_\Gamma\cdot(v_h - \widetilde{\boldsymbol{\psi}_Z^\top}\boldsymbol{N}_{Z,h}), q_h\Big\rangle_\Gamma = 0 \quad \forall q_h \in \mathcal{P}_h, \tag{3.42c}$$

$$\frac{\mathrm{d}}{\mathrm{d}t}\left(\begin{bmatrix}\widetilde{\boldsymbol{c}_{\nu,h}}\\ 0\end{bmatrix}, \boldsymbol{y}_h\right)_\Omega + \big(\nabla\cdot\boldsymbol{N}_{Z,h}, \boldsymbol{y}_h\big)_\Omega = 0 \quad \forall \boldsymbol{y}_h \in (\mathcal{X}_h)^n. \tag{3.42d}$$

We supplement this problem with the same strongly enforced BCs eq. (3.38) from the steady case, and we permit the boundary data to depend on time.

3.4.2 Integral constraints in the transient setting

As in the steady case, problem eq. (3.42) with BCs eq. (3.38) requires integral constraints for well-posedness. However, the interplay between the BCs, volumetric EOS and mass continuity equations becomes especially important in the transient setting, as we now elucidate through considerations similar to those in section 3.3.6.

First, note that eq. (3.42c) holds automatically when $q_h = 1$, as in the steady case. This suggests that at least one integral constraint will be needed for well-posedness. Next, taking constant entries of $\boldsymbol{y}_h$ in eq. (3.42d) yields, similarly to eq. (3.40), that

$$\frac{\mathrm{d}}{\mathrm{d}t}\int_\Omega (\widetilde{\boldsymbol{c}_{\nu,h}})_i \,\mathrm{d}\Omega + \int_\Gamma \pi_{\mathcal{N}_h}\big(\widetilde{g_i}\big)\,\mathrm{d}\Gamma = 0 \quad \forall i \in \{1 : n-1\}, \tag{3.43a}$$

$$\int_\Gamma \pi_{\mathcal{N}_h}\big(\widetilde{g_I}\big)\,\mathrm{d}\Gamma = 0. \tag{3.43b}$$

If g_I depends on Φ_Z by a Butler–Volmer-type BC eq. (3.27), then eq. (3.43b) constrains additive shifts in $\Phi_{Z,h}$. Otherwise, assuming g_I does not depend on p, $\boldsymbol{x}_\nu$ or Φ_Z and none of the g_i depend on Φ_Z, the (consequently undetermined) additive constant in $\Phi_{Z,h}$ can be fixed by an extra constraint $\int_\Omega \Phi_{Z,h}\,\mathrm{d}\Omega = 0$. This leaves us to consider eq. (3.43a).

To study eq. (3.43a) we assume a confined flow, in the sense that the total normal fluxes over Γ are zero. In other words, we assume that the g_i satisfy

$$\int_\Gamma \pi_{\mathcal{N}_h}(\widetilde{g_i})\,\mathrm{d}\Gamma = 0 \quad \forall i \in \{1 : n-1\}, \tag{3.44}$$

so that the compatibility conditions in eq. (3.43a) become

$$\frac{\mathrm{d}}{\mathrm{d}t}\int_\Omega (\widetilde{\boldsymbol{c}_{\nu,h}})_i\,\mathrm{d}\Omega = 0 \quad \forall i \in \{1 : n-1\}, \tag{3.45}$$

which physically states that the total number of moles of all components is conserved. Note that eq. (3.44) is satisfied whenever $g_i = \alpha_i g_I/F$ for some constants $\{\alpha_i\}_{i=1}^{n-1}$ (e.g. in symmetric cells or lithium-ion battery cells), since g_I satisfies eq. (3.43b). We now investigate how many of the $n-1$ conditions in eq. (3.45) are actually independent. Note that a general volumetric EOS relates the total concentration c_T to the partial molar volumes $\overline{\boldsymbol{V}_\nu}^\top$ and mole fractions $\boldsymbol{x}_\nu$ by (recall eq. (1.13))

$$c_T^{-1} = \overline{\boldsymbol{V}_\nu}^\top \boldsymbol{x}_\nu. \tag{3.46}$$

Hence, multiplying eq. (3.46) by c_T, we see that the entries of $\widetilde{\boldsymbol{c}_{\nu,h}}$ are related by

$$1 = \widetilde{\overline{\boldsymbol{V}_\nu}}^\top \widetilde{\boldsymbol{c}_{\nu,h}}. \tag{3.47}$$

In light of eq. (3.47), it is clear that the total molar conservation conditions eq. (3.45) may not all be independent, or may even be overdetermined. This leads us to consider three pertinent cases, depending on the functional dependence of $\overline{\boldsymbol{V}_\nu}$ on p and $\boldsymbol{x}_\nu$.

Case (i): The partial molar volumes are constant. In liquid mixtures it is often reasonable to approximate the partial molar volumes $\overline{\boldsymbol{V}_\nu}$ as being constant (recall the discussion following eq. (1.30); see also [41]). It is then clear from eq. (3.47) that only $n-2$ of the conditions in eq. (3.45) are independent. If any $n-2$ of these conditions hold, then the final one will hold as well. Thus, in this case, we must impose two additional constraints (recall that the other constraint comes from taking $q_h = 1$ in eq. (3.42c)). A reasonable choice is to enforce eq. (3.41) and a constraint that fixes the pressure such as $\int_\Omega (p_h - \bar{p})\,\mathrm{d}\Omega = 0$. If the partial molar volumes are constant then $\boldsymbol{X}_\nu^0, \rho$ and $\boldsymbol{\psi}_Z$ are independent of p. If η, ζ and $\mathbf{M}_Z$ are also modelled as being independent of p, and p does not appear in the BCs, then the user-chosen value of $\bar{p}$ will not affect the physical content of the model.

Case (ii): The partial molar volumes depend on $\boldsymbol{x}_\nu$ but not p. If the partial molar volumes are non-constant (which happens only if they depend on p or $\boldsymbol{x}_\nu$), then the

conditions in eq. (3.45) are generally independent. One must then consider whether they can all be satisfied simultaneously. If the partial molar volumes $\overline{\boldsymbol{V}_\nu}$ depend on $\boldsymbol{x}_\nu$ only, then the set of admissible concentrations $\boldsymbol{c}_\nu$ is parametrised by $\boldsymbol{x}_\nu$. Since only $n-2$ entries of $\boldsymbol{x}_\nu$ are independent, it does not seem reasonable to expect that all $n-1$ conditions in eq. (3.45) can be satisfied simultaneously, and we hypothesise that in this case the model problem eq. (3.24) may not be well-posed. We give an explicit example of how this case can produce an ill-posed model in appendix A.1.

Challengingly, in real electrolytes the partial molar volumes can vary appreciably with composition but negligibly with pressure [86, 117, 118]. To overcome the challenge of an ill-posed model one can explicitly include pressure dependence in $\overline{\boldsymbol{V}_\nu}$. In other words, one can take the bulk modulus (recall eq. (1.30)) to be small, but non-zero. However, if this dependence is too small, then to satisfy all $n-1$ conditions in eq. (3.45) the pressure may be forced to grow unphysically large. We hypothesise that this challenge could be overcome by allowing the volume of Ω to vary in time (i.e. the total volume the electrolyte occupies may vary). However, attempting this lies outside the scope of this thesis, since it would (very challengingly) require both extending the model and numerically solving a moving boundary problem. A simpler fix may be to use BCs that do not satisfy eq. (3.44) and instead allow electrolyte to "leak" into or out of Ω.

Case (iii): The partial molar volumes depend on both p and $\boldsymbol{x}_\nu$. As alluded to case (ii), if $\overline{\boldsymbol{V}_\nu}$ depends on both p and $\boldsymbol{x}_\nu$, then the set of admissible concentrations $\boldsymbol{c}_\nu$ is parametrised by the $n-1$ independent quantities $(p, \boldsymbol{x}_\nu)$. We therefore heuristically expect all $n-1$ conditions in eq. (3.45) to be satisfiable. In this case, only one additional constraint is needed (from taking $q_h = 1$ in eq. (3.42c)), and we suggest employing eq. (3.41).

Our analysis of cases (i)-(iii) only involves the total molar conservation conditions eq. (3.45) and the volumetric EOS eq. (3.46). In particular, our considerations are applicable to any transient multicomponent fluid model with a general volumetric EOS. We are not aware of these considerations being discussed elsewhere in the literature; particularly that of case (ii) where a seemingly physical choice of EOS can lead to an ill-posed problem. Although we are aware of numerical works [24, 37], which employ the EOS eq. (3.46) with constant partial molar volumes, they do not touch on the possibility of case (ii) and its associated challenges. Therefore, we believe that our considerations here may be of general interest to the multicomponent fluids community.

3.4.3 Time-stepping methods

The semi-discrete problem eq. (3.42), together with strongly enforced BCs eq. (3.38) and appropriate integral constraints of section 3.4.2, amounts to a nonlinear system of differential-algebraic equations (DAEs). We choose to solve these DAEs using implicit Runge–Kutta methods, because of their desirable stability properties and ability to provide high-order temporal accuracy [120].

3.5 Numerical examples

Our subsequent numerical examples are implemented using Firedrake [63]. We use Irksome [51, 71] for timestepping and ngsPETSc [12, 101] for mesh generation. We solve the nonlinear systems with Newton's method [35] and the sparse direct solver MUMPS [1]. Code can be found at https://bitbucket.org/abaierr/multicomponent_electrolyte_code.

3.5.1 Hull cell electroplating

To demonstrate our methods in a physically realizable setting, we simulate transient electroplating of a non-ideal binary electrolyte in a Hull cell geometry in two and three spatial dimensions. The two-dimensional domain $\Omega^{2\mathrm{D}}$ is a right trapezoid with vertices $(0,0)$, $(0,5)$, $(5,5)$ and $(10,0)$. Here, a unit of length corresponds to a physical length of 1 mm. We partition the boundary as $\partial\Omega^{2\mathrm{D}} = \Gamma_p^{2\mathrm{D}} \cup \Gamma_n^{2\mathrm{D}} \cup \Gamma_w^{2\mathrm{D}}$ where $\Gamma_p^{2\mathrm{D}}$ is the line segment between $(0,0)$ and $(0,5)$ and denotes the positive electrode, $\Gamma_n^{2\mathrm{D}}$ is the line segment between $(5,5)$ and $(10,0)$ and denotes the negative electrode, and $\Gamma_w^{2\mathrm{D}} = \partial\Omega^{2\mathrm{D}} \setminus (\Gamma_p^{2\mathrm{D}} \cup \Gamma_n^{2\mathrm{D}})$ are insulating walls. The three-dimensional domain is the extrusion of the two-dimensional domain by 5 units in the z-direction, i.e. $\Omega^{3\mathrm{D}} = \Omega^{2\mathrm{D}} \times (0,5)$ with $\Gamma_p^{3\mathrm{D}} = \Gamma_p^{2\mathrm{D}} \times (0,5)$, $\Gamma_n^{3\mathrm{D}} = \Gamma_n^{2\mathrm{D}} \times (0,5)$ and $\Gamma_w^{3\mathrm{D}} = \partial\Omega^{3\mathrm{D}} \setminus (\Gamma_p^{3\mathrm{D}} \cup \Gamma_n^{3\mathrm{D}})$. In what follows we may omit superscripts $\cdot^{2\mathrm{D}}$ and $\cdot^{3\mathrm{D}}$.

The electrolyte is composed of ethyl-methyl-carbonate (EMC) solvent and lithium hexafluorophosphate ($LiPF_6$) salt, a mixture used in lithium-ion batteries. In the notation of section 3.2, there are $n = 3$ species (EMC, Li^+ and $PF_6{}^-$) with molar masses $\boldsymbol{m} = [104.105, 6.935, 144.97]^\top \mathrm{g\,mol}^{-1}$ and equivalent charges $\boldsymbol{z} = [0, 1, -1]^\top$. We use the salt-charge transformation matrix eq. (3.13) with $\boldsymbol{\nu}_1^\top = [1,0,0]$ and $\boldsymbol{\nu}_2^\top = [0,1,1]$. This corresponds to neutralizing reactions EMC $\rightleftharpoons$ EMC and $Li^+ + PF_6{}^- \rightleftharpoons LiPF_6$. Hence, under the salt-charge transformation, the mole fractions $(\boldsymbol{x}_\nu)_i$, chemical potentials $(\boldsymbol{\mu}_\nu)_i$, fluxes $(\boldsymbol{N}_\nu)_i$ and so on, represent those of EMC for

$i = 1$ and $\mathrm{LiPF_6}$ for $i = 2$. We accordingly write $x_{\mathrm{EMC}} := (\boldsymbol{x}_\nu)_1$, $\mu_{\mathrm{EMC}} := (\boldsymbol{\mu}_\nu)_1$, $x_{\mathrm{LiPF_6}} := (\boldsymbol{x}_\nu)_2$, $\mu_{\mathrm{LiPF_6}} := (\boldsymbol{\mu}_\nu)_2$ and so on for $(\boldsymbol{N}_\nu)_i$.

The material properties are encoded in the functional dependence of η, ζ, ρ, $\boldsymbol{X}_\nu^0$ and $\mathbf{M}_Z$ on $(T, p, \boldsymbol{x}_\nu)$. We take an ambient temperature of $T = 298.15\,\mathrm{K}$. For the viscosities, we let η be a function of $\boldsymbol{x}_\nu$ as reported in [118, Table 2], and $\zeta = 10^{-6}\,\mathrm{Pa\,s}$. For ρ, $\boldsymbol{X}_\nu^0$ and $\mathbf{M}_Z$ we use the functional dependencies from [114, Table 1][10]. This leads to ρ depending on $\boldsymbol{x}_\nu$ only, and likewise for the (non-constant) partial molar volumes, placing us in case (ii) of section 3.4.2. The transport matrix $\mathbf{M}_Z$ also depends on $\boldsymbol{x}_\nu$ only, while $\boldsymbol{X}_\nu^0$ depends on both $\boldsymbol{x}_\nu$ and p, with the (negligibly small) dependence on p arising due to the non-constant partial molar volumes.

For boundary conditions on $\Gamma := \partial\Omega$ we use eq. (3.38a) with $g_{v_\parallel} = 0$. For the normal fluxes eqs. (3.38b) and (3.38c), we employ nonlinear Butler–Volmer BCs [36, 86]. Note that $\mu_{\mathrm{LiPF_6}}$ can be expressed as a known function of $(p, \boldsymbol{x}_\nu)$ only, by analytically integrating $\boldsymbol{X}_\nu^0$ and $\overline{\boldsymbol{V}_\nu}$ (cf. eq. (3.19)). The quantity $\Phi_Z - 0.5\mu_{\mathrm{LiPF_6}}/F$ then represents the potential of a reference electrode that reacts with the electrolyte through $\mathrm{Li} \rightleftharpoons \mathrm{Li^+} + \mathrm{e^-}$ [114]. We assume that the positive and negative electrodes Γ_e for $e \in \{p, n\}$ undergo the same reaction. Letting V_e denote the applied potential on electrode $e \in \{p, n\}$, and $i_0(\boldsymbol{x}_\nu)$ the exchange current density, we consider the BCs

$$g_I = -2i_0(\boldsymbol{x}_\nu)\sinh\left\{\frac{F\big[V_e - (\Phi_Z - 0.5\mu_{\mathrm{LiPF_6}}/F)\big]}{RT}\right\} \quad \text{on } \Gamma_e \text{ for } e \in \{p, n\}, \tag{3.48a}$$

$$g_I = 0 \quad \text{on } \Gamma_w, \tag{3.48b}$$

$$g_2 = g_I/(2F) \quad \text{on } \Gamma. \tag{3.48c}$$

Condition eq. (3.48a) is a standard Butler–Volmer BC, while eq. (3.48b) expresses the insulating property of the walls. Since $\boldsymbol{N} = \boldsymbol{Z}^\top \boldsymbol{N}_Z$, condition eq. (3.48c) states that the normal flux of $\mathrm{PF_6^-}$ is zero on Γ (since the electrodes only react with $\mathrm{Li^+}$). We model i_0 by $i_0(\boldsymbol{x}_\nu) = i_0^\ominus (x_{\mathrm{LiPF_6}}/x_{\mathrm{LiPF_6}}^\ominus)^{1/2}$, to resemble commonly used functional forms [86]. Moreover, we take $V_p = 0.1\,\mathrm{V}$, $V_n = 0\,\mathrm{V}$, $i_0^\ominus = 10^4\,\mathrm{A\,m^{-2}}$ and $x_{\mathrm{LiPF_6}}^\ominus = 0.075$.

Since we are in case (ii) of section 3.4.2 (non-constant partial molar volumes that do not depend on p), we do not expect a well-posed problem if no-flux BCs are imposed on EMC (i.e. $g_1 = 0$ on Γ in eq. (3.38b)). Instead we impose BCs that allow some EMC to "leak" from the positive electrode. As a simple model for this, we

[10] The formula for κ in [114, Table 1] has a typo and in the notation of that paper should read $\kappa = (48.93y_e^{3/2} - 284.8y_e^{5/2} + 817.8y_e^4)^2$. One can use the formulae from [114] to construct $\mathbf{M}_Z$, but note that the right side of [114, eq. (16.24)] is incorrect by a factor of -1.

assume a quadratic flux profile of EMC on the positive electrode, with the magnitude of the flux an unknown to be solved for. In particular, we take

$$g_1 = 0 \qquad \text{on } \Gamma_n \cup \Gamma_w, \tag{3.49a}$$

$$g_1 = \lambda_{\text{leak}} \cdot q_p \qquad \text{on } \Gamma_p, \tag{3.49b}$$

where $q_p : \Gamma_p \to \mathbb{R}$ is the unique quadratic function on Γ_p that vanishes at its endpoints and is one at its midpoint, and $\lambda_{\text{leak}} \in \mathbb{R}$ is a (time-dependent) Lagrange multiplier that determines the amount of leakage. The extra degree of freedom λ_{leak} allows us to enforce eq. (3.41) while also fixing the pressure mean, for which we take $\int_\Omega p_h \,\mathrm{d}\Omega = 0$.

As initial conditions we take a spatially uniform composition $x_{\text{LiPF}_6}|_{t=0} = x^{\ominus}_{\text{LiPF}_6}$ and $x_{\text{EMC}}|_{t=0} = 1 - 2x^{\ominus}_{\text{LiPF}_6}$ (cf. eq. (3.18)). For compositions in this regime the Reynolds and Péclet numbers for the problem are roughly $\text{Re} = 3 \times 10^{-5}$ and $\text{Pe} = 9 \times 10^{-2}$. We take all other unknowns v, p, $\boldsymbol{N}_\nu$, I, Φ_Z to be zero at $t = 0$. We numerically integrate eq. (3.42) up to a final time of 172800 seconds (two days) using the RadauIIA implicit Runge–Kutta method [120] with two stages in the two-dimensional case and one stage in the three-dimensional case, and with 200 timesteps.

We spatially discretise eq. (3.42) in a non-dimensionalised form with augmentation parameter $\gamma = 10^{-2}$. We employ a two-dimensional mesh of 5.7×10^3 triangles with maximum cell diameter $h = 0.125$, and a three-dimensional mesh of 6.3×10^3 tetrahedra with maximum cell diameter $h = 0.5$. We expect singularities in the solution at corners of Ω; in the two-dimensional case we use a finer local cell diameter of $h_{\text{c}} = 0.0125$ at the four vertices of Ω^{2D}. We employ the degree k Taylor–Hood pair [17, 109] for $(\mathcal{V}_h, \mathcal{P}_h)$ and the $\mathbb{RT}_k$–$\mathbb{DG}_{k-1}$ [96] pair for $(\mathcal{N}_h, \mathcal{X}_h)$ with $k = 4$ in two dimensions and $k = 2$ in three dimensions. The nonlinear systems at each timestep are solved using Newton's method with an absolute tolerance on the residual of 10^{-10} in the Euclidean norm. These systems consist of 1.3×10^6 unknowns in two dimensions and 3.9×10^5 unknowns in three dimensions. The greatest number of Newton iterations was taken at the first timestep (10 iterations in two and three dimensions). After the 2nd timestep, all Newton solves required at most 3 iterations.

In fig. 3.1, we plot streamlines of the EMC flux N_{EMC} and current density I at time $t = 64\,800\,\text{s}$ in two dimensions. The current density expectedly flows from the positive to negative electrode and appears to become singular at the top-right cell corner. The two-dimensional plots also reveal two convective rolls forming in the EMC flux profile. These convective rolls can also be seen in fig. 3.2, where we plot streamlines of the EMC flux at the final time $t = 172800\text{s}$ in three dimensions.

Figure 3.1: Streamlines of the EMC flux N_{EMC} (in black) and current density I (in white) from the two-dimensional simulation of section 3.5.1. The domain is coloured by the magnitude of I.

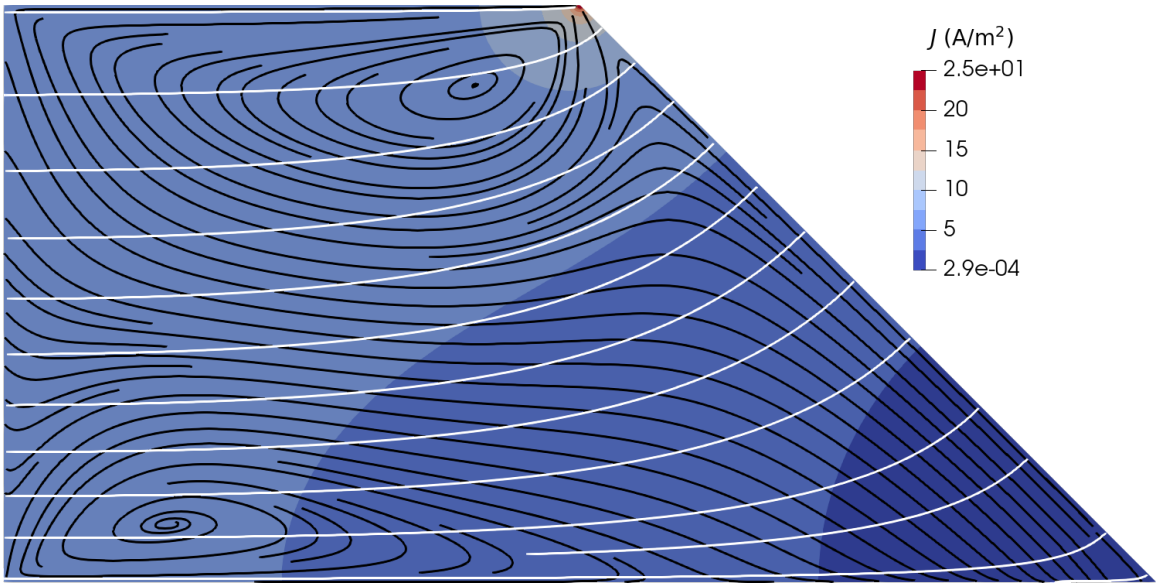

Owing to the leakage BCs eq. (3.49), the total number of moles of EMC (i.e. the value of $\int_\Omega c_1 \,\mathrm{d}\Omega$) varied by about 0.08 % over the simulation time, in both two and three dimensions. We also report maximum L^2-errors in the (nondimensionalised) mass-average constraint and mole fraction constraint:

$$\mathcal{E}_1 := \max_{0\le t\le T_{\mathrm{final}}} \left\| v_h - \widetilde{\boldsymbol{\psi}}_Z^\top \boldsymbol{N}_{Z,h} \right\|_{L^2(\Omega)^d} \quad \text{and} \quad \mathcal{E}_2 := \max_{0\le t\le T_{\mathrm{final}}} \left\| 1 - \boldsymbol{\nu}_Z^\top \boldsymbol{x}_{\nu,h} \right\|_{L^2(\Omega)} . \tag{3.50}$$

We obtained values of $(\mathcal{E}_1, \mathcal{E}_2) = (2.7 \times 10^{-4}, 5.6 \times 10^{-9})$ in two dimensions and $(\mathcal{E}_1, \mathcal{E}_2) = (2.4 \times 10^{-2}, 2.5 \times 10^{-5})$ in three dimensions.

3.5.2 Microfluidic rotating disk electrode

We again consider the binary EMC:$LiPF_6$ electrolyte from section 3.5.1, but in a setting that showcases the flexibility of our method in applying different BCs. We employ the same salt-charge transformation and material parameters η, ζ, ρ, $\boldsymbol{X}_\nu^0$ and $\mathbf{M}_Z$ at ambient temperature $T = 298.15\,\mathrm{K}$ as in section 3.5.1. We consider a three-dimensional domain Ω representing a microfluidic box containing a rotating disk electrode. Specifically, we take $\Omega = \Omega_{\mathrm{box}} \setminus \Omega_{\mathrm{disk}}$ where $\Omega_{\mathrm{box}} = (-5, 5)^3$ and $\Omega_{\mathrm{disk}} = \{(x, y, z) \in \mathbb{R}^3 : x^2 + y^2 \le 1, -0.05 \le z \le 0.05\}$. A unit of length corresponds

Figure 3.2: EMC flux N_{EMC} streamlines (coloured by its magnitude) from the three-dimensional simulation of section 3.5.1. The domain walls are coloured by the salt-charge potential Φ_Z.

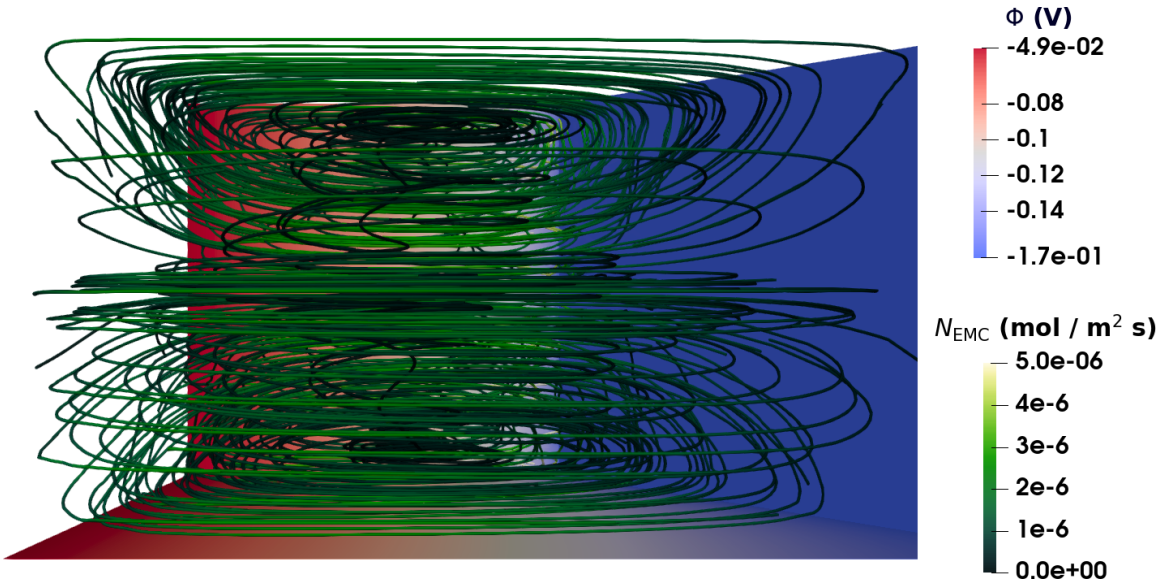

to a physical length of 12.5 µm. We decompose $\Gamma := \partial\Omega$ as $\Gamma = \Gamma_p \cup \Gamma_n \cup \Gamma_w$ where $\Gamma_p = \{(x, y, z) \in \partial\Omega_{\text{box}} : z = \pm 5\}$ denotes the top and bottom walls of the box, $\Gamma_w = \partial\Omega_{\text{box}} \backslash \Gamma_p$ the four side walls of the box, and $\Gamma_n = \partial\Omega_{\text{disk}}$ the disk boundary. The surfaces Γ_p, Γ_n, Γ_w represent, respectively, the positive electrode, negative electrode, and insulating walls.

We solve the steady problem eq. (3.37) with the following BCs. We first impose that the disk rotates with fixed angular frequency $\dot{\theta} \in \mathbb{R}$; this manifests in our model through the boundary condition eq. (3.38a) on v with $g_{v_\parallel}$ given by

$$g_{v_\parallel} = \dot{\theta}(-y, x, 0) \qquad \text{for } (x, y, z) \in \partial\Omega_{\text{disk}} = \Gamma_n, \tag{3.51a}$$

$$g_{v_\parallel} = 0 \qquad \text{on } \Gamma \setminus \partial\Omega_{\text{disk}}. \tag{3.51b}$$

We choose $\dot{\theta} = 28.79\,\text{s}^{-1}$, which leads to Reynolds and Péclet numbers of roughly $\text{Re} = 3 \times 10^{-3}$ and $\text{Pe} = 1 \times 10^{1}$. For the EMC flux $N_{h,\text{EMC}} := (\boldsymbol{N}_{\nu,h})_1$ we impose a zero normal flux condition eq. (3.38b) with $g_1 = 0$ on Γ. For the current density flux, instead of enforcing eq. (3.38c) for some function g_I, we enforce $I_h \cdot \hat{n}_\Gamma = 2F(N_{h,\text{LiPF}_6} \cdot \hat{n}_\Gamma)$ on Γ, where $N_{h,\text{LiPF}_6} := (\boldsymbol{N}_{\nu,h})_2$ (note that we implement this as a strongly enforced BC on $I_h \cdot \hat{n}_\Gamma$ and not $N_{h,\text{LiPF}_6} \cdot \hat{n}_\Gamma$). As in section 3.5.1, this BC enforces that the normal flux of PF_6^- is zero on Γ. For the LiPF_6 flux we enforce a zero normal

flux condition on the insulating walls $N_{h,\mathrm{LiPF_6}} \cdot \hat{n}_\Gamma = 0$ on Γ_w. However, instead of prescribing the value of $N_{\mathrm{LiPF_6}} \cdot \hat{n}_\Gamma$ on the electrodes $\Gamma_p \cup \Gamma_n$, we weakly enforce

$$x_{h,\mathrm{LiPF_6}} = x^{\ominus,e}_{\mathrm{LiPF_6}} \text{ on } \Gamma_e \text{ for } e \in \{p, n\}, \tag{3.52}$$

where $x^{\ominus,p}_{\mathrm{LiPF_6}} = 0.082$ and $x^{\ominus,n}_{\mathrm{LiPF_6}} = 0.068$. This is done by modifying eq. (3.37b) through the addition of boundary terms, and by enlarging the space of test functions $(\boldsymbol{W}_h)_2$ to those with zero normal trace on Γ_w only. Specifically, instead of eq. (3.37b), we consider:

$$\begin{aligned}
&\left(\begin{bmatrix} \boldsymbol{x}_{\nu,h} \\ \Phi_{Z,h} \end{bmatrix}, \nabla \cdot \begin{bmatrix} RT\widetilde{\boldsymbol{X}^0_\nu}\boldsymbol{W}_h \\ F\,\|\boldsymbol{z}\|\,K_h \end{bmatrix} \right)_\Omega - \left(p_h, \nabla \cdot \left\{ \widetilde{\boldsymbol{\psi}_Z^\top} \begin{bmatrix} \boldsymbol{W}_h \\ K_h \end{bmatrix} - \widetilde{\overline{\boldsymbol{V}_\nu}^\top} \boldsymbol{W}_h \right\} \right)_\Omega \\
&+ \left(\gamma\widetilde{\boldsymbol{\psi}_Z} v_h, \begin{bmatrix} \boldsymbol{W}_h \\ K_h \end{bmatrix} \right)_\Omega = \left(\widetilde{\mathbf{M}^\gamma_Z} \boldsymbol{N}_{Z,h}, \begin{bmatrix} \boldsymbol{W}_h \\ K_h \end{bmatrix} \right)_\Omega \\
&+ RT \cdot x^{\ominus,p}_{\mathrm{LiPF_6}} \left\langle \widetilde{(\boldsymbol{X}^0_\nu)_{22}}, (\boldsymbol{W}_h)_2 \cdot \hat{n}_\Gamma \right\rangle_{\Gamma_p} + RT \cdot x^{\ominus,n}_{\mathrm{LiPF_6}} \left\langle \widetilde{(\boldsymbol{X}^0_\nu)_{22}}, (\boldsymbol{W}_h)_2 \cdot \hat{n}_\Gamma \right\rangle_{\Gamma_n} \\
&\quad \forall \begin{bmatrix} \boldsymbol{W}_h \\ K_h \end{bmatrix} \in (\mathcal{N}_{0h} \times \mathcal{N}_h \times \mathcal{N}_{0h}) \quad \text{with } (\boldsymbol{W}_h)_2 \cdot \hat{n}_\Gamma = 0 \text{ on } \Gamma_w.
\end{aligned} \tag{3.53}$$

With the present material data, $\boldsymbol{X}^0_\nu$ is a diagonal matrix. One thus verifies by taking $(\boldsymbol{W}_h)_2$ to be non-zero in eq. (3.53), that for $e \in \{p, n\}$ the following is weakly enforced:

$$RT \cdot x_{h,\mathrm{LiPF_6}} \cdot \widetilde{(\boldsymbol{X}^0_\nu)_{22}} - \underbrace{p_h \cdot \left\{ \widetilde{(\boldsymbol{\psi}_Z^\top)_2} - \widetilde{(\overline{\boldsymbol{V}_\nu}^\top)_2} \right\}}_{:=\mathcal{I}_p} = RT \cdot x^{\ominus,e}_{\mathrm{LiPF_6}} \cdot \widetilde{(\boldsymbol{X}^0_\nu)_{22}} \quad \text{on } \Gamma_e. \tag{3.54}$$

Neglecting $\mathcal{I}_p$[11] in eq. (3.54) and dividing by $RT \cdot \widetilde{(\boldsymbol{X}^0_\nu)_{22}}$ then leads to eq. (3.52) as desired.

We discretise eq. (3.37) with aforementioned BCs and modification eq. (3.53) in a non-dimensionalised form with augmentation parameter $\gamma = 10^{-2}$. As constraints we impose eq. (3.41) along with $\int_\Omega p_h \,\mathrm{d}\Omega = 0$. We employ a curved mesh of degree 4 with 1.8×10^4 tetrahedra and maximum local cell diameter of $h = 0.1$ on the disk boundary. We employ the degree $k = 4$ Taylor–Hood pair [17, 109] for $(\mathcal{V}_h, \mathcal{P}_h)$ and the $\mathbb{RT}_k$–$\mathbb{DG}_{k-1}$ [96] pair for $(\mathcal{N}_h, \mathcal{X}_h)$. The nonlinear system consists of 1.1×10^6 unknowns and was solved using Newton's method with an absolute tolerance on the residual of 10^{-10} in the Euclidean norm. We first applied Newton's method on a coarse discretisation (with a non-curved mesh and order $k = 2$ spaces), where as an initial guess we set $x_{\mathrm{LiPF_6}} = 0.075$ and $x_{\mathrm{EMC}} = 1 - 2x_{\mathrm{LiPF_6}}$ (cf. eq. (3.18)) and we set

[11] Dimensional analysis reveals that $\mathcal{I}_p$ is smaller than the other terms in eq. (3.54) by a factor of 10^{-8}.

all other unknowns to be zero. Convergence was reached in 6 iterations. We then used the coarse solution as an initial guess for the fine discretisation (i.e. with a curved mesh and degree $k = 4$ spaces, as above), for which Newton's method converged in 3 iterations.

Figure 3.3: Streamlines of the $LiPF_6$ flux N_{LiPF_6} (coloured by its magnitude) and current density I (coloured in a transparent yellow) above Ω_{disk} for the numerical experiment of section 3.5.2. The disk is also coloured by the magnitude of N_{LiPF_6}.

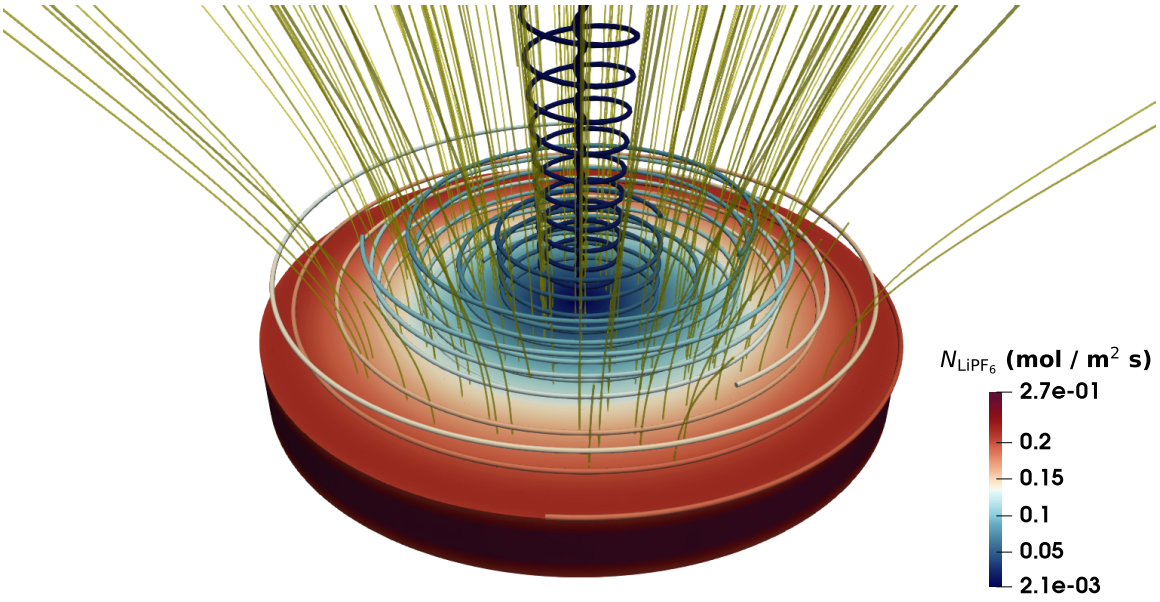

In fig. 3.3 we plot streamlines of the $LiPF_6$ flux and current density I. The rotation of the disk induces a swirling flow of $LiPF_6$, while the current density flows smoothly from the positive electrode to the negative disk electrode. These observations qualitatively reflect the expected behaviour of the solution as induced by our choice of BCs. Moreover, the L^2-errors in the (nondimensionalised) mass-average constraint, mole fraction constraint, and weakly enforced BCs eq. (3.52) are

$$\left\| v_h - \widetilde{\boldsymbol{\psi}_Z^\top} \boldsymbol{N}_{Z,h} \right\|_{L^2(\Omega)^d} = 1.3 \times 10^{-3}, \tag{3.55}$$

$$\left\| 1 - \boldsymbol{\nu}_Z^\top \boldsymbol{x}_{\nu,h} \right\|_{L^2(\Omega)} = 3.7 \times 10^{-7}, \tag{3.56}$$

$$\left\| x_{h,\mathrm{LiPF_6}} - x_{\mathrm{LiPF_6}}^{\ominus,e} \right\|_{L^2(\Gamma_p \cup \Gamma_n)} = 5.0 \times 10^{-5}. \tag{3.57}$$

In particular, the small error in the weakly enforced BC eq. (3.52) affirms the ability of our algorithm to handle a combination of flux, Dirichlet, and tangential velocity BCs.

3.5.3 Cosolvent imbalances

An appealing property of our numerical method is that it accounts for the multi-component nature of the electrolyte solvent (i.e. the neutral species in which the salts are dissolved), the effects of which may be important for battery modelling [68]. To demonstrate this, we consider an electrolyte comprised of $LiPF_6$ salt dissolved in two solvents, namely ethyl-methyl-carbonate (EMC) and ethylene-carbonate (EC). The resulting mixture has $n = 4$ species (EMC, EC, Li^+ and $PF_6{}^-$) with molar masses $\boldsymbol{m} = [104.105, 88.062, 6.935, 144.97]^\top \mathrm{g\,mol^{-1}}$ and equivalent charges $\boldsymbol{z} = [0, 0, 1, -1]^\top$. We use the salt-charge transformation matrix eq. (3.13) with $\boldsymbol{\nu}_1^\top = [1, 0, 0, 0]$, $\boldsymbol{\nu}_2^\top = [0, 1, 0, 0]$ and $\boldsymbol{\nu}_3^\top = [0, 0, 1, 1]$. This corresponds to neutralizing reactions EMC $\rightleftharpoons$ EMC, EC $\rightleftharpoons$ EC and $Li^+ + PF_6{}^- \rightleftharpoons LiPF_6$. Hence, under the salt-charge transformation, the mole fractions $(\boldsymbol{x}_\nu)_i$, chemical potentials $(\boldsymbol{\mu}_\nu)_i$, fluxes $(\boldsymbol{N}_\nu)_i$ and so on, represent those of EMC for $i = 1$, EC for $i = 2$ and $LiPF_6$ for $i = 3$. We take an ambient temperature of $T = 298.15\,\mathrm{K}$. We let ρ be

Figure 3.4: Streamlines of the EMC flux N_{EMC} (in black) and EC flux N_{EC} (in white) from the simulation of section 3.5.3. The domain is coloured by the shear viscosity η.

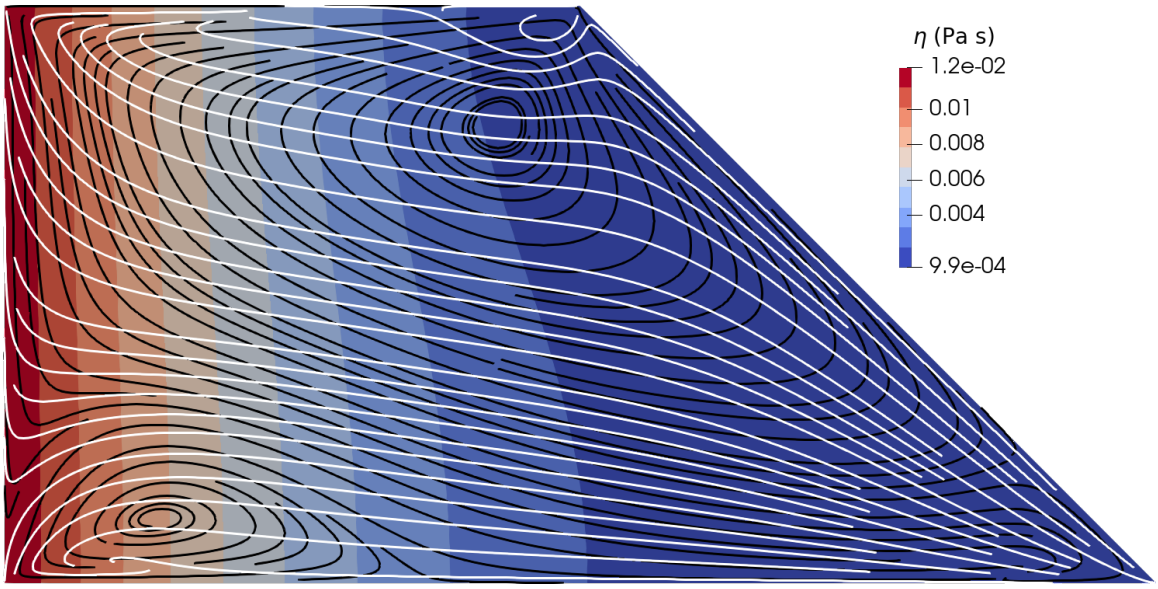

a function of $\boldsymbol{x}_\nu$ as reported in [100]. An expression for η as a function of $\boldsymbol{x}_\nu$ was obtained by fitting viscosity data reported in [100] to a degree 7 bivariate polynomial in the variables $\sqrt{x_{\mathrm{EMC}}/(x_{\mathrm{EMC}} + x_{\mathrm{EC}})}$, $\sqrt{x_{\mathrm{EC}}/(x_{\mathrm{EMC}} + x_{\mathrm{EC}})}$. We further take $\zeta = 10^{-6}\,\mathrm{Pa\,s}$, and $\boldsymbol{X}_\nu^0$ is obtained by assuming an ideal mixture (see eq. (1.29)). We compute $\mathbf{M}_Z$ by assuming constant Stefan–Maxwell diffusivities, the values of which

are obtained from the supplementary information of [94] for $1\,\mathrm{mol\,L^{-1}}$ of $\mathrm{LiPF_6}$ in vol:vol 7:3 EMC:EC solvent.

We take Ω to be the same two-dimensional Hull cell domain as in section 3.5.1. For BCs we use eq. (3.38a) with $g_{v_\parallel} = 0$. For eqs. (3.38b) and (3.38c) we use linearised Butler–Volmer BCs and we neglect the $\mu_{\mathrm{LiPF_6}}$ term in the overpotential (cf. eq. (3.27)):

$$g_I = -i_0 F(V_\mathrm{e} - \Phi_Z)/(RT) \quad \text{on } \Gamma_e \text{ for } e \in \{p, n\}, \tag{3.58a}$$

$$g_I = 0 \quad \text{on } \Gamma_w, \tag{3.58b}$$

$$g_3 = g_I/(2F) \quad \text{on } \Gamma, \tag{3.58c}$$

with $V_p = 0.1\,\mathrm{V}$, $V_n = 0\,\mathrm{V}$ and $i_0 = 10^4\,\mathrm{Am^{-2}}$. In eq. (3.38b) we further take $g_2 = 0$ on Γ, i.e. no normal flux of EC, while for EMC we impose the leak BCs eq. (3.49).

We numerically solve the transient problem eq. (3.42). As initial conditions we take a spatially uniform composition $x_{\mathrm{LiPF_6}}|_{t=0} = 0.077$, $x_{\mathrm{EMC}}|_{t=0} = 0.509$ and $x_{\mathrm{EC}}|_{t=0} = 1 - 0.509 - (2 \cdot 0.077) = 0.337$ (cf. eq. (3.18)). In this regime the Reynolds and Péclet numbers for the problem are roughly $\mathrm{Re} = 3 \times 10^{-5}$ and $\mathrm{Pe} = 9 \times 10^{-1}$. We take all other unknowns v, p, $\boldsymbol{N}_\nu$, I, Φ_Z to be zero at $t = 0$. As constraints we impose eq. (3.41) along with $\int_\Omega p_h \,\mathrm{d}\Omega = 0$. We use the same mesh, finite element spaces $(\mathcal{V}_h, \mathcal{P}_h)$ and $(\mathcal{N}_h, \mathcal{X}_h)$, and timestepping scheme as in the two-dimensional case of section 3.5.1. The nonlinear systems at each timestep consist of 1.7×10^6 unknowns and are solved using Newton's method with an absolute tolerance on the residual of 10^{-10} in the Euclidean norm. The first two timesteps required at most 5 Newton iterations, and all subsequent timesteps required at most 3 iterations. Note that the initial Newton solves in section 3.5.1 required more iterations due to the nonlinear BCs eq. (3.48a).

In fig. 3.4 we plot streamlines of the EMC and EC fluxes N_{EMC}, N_{EC} at time $t = 64\,800\,\mathrm{s}$. The flux profiles are emphatically different, underscoring the multi-component nature of the solvent. Moreover, in fig. 3.4 we colour the domain by the shear viscosity $\eta = \eta(\boldsymbol{x}_\nu)$, which changes by an order of magnitude across the cell due to the spatially varying EMC:EC ratio. Specifically, at $t = 64\,800\,\mathrm{s}$ the ratio $x_{\mathrm{EMC}}/x_{\mathrm{EC}} \approx 1.4$ near the positive (left) electrode and $x_{\mathrm{EMC}}/x_{\mathrm{EC}} \approx 1.6$ near the negative (right) electrode. The large variation in η arises due to its strong dependence on the EMC:EC ratio.

3.6 Conclusions

We have presented a broad family of finite element algorithms for numerically solving the electroneutral NSOSM equations. To the best of our knowledge, this chapter represents the first work in the finite element literature on electroneutral NSOSM flow. The flexibility of our algorithms in handling transient and steady flow under different boundary conditions was substantiated in our numerical experiments. Our numerical experiment involving EMC-EC-$LiPF_6$ flow also demonstrated the scientific potential of our algorithms in studying how the multicomponent nature of electrolytes may impact, for example, locally varying material properties of the mixture.

Chapter 4

Extensions to anisothermal flows

4.1 Introduction

The purpose of this chapter is to demonstrate how the numerical framework of chapters 2 and 3 can be extended to handle *anisothermal flows*, where the temperature T is not constant. Anisothermality is of clear scientific importance, since in most applications it is difficult, if not impossible, to achieve nearly exact isothermal conditions. While assuming isothermality is sometimes expedient, in many applications the temperature varies substantially and this assumption breaks down. In such regimes, heat transport and thermal effects are crucial to the underlying physics, and may even constitute the primary phenomena of interest [14]. Examples of applications involving anisothermal multicomponent fluids include batteries, where thermal management is crucial to safety, performance and degradation [23]; combustion, where chemical reactions produce heat, and reaction rates depend on the temperature [56]; and atmospheric physics [103], where temperature varies throughout the layers of the atmosphere and couples to the chemical behaviour of its constituent species.

The most common mechanism of heat transport in applications is described by *Fourier's law*, which states that the heat flow is proportional to the negative temperature gradient. The constant of proportionality is given by κ, the *thermal conductivity*, and this mechanism is captured by the Onsager–Stefan–Maxwell (OSM) framework (see eq. (1.78)). The OSM framework is also capable of modelling the *Soret effect* [105], in which thermal gradients drive mass transport. Mass transport by the Soret effect has been proposed in separation processes [55, 125], and this mechanism is sometimes referred to as *thermodiffusion*. Reciprocal to the Soret effect is the *Dufour effect* [42], in which concentration gradients drive heat transport. The Soret and Dufour effects are quantified in OSM theory by the *thermal diffusion coefficients*, D_i^T (see eq. (1.77) and [14]). Often in applications, the Soret and Dufour effects can be

neglected. Even when this is the case, however, thermality plays a crucial role within the OSM framework, since transport coefficients (e.g. diffusivities or viscosities) and properties of equilibrium thermodynamics (e.g. densities or excess properties) are generally temperature-dependent [56, 60].

Our forthcoming numerical discretisation of the anisothermal OSM equations does not require a great deal of discussion, since we will show that the numerical framework developed in chapters 2 and 3 adapts straightforwardly to the anisothermal regime. This is largely due to the structure of the anisothermal OSM constitutive law (see eq. (1.75) and [113]), which relates the generalised velocities and driving forces by a transport matrix that is symmetric positive-semidefinite and has a one-dimensional nullspace. This same structure was exploited in chapters 2 and 3, and the ideas readily extend to the anisothermal setting.

The main subtlety regarding the discretisation of anisothermal Navier–Stokes–OSM (NSOSM) flow lies in the choice of energy balance law to discretise. There are several possible formulations, all of which are equivalent at the continuous level, but are generally not equivalent upon discretisation. The most obvious choice is the equation for the specific total energy, eq. (1.50c). Discretisation of this equation by a sensible numerical scheme would have the advantage of straightforwardly yielding an *energy preserving* method for unforced systems. However, in this chapter we are slightly more ambitious, and we wish to devise a scheme that is both energy preserving, and ensures that the total entropy is non-decreasing (i.e. the scheme is *entropy dissipating*, again for isolated, unforced systems). This latter goal is readily achieved by discretising the entropy balance law eq. (1.59), since the entropy production function g_S is, by construction, pointwise non-negative (see eq. (1.72) and the discussion thereafter). If desired, exact total energy conservation can additionally be enforced through the suitable introduction of a Lagrange multiplier. At an implementation level, the Lagrange multiplier approach is trivial to incorporate, which is why we discuss it here. Devising an anisothermal NSOSM scheme that is both energy preserving and entropy dissipating *intrinsically* (i.e. without Lagrange multipliers) is challenging, and outside the scope of this thesis.

The remainder of this chapter is organised as follows. In section 4.2 we outline the equations governing anisothermal NSOSM flow. In section 4.3 we show how these equations are readily discretised by adapting the numerical framework of chapters 2 and 3. Numerical experiments demonstrating our ability to simulate anisothermal multicomponent flow are given in section 4.4, and conclusions are drawn in section 4.5.

4.2 Continuous problem

We consider an anisothermal, chemically nonreacting mixture of $n \geq 2$ species, on a bounded and connected Lipschitz spatial domain $\Omega \subset \mathbb{R}^d$, with spatial dimension $d \in \{2, 3\}$. For simplicity, we assume the species to be uncharged; at the end of this section we briefly outline how one can handle the charged, locally electroneutral case.

4.2.1 Governing anisothermal equations

Important thermodynamic state variables include T, p and $c_1, \ldots, c_n$, where T is the temperature, p is the pressure and c_i is the concentration of species $i \in \{1 : n\}$. In contrast to the previous chapters, we now permit T to vary in space and time, along with the other state variables $p, c_1, \ldots, c_n$. The total molar concentration is $c_T = \sum_{i=1}^n c_i$ and the mass density is $\rho = \sum_{i=1}^n m_i c_i$, where m_i is the molar mass of species i. Composition is expressed using mole fractions $x_i = c_i/c_T$, for which $\sum_{i=1}^n x_i = 1$. Note that the local thermodynamic state of the mixture is fully characterised by the state variables $T, p, x_1, \ldots, x_n$ (recall section 1.2).

The equations governing the balance of mass and momentum are given by (recall eqs. (1.50a), (1.50b), and (1.66))

$$\frac{\partial(\rho v)}{\partial t} + \nabla \cdot (\rho v \otimes v) + \nabla p - \nabla \cdot \tau = 0, \quad \text{in } \Omega, \tag{4.1}$$

$$\frac{\partial c_i}{\partial t} + \nabla \cdot N_i = 0 \quad \text{in } \Omega \quad \forall i \in \{1 : n\}. \tag{4.2}$$

Here v is the barycentric velocity, τ is the viscous stress and $N_i = c_i v_i$ is the molar flux[1] of species i. These balance laws were employed in chapter 3 (recall eqs. (3.2) and (3.3)); here, for simplicity we omit source terms since they obfuscate the energy balance. Recall that v must satisfy the mass-average constraint (see eq. (1.44)):

$$v = \sum_{j=1}^n \omega_j v_j \quad \text{in } \Omega, \tag{4.3}$$

where we have introduced the mass fractions $\omega_j := m_j c_j/\rho$. Moreover, we assume that τ satisfies the Newtonian constitutive law (see eq. (1.74))

$$\tau = 2\eta\epsilon(v) + (\zeta - 2\eta/d)(\nabla \cdot v)\mathbb{I}. \tag{4.4}$$

[1] In this chapter, there is no major advantage to using molar fluxes N_i as opposed to mass fluxes $J_i = m_i N_i$. For the sake of fixing a convention, we choose to work with molar fluxes.

Here, $\epsilon(v)$ is the symmetric gradient of v, $\mathbb{I}$ is the $d \times d$ identity matrix, $\eta > 0$ is the shear viscosity and $\zeta > 0$ is the bulk viscosity. As in chapter 3, we permit η and ζ to depend on the thermodynamic state variables T, p and $x_1, \ldots, x_n$.

As discussed in section 4.1, we shall employ the entropy balance law as our time evolution equation that implicitly determines the temperature. This facilitates the straightforward development of an entropy-dissipating discretisation. The entropy balance equation is given by (recall eq. (1.59))

$$\frac{\partial(\rho s)}{\partial t} + \nabla \cdot (\rho s v) + \nabla \cdot J_s = g_S, \tag{4.5}$$

where s is the *specific entropy*, J_s is the *entropy flux* and g_S is the *entropy production function*. It will be convenient to eliminate ρ from eq. (4.5) by working directly with the *volumetric entropy* $s_V := \rho s$. Written in terms of s_V, eq. (4.5) becomes

$$\frac{\partial s_V}{\partial t} + \nabla \cdot (s_V v) + \nabla \cdot J_s = g_S. \tag{4.6}$$

Note that s_V depends on $T, p, x_1, \ldots, x_n$ only, i.e. $s_V = s_V(T, p, x_1, \ldots, x_n)$. We assume that this functional dependence is known[2]. The entropy flux is (see eq. (1.61))

$$J_s = \frac{J'_q}{T} + \sum_{i=1}^{n} \overline{S_i} c_i v_i^d = J'_s + \sum_{i=1}^{n} \overline{S_i}\big(N_i - c_i v\big), \tag{4.7}$$

where J'_q is the *irreversible heat flux* (recall eq. (1.60)), $J'_s := \frac{J'_q}{T}$ the *irreversible entropy flux*, the $\overline{S_i}$ are partial molar entropies (recall eq. (1.10)), and $v_i^d = v_i - v$ are *diffusive velocities* (recall eq. (1.51)). The entropy production is (recall eq. (1.72))

$$g_S = \frac{1}{T}\Big\{2\eta\big(\epsilon^0(v) : \epsilon^0(v)\big) + \zeta(\nabla \cdot v)^2 + \sum_{i,j=0}^{n} v_i \cdot \mathfrak{M}_{ij} v_j\Big\}, \tag{4.8}$$

where $\epsilon^0(v) := \epsilon(v) - \frac{\mathbb{I}}{d}\nabla \cdot v$ denotes the traceless part of $\epsilon(v)$, $\mathfrak{M}$ is the *thermodiffusion transport matrix* (recall eq. (1.75)), and $v_0 = \frac{J'_q}{c_{p,V} T} = \frac{J'_s}{c_{p,V}}$ is the thermal velocity (recall eq. (1.76)) where $c_{p,V}$ is the volumetric heat capacity.

The properties of $\mathfrak{M}$ that are crucial here are entirely analogous to those concerning $\boldsymbol{M}$ in chapter 2 (recall eq. (2.6)), and of $\mathbf{M}$ in chapter 3 (recall eq. (3.7)). In particular, it holds that $\mathfrak{M}$ is symmetric [88, 89], and positive-semidefinite with nullspace spanned by the vector $l \in \mathbb{R}^{n+1}$ where $l_0 = 0$ and $l_i = 1$ for $i \in \{1 : n\}$

[2]For example, if the functional dependence of the chemical potentials μ_i on $T, p, x_1, \ldots, x_n$ is known, then one can recover the partial molar entropies and volumes by Maxwell relations: $\overline{S_i} = -\frac{\partial \mu_i}{\partial T}$ and $\overline{V_i} = \frac{\partial \mu_i}{\partial p}$ (recall eq. (1.11)). From here, one can recover s_V by Euler relations (recall eq. (1.12)), namely: $s_V = \sum_{i=1}^{n} c_i \overline{S_i}$ where $c_i = x_i c_T$ and $c_T^{-1} = \sum_{i=1}^{n} x_i \overline{V_i}$.

(recall eq. (1.73)). One can relate the $(n+1)\times(n+1)$ thermodiffusion matrix $\mathfrak{M}$ to the $n\times n$ isothermal transport matrix $\boldsymbol{M}$ from eq. (2.6) by the formula [113]

$$\mathfrak{M}=\begin{bmatrix}\mathfrak{M}_{00} & \mathfrak{M}_0^\top\\ \mathfrak{M}_0 & \boldsymbol{M}+\frac{\mathfrak{M}_0\mathfrak{M}_0^\top}{\mathfrak{M}_{00}}\end{bmatrix}. \tag{4.9}$$

Here, the scalar $\mathfrak{M}_{00}$, and the $n\times 1$ vector $\mathfrak{M}_0$, are given by

$$\mathfrak{M}_{00}=\frac{c_{p,V}^2T}{\kappa}\quad\text{and}\quad\mathfrak{M}_{0i}=-\frac{c_{p,V}}{\kappa}\sum_{j=1}^{n}\boldsymbol{M}_{ij}\frac{D_j^T}{m_jc_j}\quad\forall i\in\{1:n\}, \tag{4.10}$$

where $\kappa>0$ is the *thermal conductivity*, and the D_i^T for $i\in\{1:n\}$ are *thermal diffusion coefficients* (recall eq. (1.77)). We note that only $n-1$ of the D_i^T are independent, and they satisfy $\sum_{i=1}^n D_i^T=0$ [14, 113]. Altogether, eqs. (2.6), (4.9), and (4.10) show that $\mathfrak{M}$ is fully parametrized by κ, D_i^T and the *Stefan–Maxwell diffusivities* $\mathscr{D}_{ij}$ (recall eq. (2.6)). So long as $\mathfrak{M}$ remains positive-semidefinite of rank n, we shall permit the transport properties κ, D_i^T and $\mathscr{D}_{ij}$ to be functions of the state variables $T,p,x_1,\dots,x_n$.

The anisothermal Onsager–Stefan–Maxwell (OSM) equations [14, 113] close the balance laws eqs. (4.2) and (4.6). The OSM equations read (recall eq. (1.75)):

$$\sum_{j=0}^{n}\mathfrak{M}_{ij}v_j=d_i=\begin{cases}-c_{p,V}\nabla T, & i=0,\\ -c_i\nabla\mu_i-c_i\overline{S_i}\nabla T+\omega_i\nabla p, & i\in\{1:n\},\end{cases} \tag{4.11}$$

where the driving forces d_i were defined in eqs. (1.63) and (1.76), which involves the species chemical potentials μ_i (recall eq. (1.3)). If desired, one can formulate our forthcoming numerical scheme using chemical potentials, as was done in chapter 2. However, following chapter 3, we instead choose to reformulate the driving forces using mole fraction gradients. This will lead to a cancellation of the ∇T term in the diffusional driving forces. Indeed, since $\mu_i=\mu_i(T,p,x_1,\dots,x_n)$, by the chain rule and Maxwell relations eq. (1.11), one has

$$\nabla\mu_i=-\overline{S_i}\nabla T+\overline{V_i}\nabla p+RT\sum_{j=1}^{n}\boldsymbol{X}_{ij}\nabla x_j, \tag{4.12}$$

where $\boldsymbol{X}=\boldsymbol{X}(T,p,x_1,\dots,x_n)$ is an $n\times n$ matrix of *thermodynamic factors*, which captures the partial derivatives of chemical potentials with respect to composition (cf. eq. (3.19)). Substituting eq. (4.12) into eq. (4.11), we find that

$$\sum_{j=0}^{n}\mathfrak{M}_{ij}v_j=d_i=\begin{cases}-c_{p,V}\nabla T, & i=0,\\ -c_iRT\sum_{j=1}^{n}\boldsymbol{X}_{ij}\nabla x_j+\big(\omega_i-c_i\overline{V_i}\big)\nabla p, & i\in\{1:n\},\end{cases} \tag{4.13}$$

revealing that the diffusional driving forces d_i for $i\in\{1:n\}$ are independent of ∇T.

4.2.2 Anisothermal augmentation strategy

Analogously to sections 2.2.3 and 3.2.3 in the previous chapters, we shall weakly incorporate the mass-average constraint eq. (4.3), and simultaneously address the fact that $\mathfrak{M}$ is singular, using an augmentation strategy [4, 45, 64, 112]. A discussion on this strategy in the anisothermal setting is given in [113], which we now outline.

Let $\gamma > 0$ be a user-chosen augmentation parameter. It will be convenient to introduce $\omega_0 := 0$, so that the mass-average constraint eq. (4.3) can be written as a sum indexed by $j \in \{0 : n\}$ instead of $j \in \{1 : n\}$. Namely, with $\omega_0 := 0$, we have

$$v = \sum_{j=0}^{n} \omega_j v_j. \tag{4.14}$$

Hence, for any $i \in \{0 : n\}$, multiplying eq. (4.14) by $\gamma\omega_i$ yields

$$\sum_{j=0}^{n} \gamma\omega_i\omega_j v_j = \gamma\omega_i v. \tag{4.15}$$

Adding eq. (4.15) to eq. (4.13), we obtain the augmented anisothermal OSM equations

$$\sum_{j=0}^{n} \mathfrak{M}^{\gamma}_{ij} v_j = d_i + \gamma\omega_i v \quad \forall i \in \{0 : n\}, \tag{4.16}$$

where $\mathfrak{M}^{\gamma}$ is a symmetric positive-definite *augmented thermodiffusion matrix*,

$$\mathfrak{M}^{\gamma}_{ij} := \mathfrak{M}_{ij} + \gamma\omega_i\omega_j. \tag{4.17}$$

Since $\omega_0 = 0$, we have $\mathfrak{M}^{\gamma}_{ij} = \mathfrak{M}_{ij}$ whenever $i = 0$ or $j = 0$. In fact, one has [113]

$$\mathfrak{M}^{\gamma} = \begin{bmatrix} \mathfrak{M}_{00} & \mathfrak{M}_0^{\top} \\ \mathfrak{M}_0 & \boldsymbol{M}^{\gamma} + \frac{\mathfrak{M}_0\mathfrak{M}_0^{\top}}{\mathfrak{M}_{00}} \end{bmatrix}, \tag{4.18}$$

where $\boldsymbol{M}^{\gamma}$ is the augmented isothermal transport matrix from eq. (2.14). Having incorporated the mass-average constraint in the OSM equations through augmentation, following the previous chapters we only explicitly enforce the divergence of the mass-average constraint. Written in terms of molar fluxes, this means that we enforce

$$\nabla \cdot v = \nabla \cdot \left(\sum_{j=1}^{n} \frac{m_j N_j}{\rho} \right) = \nabla \cdot \left(\sum_{j=1}^{n} \psi_j N_j \right), \tag{4.19}$$

where $\psi_j := \frac{m_j}{\rho}$. The same notation for $\boldsymbol{\psi}$ was used in chapter 3 (see eq. (3.11)). Also, following the previous chapters (recall eqs. (2.13b) and (3.22)), for symmetry we augment the momentum balance eq. (4.1) with the mass-average constraint:

$$\frac{\partial(\rho v)}{\partial t} + \nabla \cdot (\rho v \otimes v) + \nabla p - \nabla \cdot \tau + \gamma v - \gamma \sum_{j=1}^{n} \psi_j N_j = 0. \tag{4.20}$$

Finally, we shall express the augmented OSM equations eq. (4.16) in terms of the fluxes $J'_s, N_1, \ldots, N_n$ instead of the velocities $v_0, v_1, \ldots, v_n$. Since

$$J'_s = c_{p,V} v_0, \quad N_i = c_i v_i \quad \forall i \in \{1:n\}, \tag{4.21}$$

this motivates us to define the scaled transport matrix (in analogy to eq. (2.17))

$$\hat{\mathfrak{M}} := \operatorname{diag}(c_{p,V}^{-1}, c_1^{-1}, \ldots, c_n^{-1}) \mathfrak{M} \operatorname{diag}(c_{p,V}^{-1}, c_1^{-1}, \ldots, c_n^{-1}), \tag{4.22}$$

where $\operatorname{diag}(a_0, \ldots, a_n)$ is the diagonal matrix with i-th diagonal entry given by a_i. The augmented analogue of $\hat{\mathfrak{M}}$ is $\hat{\mathfrak{M}}^\gamma$, given by the formula

$$\hat{\mathfrak{M}}^\gamma := \operatorname{diag}(c_{p,V}^{-1}, c_1^{-1}, \ldots, c_n^{-1}) \mathfrak{M}^\gamma \operatorname{diag}(c_{p,V}^{-1}, c_1^{-1}, \ldots, c_n^{-1}). \tag{4.23}$$

Using the rescaled matrix $\hat{\mathfrak{M}}^\gamma$ and eq. (4.13), one verifies that eq. (4.16) becomes:

$$\hat{\mathfrak{M}}^\gamma_{i0} J'_s + \sum_{j=1}^n \hat{\mathfrak{M}}^\gamma_{ij} N_j = \begin{cases} -\nabla T, & i = 0, \\ -RT \sum_{j=1}^n \boldsymbol{X}_{ij} \nabla x_j + \big(\psi_i - \overline{V_i}\big) \nabla p + \gamma \psi_i v & i \in \{1:n\}. \end{cases} \tag{4.24}$$

Equation (4.24) is our desired formulation of the anisothermal OSM equations. Indeed, it has the advantage of being expressed in terms of the fluxes $J'_s, N_1, \ldots, N_n$, it involves a symmetric positive-definite matrix $\hat{\mathfrak{M}}^\gamma$, and the terms on the right-hand side of eq. (4.24) are amenable to integration by parts in a weak formulation.

4.2.3 Full anisothermal problem statement

As in the previous chapters, we use boldface notation for vectors and matrices indexed by $i \in \{1:n\}$ (or, where it is clear from context, $i \in \{0:n\}$). Hence, for example, we write $\boldsymbol{c} = [c_1, \ldots, c_n]^\top$, which is to be interpreted as an $n \times 1$ vector. For $\mathbb{R}^d$-valued quantities we write, for example, $\boldsymbol{N} = [N_1, \ldots, N_n]^\top$, which is to be interpreted as an $n \times d$ matrix, and the divergence acts on its rows, so that $\nabla \cdot \boldsymbol{N}$ is an $n \times 1$ vector.

The full anisothermal problem is obtained by combining eqs. (4.2), (4.6), (4.19), (4.20), and (4.24). In particular, the unknown functions of space and time to be solved for are the velocity v, irreversible entropy flux J'_s, molar fluxes $\boldsymbol{N}$, temperature T,

pressure p, and mole fractions $\boldsymbol{x}$, such that, in block-matrix notation:

$$\begin{aligned} &\frac{\partial(\rho v)}{\partial t} + \nabla\cdot(\rho v\otimes v) + \nabla p + \gamma\big(v - \boldsymbol{\psi}^\top \boldsymbol{N}\big) \\ &\qquad -\nabla\cdot\Big(2\eta\epsilon(v) + (\zeta - 2\eta/d)(\nabla\cdot v)\mathbb{I}\Big) = 0, \end{aligned} \tag{4.25a}$$

$$-\begin{bmatrix} 1 & 0 \\ 0 & RT\boldsymbol{X} \end{bmatrix}\begin{bmatrix} \nabla T \\ \nabla \boldsymbol{x} \end{bmatrix} + \begin{bmatrix} 0 \\ \boldsymbol{\psi} - \overline{\boldsymbol{V}} \end{bmatrix}\nabla p + \gamma\begin{bmatrix} 0 \\ \boldsymbol{\psi} \end{bmatrix} v = \hat{\mathfrak{M}}^\gamma \begin{bmatrix} J_s' \\ \boldsymbol{N} \end{bmatrix}, \tag{4.25b}$$

$$\frac{\partial s_V}{\partial t} + \nabla\cdot(s_V v) + \nabla\cdot\Big(J_s' + \overline{\boldsymbol{S}}^\top\big(\boldsymbol{N} - \boldsymbol{c}v\big)\Big) = g_S, \tag{4.25c}$$

$$\nabla\cdot\big(v - \boldsymbol{\psi}^\top\boldsymbol{N}\big) = 0, \tag{4.25d}$$

$$\frac{\partial \boldsymbol{c}}{\partial t} + \nabla\cdot\boldsymbol{N} = 0. \tag{4.25e}$$

Before clarifying the notation in eq. (4.25), note that eq. (4.25a) can be viewed as the equation for velocity v, eq. (4.25b) for the fluxes J_s' and $\boldsymbol{N}$, eq. (4.25c) for temperature T, eq. (4.25d) for pressure p, and eq. (4.25e) for mole fractions $\boldsymbol{x}$.

In eq. (4.25a), we recall that ρ is the density, $\gamma > 0$ a user-chosen augmentation parameter, $(\boldsymbol{\psi})_i = \psi_i = \frac{m_i}{\rho}$, while η and ζ are the shear and bulk viscosities, respectively. In eq. (4.25b), $\boldsymbol{X}$ is a matrix of thermodynamic factors (recall eq. (4.12)), $(\overline{\boldsymbol{V}})_i = \overline{V_i}$ are partial molar volumes, and the transport matrix $\hat{\mathfrak{M}}^\gamma$ is given by eq. (4.23). In eq. (4.25c), s_V is the volumetric entropy, $(\overline{\boldsymbol{S}})_i = \overline{S_i}$ are partial molar entropies, and $(\boldsymbol{c})_i = c_i$ are the concentrations. The entropy production g_S in eq. (4.25c) can be expressed in terms of the unknowns as (cf. eq. (4.8))

$$g_S = \frac{1}{T}\left\{2\eta\big(\epsilon^0(v) : \epsilon^0(v)\big) + \zeta(\nabla\cdot v)^2 + \left(\begin{bmatrix} J_s' \\ \boldsymbol{N} \end{bmatrix}^\top \hat{\mathfrak{M}}\begin{bmatrix} J_s' \\ \boldsymbol{N} \end{bmatrix}\right)\right\}. \tag{4.26}$$

Note that in eq. (4.26), we use $\hat{\mathfrak{M}}$ instead of its augmented analogue $\hat{\mathfrak{M}}^\gamma$. This is because there is no need for $\hat{\mathfrak{M}}$ to be positive-definite in eq. (4.26), and using $\hat{\mathfrak{M}}^\gamma$ in its place would violate the invariance of diffusional entropy production under a common additive shift in the species velocities. Note also that $\rho, \boldsymbol{\psi}, \eta, \zeta, \boldsymbol{X}, \overline{\boldsymbol{V}}, \hat{\mathfrak{M}}, \hat{\mathfrak{M}}^\gamma, s_V, \overline{\boldsymbol{S}}$ and $\boldsymbol{c}$ are all material properties and are functions of the state variables $T, p, \boldsymbol{x}$ only. In all cases, we assume this functional dependence to be known, and Lipschitz continuous.

The system in eq. (4.25) must be closed with suitable initial conditions (ICs) and boundary conditions (BCs). Regarding BCs, let $\Gamma := \partial\Omega$ denote the boundary of Ω and $\hat{n}_\Gamma$ the unit outward normal on Γ. The simplest choice of BCs is, in direct analogy to those considered in section 3.3.1, given by:

$$v = [(\boldsymbol{\psi}^\top\boldsymbol{N})\cdot\hat{n}_\Gamma]\hat{n}_\Gamma + g_{v_\parallel} \quad \text{on } \Gamma, \tag{4.27a}$$

$$N_i \cdot \hat{n}_\Gamma = g_i \qquad \text{on } \Gamma \quad \forall i \in \{1:n\}, \tag{4.27b}$$

$$J_s' \cdot \hat{n}_\Gamma = g_s \qquad \text{on } \Gamma. \tag{4.27c}$$

The functions $g_{v_\parallel} : \Gamma \to \mathbb{R}^d$, $g_i : \Gamma \to \mathbb{R}$ and $g_s : \Gamma \to \mathbb{R}$ are prescribed data. As in section 3.3.1, we assume $g_{v_\parallel} \cdot \hat{n}_\Gamma = 0$ on Γ, so that eq. (4.27a) enforces the mass-average constraint in the normal direction and $v = g_{v_\parallel}$ in the tangential directions. Moreover, as in section 3.3.1, we permit the prescribed normal fluxes g_i, g_s to be known algebraic functions of the state variables $T, p, \boldsymbol{x}$.

4.2.4 Adaptations in the locally electroneutral case

The previous discussions can be adapted, *mutatis mutandis*, to handle the flow of anisothermal, locally electroneutral multicomponent electrolyte flows. In other words, the framework of chapter 3, which employs the *salt-charge transformation* [114], can be readily extended to the anisothermal setting.

The relevant adaptations are summarised below. As in section 3.2, we now assume there are $n \geq 3$ species, with equivalent charges z_i for $i \in \{1:n\}$. Let $n_c \geq 2$ denote the number of charged species; we list the species so that the first $(n - n_c)$ species are uncharged, and the last two species are oppositely charged. We assume the local electroneutrality condition (recall eq. (3.1)),

$$\sum_{j=1}^{n} z_j c_j = 0 \quad \text{in } \Omega. \tag{4.28}$$

Following section 3.2.2, one employs an $n \times n$ salt-charge transformation matrix $\boldsymbol{Z}$ (see eq. (3.13)). The concentrations, mole fractions and fluxes transform as

$$\boldsymbol{c}_Z := \boldsymbol{Z}^{-\top} \boldsymbol{c} = \begin{bmatrix} \boldsymbol{c}_\nu \\ 0 \end{bmatrix}, \tag{4.29a}$$

$$\boldsymbol{x}_Z := \boldsymbol{Z}^{-\top} \boldsymbol{x} = \begin{bmatrix} \boldsymbol{x}_\nu \\ 0 \end{bmatrix}, \tag{4.29b}$$

$$\boldsymbol{N}_Z := \boldsymbol{Z}^{-\top} \boldsymbol{N} = \begin{bmatrix} \boldsymbol{N}_\nu \\ I^\top / (F \, \|\boldsymbol{z}\|) \end{bmatrix}. \tag{4.29c}$$

Recall that the condition $(\boldsymbol{c}_Z)_n = (\boldsymbol{x}_Z)_n = 0$ is equivalent to electroneutrality eq. (4.28). We refer to $\boldsymbol{c}_\nu$ as the *component concentrations*, while $\boldsymbol{x}_\nu$ are the *component (molar) fractions* and $\boldsymbol{N}_\nu$ the *component (molar) fluxes*. Moreover, $I = F \boldsymbol{N}^\top \boldsymbol{z}$ represents the electrical current density, where F is the Faraday constant. The electrochemical potentials transform as

$$\boldsymbol{\mu}_Z := \boldsymbol{Z} \boldsymbol{\mu} = \begin{bmatrix} \boldsymbol{\mu}_\nu \\ F \, \|\boldsymbol{z}\| \, \Phi_Z \end{bmatrix}, \tag{4.30}$$

which defines the *component chemical potentials* $\boldsymbol{\mu}_\nu$ and the *salt-charge potential* Φ_Z.

Partial molar properties also transform. For the partial molar volumes, one has:

$$\overline{\boldsymbol{V}_Z} := \boldsymbol{Z}\overline{\boldsymbol{V}} = \frac{\partial \boldsymbol{\mu}_Z}{\partial p} = \begin{bmatrix} \overline{\boldsymbol{V}_\nu} \\ F\,\|\boldsymbol{z}\|\,\frac{\partial \Phi_Z}{\partial p} \end{bmatrix}, \tag{4.31}$$

where the *component partial molar volumes* $\overline{\boldsymbol{V}_\nu}$ were already introduced in eq. (3.20); experimentally, they can be recovered from density measurements [86]. The quantity $\frac{\partial \Phi_Z}{\partial p}$ can be viewed as an *electrostriction coefficient*, and it quantifies the change in molar volume of the system with respect to charge density [99]. However, under electroneutrality, $\frac{\partial \Phi_Z}{\partial p}$ does not show up anywhere in the governing equations and it can thus be ignored. On the other hand, the partial molar entropies transform as

$$\overline{\boldsymbol{S}_Z} := \boldsymbol{Z}\overline{\boldsymbol{S}} = -\frac{\partial \boldsymbol{\mu}_Z}{\partial T} = \begin{bmatrix} \overline{\boldsymbol{S}_\nu} \\ -F\,\|\boldsymbol{z}\|\,\frac{\partial \Phi_Z}{\partial T} \end{bmatrix}, \tag{4.32}$$

which defines $\overline{\boldsymbol{S}_\nu} := -\frac{\partial \boldsymbol{\mu}_\nu}{\partial T}$, the *component partial molar entropies*. The additional quantity $\frac{\partial \Phi_Z}{\partial T}$ turns out to be quite subtle. Unlike $\frac{\partial \Phi_Z}{\partial p}$, this quantity *does* show up in the governing electroneutral equations, in particular the entropy balance law eq. (4.6). Indeed, under the salt-charge transformation, the entropy flux (recall eq. (4.7)) becomes

$$J_s = J_s' + \overline{\boldsymbol{S}}^\top \big(\boldsymbol{N} - \boldsymbol{c}v\big) = J_s' + \overline{\boldsymbol{S}_\nu}^\top \big(\boldsymbol{N}_\nu - \boldsymbol{c}_\nu v\big) - I\frac{\partial \Phi_Z}{\partial T}. \tag{4.33}$$

Equation (4.33) shows that $\frac{\partial \Phi_Z}{\partial T}$ apparently quantifies the excess flow of entropy due to the electrical current. However, since J_s only appears in the entropy balance law eq. (4.6) through its divergence, it is interesting to note that

$$\nabla \cdot J_s = \nabla \cdot \Big(J_s' + \overline{\boldsymbol{S}_\nu}^\top \big(\boldsymbol{N}_\nu - \boldsymbol{c}_\nu v\big)\Big) - I \cdot \nabla\Big(\frac{\partial \Phi_Z}{\partial T}\Big), \tag{4.34}$$

since $\nabla \cdot I = 0$ under electroneutrality (see eq. (3.15)). In particular, so long as $\frac{\partial \Phi_Z}{\partial T}$ is a constant (or approximately so), its value is not of physical importance in the present model. Since we are not aware of discussions on $\frac{\partial \Phi_Z}{\partial T}$ in the literature on OSM flow, for the sake of simplicity we shall assume that it can be neglected. If, however, a model for this quantity were to be provided, then it could straightforwardly be incorporated into our numerical framework.

The vector $\boldsymbol{\psi}$ and transport matrix $\hat{\mathfrak{M}}$ transform by (cf. eq. (3.17))

$$\boldsymbol{\psi}_Z := \boldsymbol{Z}\boldsymbol{\psi}, \quad \hat{\mathfrak{M}}_Z := \begin{bmatrix} 1 & 0 \\ 0 & \boldsymbol{Z} \end{bmatrix} \hat{\mathfrak{M}} \begin{bmatrix} 1 & 0 \\ 0 & \boldsymbol{Z}^\top \end{bmatrix}, \quad \hat{\mathfrak{M}}^\gamma_Z := \begin{bmatrix} 1 & 0 \\ 0 & \boldsymbol{Z} \end{bmatrix} \hat{\mathfrak{M}}^\gamma \begin{bmatrix} 1 & 0 \\ 0 & \boldsymbol{Z}^\top \end{bmatrix}. \tag{4.35}$$

With these quantities at hand, one can utilise the salt-charge transformation to show that the analogue of eq. (4.25) in the electroneutral setting is as follows. The unknown

functions of space and time to be solved for are the velocity v, irreversible entropy flux J'_s, component molar fluxes $\boldsymbol{N}_\nu$, current density I, temperature T, pressure p, component fractions $\boldsymbol{x}_\nu$, and salt-charge potential Φ_Z, such that:

$$\begin{aligned}\frac{\partial(\rho v)}{\partial t} + \nabla\cdot(\rho v\otimes v) + \nabla p + \gamma\big(v - \boldsymbol{\psi}_Z^\top \boldsymbol{N}_Z\big) \\ -\nabla\cdot\Big(2\eta\epsilon(v) + (\zeta - 2\eta/d)(\nabla\cdot v)\mathbb{I}\Big) = 0,\end{aligned} \tag{4.36a}$$

$$-\begin{bmatrix}1 & 0 & 0\\ 0 & RT\boldsymbol{X}_\nu^0 & 0\\ 0 & 0 & F\,\|\boldsymbol{z}\|\end{bmatrix}\begin{bmatrix}\nabla T\\ \nabla\boldsymbol{x}_\nu\\ \nabla\Phi_Z\end{bmatrix} + \begin{bmatrix}0\\ \left(\boldsymbol{\psi}_Z - \begin{bmatrix}\overline{\boldsymbol{V}_\nu}\\ 0\end{bmatrix}\right)\end{bmatrix}\nabla p + \gamma\begin{bmatrix}0\\ \boldsymbol{\psi}_Z\end{bmatrix} v = \hat{\mathfrak{M}}_Z^\gamma\begin{bmatrix}J'_s\\ \boldsymbol{N}_Z\end{bmatrix}, \tag{4.36b}$$

$$\frac{\partial s_V}{\partial t} + \nabla\cdot(s_V v) + \nabla\cdot\Big(J'_s + \overline{\boldsymbol{S}_\nu}^\top\big(\boldsymbol{N}_\nu - \boldsymbol{c}_\nu v\big)\Big) = g_S, \tag{4.36c}$$

$$\nabla\cdot\big(v - \boldsymbol{\psi}_Z^\top\boldsymbol{N}_Z\big) = 0, \tag{4.36d}$$

$$\frac{\partial}{\partial t}\begin{bmatrix}\boldsymbol{c}_\nu\\ 0\end{bmatrix} + \begin{bmatrix}\nabla\cdot\boldsymbol{N}_\nu\\ \nabla\cdot I\end{bmatrix} = 0. \tag{4.36e}$$

Note that $\boldsymbol{X}_\nu^0$ in eq. (4.36b) is the matrix of thermodynamic factors under electroneutrality from eq. (3.19). Also, it may be helpful to recall that $\boldsymbol{N}_Z$ is defined in eq. (4.29c). In the salt-charge basis, the entropy production g_S in eq. (4.36c) can be expressed as (cf. eq. (4.26))

$$g_S = \frac{1}{T}\left\{2\eta\big(\epsilon^0(v) : \epsilon^0(v)\big) + \zeta(\nabla\cdot v)^2 + \left(\begin{bmatrix}J'_s\\ \boldsymbol{N}_Z\end{bmatrix}^\top\hat{\mathfrak{M}}_Z\begin{bmatrix}J'_s\\ \boldsymbol{N}_Z\end{bmatrix}\right)\right\}. \tag{4.37}$$

It is worth comparing eq. (4.36) with eq. (3.24) (the isothermal case), and eq. (4.25) (the uncharged case). Comparing eqs. (3.24) and (4.36), we see that the main difference is the inclusion of temperature in eq. (4.36b), and the entropy balance law eq. (4.36c). On the other hand, comparing eqs. (4.25) and (4.36), we see that the main difference is the salt-charge potential in eq. (4.36b), and the solenoidal condition on I in eq. (4.36e).

Overall, although eqs. (3.24), (4.25), and (4.36) are notationally cumbersome, and certainly are not identical, they are structurally very similar. In particular, with suitable adaptations, they can all be discretised using the same strategies from chapter 3.

4.3 Discretisation

In this section we outline how the governing anisothermal equations can be discretised using the ideas from chapter 3. For brevity, we will focus on the equations for the

uncharged case, in eq. (4.25). However, the same discretisation strategy applies to the charged, locally electroneutral equations in eq. (4.36), and we will numerically simulate this case in section 4.4.2.

4.3.1 Finite element spaces and reconstruction operators

We use the standard notation for Lebesgue and Sobolev spaces $L^2(\Omega)$, $W^{1,\infty}(\Omega)$, $H^1(\Omega)$, $H(\mathrm{div};\Omega)$ and their norms [48]. Moreover, we write $L^2_0(\Omega) := \{q \in L^2(\Omega) : (q,1)_\Omega = 0\}$ for the subspace of functions in $L^2(\Omega)$ with vanishing mean. We write $H^1_0(\Omega) := \{u \in H^1(\Omega) : u|_\Gamma = 0\}$ and $H_0(\mathrm{div};\Omega) := \{u \in H(\mathrm{div};\Omega) : (u \cdot \hat{n}_\Gamma)|_\Gamma = 0\}$ for subspaces with vanishing traces (recall $\Gamma := \partial\Omega$ with outward unit normal $\hat{n}_\Gamma$).

Following section 3.3.3, we introduce finite dimensional finite element subspaces that may depend on a parameter $h \in (0,\infty)$ representing, for example, the mesh size:

$$\mathcal{V}_h \subset H^1(\Omega)^d, \qquad \mathcal{V}_{0h} := \mathcal{V}_h \cap H^1_0(\Omega)^d, \tag{4.38a}$$

$$\mathcal{P}_h \subset L^2(\Omega), \qquad \mathcal{P}_{0h} := \mathcal{P}_h \cap L^2_0(\Omega), \tag{4.38b}$$

$$\mathcal{N}_h \subset H(\mathrm{div};\Omega), \qquad \mathcal{N}_{0h} := \mathcal{N}_h \cap H_0(\mathrm{div};\Omega), \tag{4.38c}$$

$$\mathcal{X}_h \subset L^2(\Omega), \qquad \mathcal{X}_{0h} := \mathcal{X}_h \cap L^2_0(\Omega), \tag{4.38d}$$

$$\mathcal{S}_h \subset W^{1,\infty}(\Omega). \tag{4.38e}$$

We assume that $\mathcal{P}_h, \mathcal{X}_h$ and $\mathcal{S}_h$ contain the constant functions, i.e. $1 \in \mathcal{P}_h \cap \mathcal{X}_h \cap \mathcal{S}_h$.

Following section 3.3.3, we seek the discrete velocity $v_h \in \mathcal{V}_h$ and pressure $p_h \in \mathcal{P}_h$. We seek the discrete molar fluxes $(\boldsymbol{N}_h)_i \in \mathcal{N}_h$ for $i \in \{1:n\}$ and irreversible entropy flux $J'_{s,h} \in \mathcal{N}_h$. We seek the discrete mole fractions $(\boldsymbol{x}_h)_i \in \mathcal{X}_h$ for $i \in \{1:n\}$ and temperature $T_h \in \mathcal{X}_h$. We additionally discretise the volumetric entropy, $s_{V,h} \in \mathcal{S}_h$.

We assume that $(\mathcal{V}_h, \mathcal{P}_h)$ forms an inf-sup stable Stokes pair [49], in the sense of eq. (3.32). Likewise, we assume that $(\mathcal{N}_h, \mathcal{X}_h)$ forms a divergence-free and inf-sup stable mixed-Poisson pair [49], in the sense of eq. (3.33). In practice, in our numerical experiments we employ the degree $k \geq 2$ Taylor–Hood pair [17, 109] for $(\mathcal{V}_h, \mathcal{P}_h)$. For $(\mathcal{N}_h, \mathcal{X}_h)$ we employ the $\mathbb{RT}_k$–$\mathbb{DG}_{k-1}$ [96] pair, although the $\mathbb{BDM}_k$–$\mathbb{DG}_{k-1}$ pair [22, 85] is equally viable. For $\mathcal{S}_h$ we employ the $\mathbb{CG}_{k-1}$ finite element space of continuous piecewise degree $k-1$ polynomials.

Following section 3.3.4, we shall employ Lipschitz continuous smoothing operators

$$\pi_{\mathcal{P}_h} : \mathcal{P}_h \to \mathcal{P}_h \cap W^{1,\infty}(\Omega) \quad \text{and} \quad \pi_{\mathcal{X}_h} : \mathcal{X}_h \to \mathcal{X}_h \cap W^{1,\infty}(\Omega). \tag{4.39}$$

In practice, we take these to be the $L^2(\Omega)$-projection of $\mathcal{P}_h$ into $\mathcal{P}_h \cap W^{1,\infty}(\Omega)$ and likewise for $\mathcal{X}_h$. The *reconstructions* of T_h, p_h and $\boldsymbol{x}_h$ are defined as

$$\widetilde{T_h} := \pi_{\mathcal{X}_h} T_h, \qquad \widetilde{p_h} := \pi_{\mathcal{P}_h} p_h \qquad \widetilde{(\boldsymbol{x}_h)}_i := \pi_{\mathcal{X}_h}(\boldsymbol{x}_h)_i \Big/ \sum_{j=1}^{n} \pi_{\mathcal{X}_h}(\boldsymbol{x}_h)_j. \tag{4.40}$$

Note that the reconstructed mole fractions are normalised to exactly sum to unity. We then write $\widetilde{\boldsymbol{X}}$, $\widetilde{\boldsymbol{\psi}}$, $\widetilde{\overline{\boldsymbol{V}}}$, $\widetilde{\rho}$, and so on, to denote properties evaluated with the reconstructed $\widetilde{T_h}$, $\widetilde{p_h}$ and $\widetilde{\boldsymbol{x}_h}$ (as opposed to T_h, p_h and $\boldsymbol{x}_h$). Exactly as in chapter 3, we use these reconstructed properties because they ensure the weak differentiability of quantities arising in our discretisation.

4.3.2 Spatially discrete problem

We discretise eq. (4.25) in space (but not time) by multiplying the equations by suitable test functions and integrating over Ω. We use $(\cdot,\cdot)_\Omega$ and $\langle\cdot,\cdot\rangle_\Gamma$ to denote the L^2-inner products on Ω and Γ, respectively. The pressure and viscous terms in eq. (4.25a), in addition to the gradient terms on the left-hand side of eq. (4.25b), are integrated by parts, and the boundary terms vanish owing to our BCs below. Density consistency terms (recall eq. (2.66)) are also incorporated in eq. (4.25d). An equation for $s_{V,h}$ is obtained by taking the $L^2(\Omega)$-projection of the equation $s_{V,h} = \widetilde{s_V}$, which is feasible since s_V is a function of $T, p, \boldsymbol{x}$ only.

Altogether, we obtain the following semi-discrete problem. We seek time-dependent discrete functions $v_h \in \mathcal{V}_h$, $p_h \in \mathcal{P}_h$, $\boldsymbol{N}_h \in (\mathcal{N}_h)^n$, $J'_{s,h} \in \mathcal{N}_h$, $\boldsymbol{x}_h \in (\mathcal{X}_h)^n$, $T_h \in \mathcal{X}_h$, and $s_{V,h} \in \mathcal{S}_h$, such that:

$$\begin{aligned}
&\frac{\mathrm{d}}{\mathrm{d}t}\big(\widetilde{\rho} v_h, u_h\big)_\Omega + \Big(\nabla\cdot(\widetilde{\rho} v_h \otimes v_h) + \gamma\big(v_h - \widetilde{\boldsymbol{\psi}^\top}\boldsymbol{N}_h\big), u_h\Big)_\Omega - \big(p_h, \nabla\cdot u_h\big)_\Omega \\
&+ \Big(2\widetilde{\eta}\epsilon(v_h) + (\widetilde{\zeta} - 2\widetilde{\eta}/d)(\nabla\cdot v_h)\mathbb{I}, \epsilon(u_h)\Big)_\Omega = 0 \quad \forall u_h \in \mathcal{V}_{0h},
\end{aligned} \tag{4.41a}$$

$$\begin{aligned}
&\left(\begin{bmatrix} T_h \\ \boldsymbol{x}_h \end{bmatrix}, \nabla\cdot\begin{bmatrix} K_h \\ RT\widetilde{\boldsymbol{X}}\boldsymbol{W}_h \end{bmatrix}\right)_\Omega - \left(p_h, \nabla\cdot\left\{\left(\widetilde{\boldsymbol{\psi}^\top} - \widetilde{\overline{\boldsymbol{V}}^\top}\right)\boldsymbol{W}_h\right\}\right)_\Omega \\
&+ \Big(\gamma\widetilde{\boldsymbol{\psi}} v_h, \boldsymbol{W}_h\Big)_\Omega = \left(\widetilde{\hat{\mathfrak{M}}^\gamma}\begin{bmatrix} J'_{s,h} \\ \boldsymbol{N}_h \end{bmatrix}, \begin{bmatrix} K_h \\ \boldsymbol{W}_h \end{bmatrix}\right)_\Omega \quad \forall \begin{bmatrix} K_h \\ \boldsymbol{W}_h \end{bmatrix} \in (\mathcal{N}_{0h})^{n+1},
\end{aligned} \tag{4.41b}$$

$$\frac{\mathrm{d}}{\mathrm{d}t}(s_{V,h}, L_h)_\Omega + \Big(\nabla\cdot\big((s_{V,h} v_h) + J'_{s,h} + \widetilde{\overline{\boldsymbol{S}}^\top}(\boldsymbol{N}_h - \widetilde{\boldsymbol{c}} v_h)\big) - g_{S,h}, L_h\Big)_\Omega = 0 \quad \forall L_h \in \mathcal{X}_h, \tag{4.41c}$$

$$\Big(\nabla\cdot(v_h - \widetilde{\boldsymbol{\psi}^\top}\boldsymbol{N}_h), q_h\Big)_\Omega - \Big\langle \hat{n}_\Gamma\cdot(v_h - \widetilde{\boldsymbol{\psi}^\top}\boldsymbol{N}_h), q_h\Big\rangle_\Gamma = 0 \quad \forall q_h \in \mathcal{P}_h, \tag{4.41d}$$

$$\frac{\mathrm{d}}{\mathrm{d}t}\big(\widetilde{\boldsymbol{c}}_h, \boldsymbol{y}_h\big)_\Omega + \big(\nabla\cdot\boldsymbol{N}_h, \boldsymbol{y}_h\big)_\Omega = 0 \quad \forall \boldsymbol{y}_h \in (\mathcal{X}_h)^n, \tag{4.41e}$$

$$\big(s_{V,h} - \widetilde{s_V}, r_h\big)_\Omega = 0 \quad \forall r_h \in \mathcal{S}_h, \tag{4.41f}$$

where the discrete entropy production $g_{S,h}$ in eq. (4.41c) is defined as (cf. eq. (4.26))

$$g_{S,h} := \frac{1 + l_h}{\widetilde{T_h}} \left\{ 2\widetilde{\eta}\big(\epsilon^0(v_h) : \epsilon^0(v_h)\big) + \widetilde{\zeta}(\nabla \cdot v_h)^2 + \left(\begin{bmatrix} J'_{s,h} \\ \boldsymbol{N}_h \end{bmatrix}^\top \widetilde{\hat{\mathfrak{M}}} \begin{bmatrix} J'_{s,h} \\ \boldsymbol{N}_h \end{bmatrix} \right) \right\}, \tag{4.42}$$

and $l_h \in \mathbb{R}$ is a Lagrange multiplier which, if desired, can be used to enforce exact energy preservation. We discuss our energy preservation strategy in section 4.3.3; if this is not desired, one can simply take $l_h = 0$ in eq. (4.42).

Moreover, in exact analogy to section 3.3.5, we strongly impose the following discrete analogue of the BCs in eq. (4.27):

$$v_h = \pi_{\mathcal{V}_h}\Big([(\widetilde{\boldsymbol{\psi}^\top} \boldsymbol{N}_h) \cdot \hat{n}_\Gamma] \hat{n}_\Gamma + g_{v_\parallel} \Big) \quad \text{on } \Gamma, \tag{4.43a}$$

$$(\boldsymbol{N}_h)_i \cdot \hat{n}_\Gamma = \pi_{\mathcal{N}_h}\big(\widetilde{g_i}\big) \quad \text{on } \Gamma \quad \forall i \in \{1 : n\}, \tag{4.43b}$$

$$J'_{s,h} \cdot \hat{n}_\Gamma = \pi_{\mathcal{N}_h}\big(\widetilde{g_s}\big) \quad \text{on } \Gamma, \tag{4.43c}$$

where $\pi_{\mathcal{V}_h}$ and $\pi_{\mathcal{N}_h}$ are $L^2(\Gamma)$-projection operators onto the discrete trace spaces, as defined in eq. (3.39).

Equations (4.41) and (4.43), with suitable initial conditions, define our semi-discrete scheme. However, we should emphasise that, in exact analogy to section 3.4.2, for well-posedness the discrete problem must be supplemented with *integral constraints*. One must choose these on a case-by-case basis, depending on the functional dependence of the material properties on $T, p, \boldsymbol{x}$, and on the boundary conditions.

4.3.3 Structure preservation and timestepping

At the continuous level, the governing Navier–Stokes–OSM equations are entropy dissipating and energy preserving. To see this for the entropy, integrate eq. (4.6) over Ω and apply the divergence theorem, to obtain

$$\frac{\mathrm{d}}{\mathrm{d}t} \int_\Omega s_V \,\mathrm{d}\Omega + \int_\Gamma (s_V v + J_s) \cdot \hat{n}_\Gamma \,\mathrm{d}\Gamma = \int_\Omega g_S \,\mathrm{d}\Omega. \tag{4.44}$$

Hence, subject to the no-flux conditions

$$v \cdot \hat{n}_\Gamma = 0, \quad J_s \cdot \hat{n}_\Gamma = 0 \quad \text{on } \Gamma, \tag{4.45}$$

it holds that

$$\frac{\mathrm{d}}{\mathrm{d}t} \int_\Omega s_V \,\mathrm{d}\Omega = \int_\Omega g_S \,\mathrm{d}\Omega \geq 0, \tag{4.46}$$

since $g_S \geq 0$ pointwise. Thus the entropy of the system, $\int_\Omega s_V \,\mathrm{d}\Omega$, is non-decreasing under the BCs eq. (4.45). Regarding the energy, one can similarly integrate eq. (1.49) over Ω, and apply the divergence theorem, to obtain

$$\frac{\mathrm{d}}{\mathrm{d}t}\int_\Omega \rho e_{\mathrm{tot}} \,\mathrm{d}\Omega + \int_\Gamma (\rho e_{\mathrm{tot}} v - \sigma v + J_q) \cdot \hat{n}_\Gamma \,\mathrm{d}\Gamma = 0. \tag{4.47}$$

Here, e_{tot} is the specific energy, so ρe_{tot} is the volumetric energy. Thus the energy of the system, $\int_\Omega \rho e_{\mathrm{tot}} \,\mathrm{d}\Omega$, remains constant under the BCs

$$v = 0, \quad J_q \cdot \hat{n}_\Gamma = 0 \quad \text{on } \Gamma. \tag{4.48}$$

When the data $g_{v_\parallel}, g_i$ and g_s in eq. (4.27) are zero, at the continuous level one has:

$$v = 0, \quad N_i \cdot \hat{n}_\Gamma = 0 \;\; \forall i \in \{1:n\}, \quad J_s' \cdot \hat{n}_\Gamma = 0 \quad \text{on } \Gamma. \tag{4.49}$$

Using $J_s' = \frac{J_q'}{T}$ and eqs. (1.51), (1.60), (1.61), and (4.49), we find that

$$J_s \cdot \hat{n}_\Gamma = 0, \quad J_q \cdot \hat{n}_\Gamma = 0 \quad \text{on } \Gamma. \tag{4.50}$$

Hence eqs. (4.45) and (4.48) are satisfied. Thus entropy dissipation and energy preservation both hold at the continuous level, for vanishing boundary data in eq. (4.27). We now investigate the extent to which this holds discretely.

At the semi-discrete level (i.e. without discretising in time), entropy dissipation follows readily by taking $L_h = 1$ in eq. (4.41c). The divergence theorem then yields

$$\frac{\mathrm{d}}{\mathrm{d}t}\int_\Omega s_{V,h} \,\mathrm{d}\Omega + \int_\Gamma \Big((s_{V,h} v_h) + J_{s,h}' + \widetilde{\overline{\boldsymbol{S}}^\top}(\boldsymbol{N}_h - \widetilde{\boldsymbol{c}} v_h) \Big) \cdot \hat{n}_\Gamma \,\mathrm{d}\Gamma = \int_\Omega g_{S,h} \,\mathrm{d}\Omega, \tag{4.51}$$

and, owing to the BCs eq. (4.43) together with the assumption that the boundary data is zero, the boundary term in eq. (4.51) vanishes. One therefore obtains

$$\frac{\mathrm{d}}{\mathrm{d}t}\int_\Omega s_{V,h} \,\mathrm{d}\Omega = \int_\Omega g_{S,h} \,\mathrm{d}\Omega. \tag{4.52}$$

Inspection of eq. (4.42) reveals that $g_{S,h} \geq 0$ pointwise, so long as $l_h \geq -1$. Hence, in this case, the numerical scheme is entropy dissipating.

In general, due to spatial discretisation error, exact energy preservation cannot be expected without further work. A straightforward way of accomplishing this is to treat the Lagrange multiplier l_h in eq. (4.42) as an additional time-dependent scalar unknown to be solved for. An additional equation that implicitly determines l_h must then be chosen. We take this equation to be the statement of discrete energy preservation:

$$\frac{\mathrm{d}}{\mathrm{d}t}\int_\Omega \frac{1}{2}\widetilde{\rho}(v_h \cdot v_h) + \widetilde{\rho e_{\mathrm{int}}} \,\mathrm{d}\Omega = 0. \tag{4.53}$$

The expression in the integrand is obtained by noting that the specific total energy is given by eq. (1.48), where the volumetric internal energy ρe_{int} is a function of $T, p, \boldsymbol{x}$.

Owing to eq. (4.53), our semi-discrete scheme is, by construction, energy preserving. Assuming that $l_h \geq -1$ holds (which can always be checked *a posteriori*), by eq. (4.52) it is also entropy dissipating. In practice, we observe numerically that $|l_h| \ll 1$, and we expect that $l_h \to 0$ under mesh refinement. Indeed, note that $l_h = 0$ recovers the correct expression for the entropy production, which was obtained from the total energy balance to begin with (recall section 1.5). Another argument to be made for using l_h is that its use amounts to rescaling the transport properties η, ζ and $\widetilde{\hat{\mathfrak{M}}}$ in the entropy production by a factor of $(1 + l_h)$. For $|l_h|$ small, this rescaling will likely be within the extent of experimental uncertainty in η, ζ and $\widetilde{\hat{\mathfrak{M}}}$.

Finally, we should mention how entropy dissipation and energy preservation can be retained once a timestepping scheme is applied to the semi-discrete problem. Following section 3.4.3, we shall focus our attention on implicit Runge–Kutta (IRK) methods [120]. A general n_s-stage IRK method can be described by a *Butcher tableau*,

$$\begin{array}{c|c} c^{\text{irk}} & A^{\text{irk}} \\ \hline & b^{\text{irk}} \end{array}, \tag{4.54}$$

where $b^{\text{irk}}, c^{\text{irk}} \in \mathbb{R}^{n_s}$ and $A^{\text{irk}} \in \mathbb{R}^{n_s \times n_s}$ are coefficients determining the method [120].

Once a finite element basis has been chosen, our semi-discrete problem in eqs. (4.41), (4.43), and (4.53) amounts to an index-1 differential algebraic equation of the form

$$\frac{\mathrm{d}y}{\mathrm{d}t} = f(y, z), \tag{4.55}$$

$$0 = g(y, z), \tag{4.56}$$

where $y \in \mathbb{R}^{D_1}$ and $z \in \mathbb{R}^{D_2}$, for some integers $D_1, D_2 \geq 2$ and functions f, g whose precise form is unimportant. Without any loss of generality, the finite element basis can be chosen such that the first two degrees of freedom are the entropy and energy,

$$\begin{aligned} y_1 &= \int_\Omega s_{V,h} \, \mathrm{d}\Omega, \\ y_2 &= \int_\Omega \frac{1}{2} \widetilde{\rho}(v_h \cdot v_h) + \widetilde{\rho e_{\text{int}}} \, \mathrm{d}\Omega, \end{aligned} \tag{4.57}$$

and it holds that $f_1(y, z) \geq 0$ and $f_2(y, z) = 0$ whenever $g(y, z) = 0$, due to the discussion above. Note that this choice of basis is purely a theoretical device; in implementations one usually works with locally supported bases, but all choices of

bases are mathematically equivalent. When the IRK method with Butcher tableau eq. (4.54) is applied to eq. (4.55), the value of y^{k+1} at timestep $k+1$ is given by

$$y^{k+1} = y^k + \Delta t \sum_{i=1}^{n_s} b_i^{\text{irk}} f(Y^{ki}, B^{ki}), \tag{4.58}$$

where Δt is the timestep, and Y^{ki}, B^{ki} are stage values which satisfy $g(Y^{ki}, B^{ki}) = 0$, in addition to other equations [120, sec. (VI.1), eq. (1.11)]. Therefore, we see from eq. (4.58) that fully-discrete entropy dissipation and energy preservation,

$$y_1^{k+1} \geq y_1^k, \qquad y_2^{k+1} = y_2^k, \tag{4.59}$$

will hold if $b_i^{\text{irk}} \geq 0$ for all $i \in \{1 : n_s\}$. In this case, we say that the IRK method has *positive quadrature weights*. Any Runge–Kutta method that is *algebraically stable* has positive quadrature weights [120], which includes the backward Euler method, and the higher-order methods of Gauss, RadauIA, RadauIIA and LobattoIIIC.

We have therefore shown that, by employing any algebraically stable IRK method, entropy dissipation and energy preservation are retained during timestepping. It should be emphasised, of course, that in a numerical implementation, this will only be true up to solver tolerances, quadrature error, and rounding error.

4.4 Numerical examples

In this section, we present numerical examples which demonstrate the feasibility of our proposed anisothermal discretisations. All examples were implemented using Firedrake [63]. Irksome [51, 71] was used for timestepping, and we generated the meshes using ngsPETSc [12, 101]. We solved all nonlinear systems using Newton's method [35], together with the sparse direct solver MUMPS [1].

4.4.1 Structure preservation in a lid-driven cavity

To show that our discretisation is capable of energy preservation and entropy dissipation, we consider the lid-driven cavity flow of an ideal gaseous mixture of $n = 2$ species, in $d = 2$ spatial dimensions.

In this simulation, we treat all quantities arising in the governing problem eq. (4.25) as being physically nondimensional. We use molar masses of $m_1 = 1.25$ and $m_2 = 0.75$. For the equilibrium thermodynamic properties of the mixture, we set $R = 1$ for the gas constant, and we assume a calorically perfect ideal gaseous mixture, as in

eq. (1.27). We assume the gases to be monatomic, so that their partial molar heat capacities are $\overline{C_{p,1}} = \overline{C_{p,2}} = \frac{5}{2}R$. For the transport properties, we take Stefan–Maxwell diffusivities of $\mathscr{D}_{12} = \mathscr{D}_{21} = 1.1$, a thermal conductivity of $\kappa = 1.2$, thermal diffusion coefficients of $D_1^T = 1.3 = -D_2^T$, a shear viscosity of $\eta = 1.4$ and a bulk viscosity of $\zeta = 1.5$.

We simulate the system from an initial time of $t = 0$, up to a final time of $t = 1.2$. As initial conditions, we set $x_1|_{t=0} = x_2|_{t=0} = 0.5$ for the mole fractions, $p|_{t=0} = 0.9$ for the pressure and $T|_{t=0} = 0.8$ for the temperature, uniformly in the domain Ω. We take $\Omega = (0,1)^2$ to be the unit square. We employ the boundary conditions in eq. (4.27), with zero normal fluxes $g_1 = g_2 = g_s = 0$ on $\Gamma := \partial\Omega$. We set the tangential velocity $g_{v_\parallel}$ to be zero on the top, left, and bottom boundaries of Ω. On the right boundary of Ω, we impose a quadratic forcing profile, which grows linearly in magnitude with the time t, and is subsequently ramped down to zero at $t = 1$. We accomplish this by taking:

$$g_{v_\parallel}(x,y) = t \cdot g_t(t) \begin{bmatrix} 0 \\ 0.75y(1-y) \end{bmatrix} \qquad \forall (x,y) \in \Gamma \text{ with } x = 1 \text{ and } 0 \leq y \leq 1, \tag{4.60}$$

where g_t is a piecewise linear function which stops the forcing once $t \geq 1$:

$$g_t(t) = \begin{cases} 1 & \text{if } 0 \leq t \leq 0.98, \\ 1 - \big(50 \cdot (t - 0.98)\big) & \text{if } 0.98 \leq t \leq 1, \\ 0 & \text{if } t \geq 1. \end{cases} \tag{4.61}$$

Hence, the energetics of the system will be affected by the forcing (cf. the σv term in eq. (4.47)) up to time $t = 1$. Once $t > 1$, the system becomes unforced; energy preservation and entropy dissipation must then hold. We now verify that this is captured in our numerical discretisation.

We solve the discrete problem eq. (4.41) using a mesh of 852 triangles. For discrete finite element spaces we employ the degree k Taylor–Hood pair [17, 109] for $(\mathcal{V}_h, \mathcal{P}_h)$, the $\mathbb{RT}_k$–$\mathbb{DG}_{k-1}$ [96] pair for $(\mathcal{N}_h, \mathcal{X}_h)$, and $\mathcal{S}_h = \mathbb{CG}_{k-1}$ with degree $k = 5$. The nonlinear systems at each timestep are solved using Newton's method with an absolute tolerance on the residual of 10^{-10} in the Euclidean norm. Each nonlinear system consists of 3.4×10^5 unknowns.

For timestepping, we employ the RadauIIA implicit Runge–Kutta method [120] with two stages, with a timestep of $\Delta t = 0.01$. After the 100th timestep (i.e. once $t > 1$), the system becomes unforced, and we then employ the Lagrange multiplier strategy of section 4.3.3 to enforce energy preservation eq. (4.53). Note that high-order (i.e. of order greater than one) timestepping methods are not expected to be beneficial

in the present example, since g_t is not continuously differentiable and therefore the exact solution is not smooth in time. Nonetheless, we employ the RadauIIA method with two stages here, for the sake of demonstrating that structure preservation is possible with multi-stage Runge–Kutta methods.

Figure 4.1: Plot of the change in entropy, total energy, kinetic energy and internal energy, starting from time $t = 0.98$, for the simulation in section 4.4.1. The total energy is preserved for $t > 1$, which is when the system is unforced. The Lagrange multiplier l_h is also plotted.

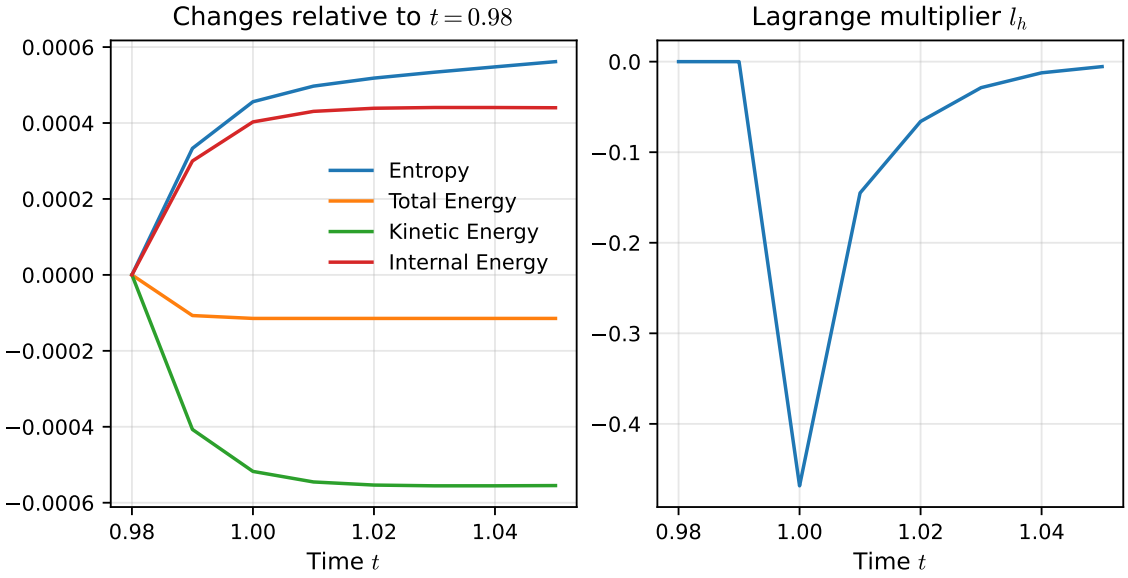

In fig. 4.1, we plot the change in entropy $\int_\Omega s_{V,h}\,\mathrm{d}\Omega$, kinetic energy $\int_\Omega \frac{1}{2}\widetilde{\rho}(v_h \cdot v_h)\,\mathrm{d}\Omega$, internal energy $\int_\Omega \widetilde{\rho e_{\mathrm{int}}}\,\mathrm{d}\Omega$, and total energy $\int_\Omega \frac{1}{2}\widetilde{\rho}(v_h \cdot v_h) + \widetilde{\rho e_{\mathrm{int}}}\,\mathrm{d}\Omega$. The plot starts from time $t = 0.98$ when the forcing begins to be ramped down (recall eq. (4.61)), and goes up to time $t = 1.05$ after which the energetics of the system do not change much. We see that the entropy increases over the plotted timesteps, while the total energy is preserved over the timesteps for $t > 1$, which is when the system is unforced. Indeed, for $t > 1$, we compute that the change in total energy always remains below 10^{-14}, although it is not exactly zero due to rounding error and solver tolerances. The value of the Lagrange multiplier l_h is also plotted in fig. 4.1 as a function of time. In particular, we see that $l_h \geq -1$ holds for all time, which ensures that entropy production remains non-negative. Finally, in fig. 4.2 we plot the temperature T and streamlines of the velocity v at time $t = 1.04$, shortly after the forcing is stopped.

Figure 4.2: Streamlines of the velocity v from the simulation of section 4.4.1 at time $t = 1.04$. The domain is coloured by the temperature T.

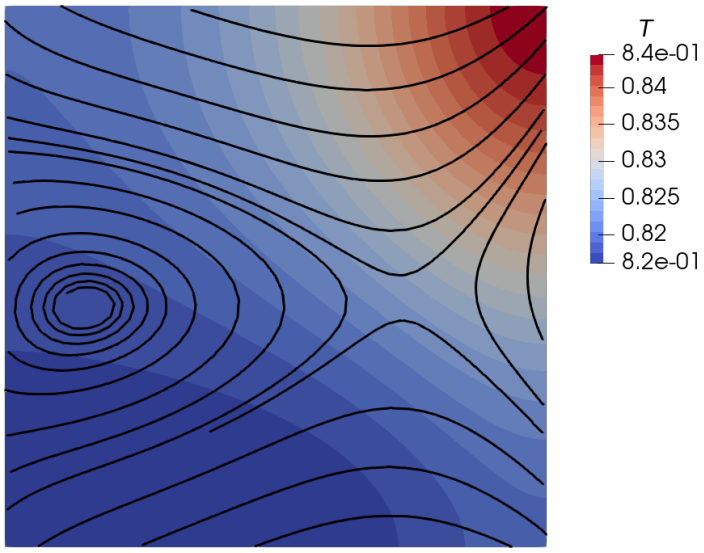

4.4.2 Anisothermal cosolvent electrolyte

In this example, we repeat the cosolvent electrolyte simulation from section 3.5.3, but now in the anisothermal setting where the governing equations are given by eq. (4.36). Recall that this simulation involves an electrolyte comprised of $LiPF_6$ salt dissolved in two solvents, namely ethyl-methyl-carbonate (EMC) and ethylene-carbonate (EC).

We use the same material properties from section 3.5.3, but in the anisothermal setting we must also specify the component partial molar heat capacities. Note that by a Maxwell relation (cf. eq. (1.7)), these are given by

$$\overline{\boldsymbol{C}}_{p,\nu} = T\frac{\partial \overline{\boldsymbol{S}_\nu}}{\partial T}, \tag{4.62}$$

where the component partial molar entropies $\overline{\boldsymbol{S}_\nu}$ were introduced in eq. (4.32). We take $\overline{\boldsymbol{C}}_{p,\nu,\mathrm{EMC}} = 183\,\mathrm{J\,K^{-1}\,mol^{-1}}$ and $\overline{\boldsymbol{C}}_{p,\nu,\mathrm{EC}} = 130\,\mathrm{J\,K^{-1}\,mol^{-1}}$, and we assume these to be constant. These values were obtained using empirical correlations from [54, Table IV] at temperature $T = 298.15\,\mathrm{K}$. Lacking data for the partial molar heat capacity of $LiPF_6$ dissolved in an EMC:EC mixture, we make the approximation that $\overline{\boldsymbol{C}}_{p,\nu,\mathrm{LiPF_6}} = 0$, i.e. we assume that $LiPF_6$ does not contribute to the total heat capacity. This is a crude but acceptable approximation in the current simulation where $LiPF_6$ is relatively dilute, with its component fraction value fluctuating around $x_{\mathrm{LiPF_6}} \approx 0.077$. The additional transport properties to be specified are the thermal conductivity κ and thermal diffusion coefficients D_i^T (see eq. (1.78)). Lacking data

for the D_i^T, we set these to be zero; the Soret and Dufour effects are expected to be negligible in this system. We are also not aware of any thermal conductivity data in the literature for EMC:EC mixtures. We therefore take the thermal conductivity to be $\kappa = 0.16\,\mathrm{W\,m^{-1}\,K^{-1}}$, since similar thermal conductivity values have been reported in the literature for structurally similar chemicals at $T = 298.15\,\mathrm{K}$ (see [31, supplementary material, fig. S7]).

We employ the same Hull cell domain Ω, boundary conditions, initial conditions, and integral constraints as in section 3.5.3. For the temperature, we use an initial condition of $T|_{t=0} = 298.15\,\mathrm{K}$. For the thermal boundary conditions, instead of prescribing the normal component of the irreversible entropy flux, as in eq. (4.27c), we consider the Robin-type BCs

$$J_q' \cdot \hat{n}_\Gamma = \frac{\kappa_{\mathrm{wall}}}{l_{\mathrm{wall}}}(T - T_{\mathrm{wall}}) \quad \text{on } \Gamma, \tag{4.63}$$

where $J_q' = TJ_s'$ is the irreversible heat flux, while κ_{wall}, l_{wall} and T_{wall} are prescribed. Physically, eq. (4.63) is a statement of Fourier's law, expressing that the walls (i.e. the domain boundary Γ) are thermally conducting, with thermal conductivity κ_{wall} and thickness l_{wall}. Moreover, T_{wall} represents the ambient temperature directly outside the wall. We set $\kappa_{\mathrm{wall}} = 0.1 \cdot \kappa = 0.016\,\mathrm{W\,m^{-1}\,K^{-1}}$, and $l_{\mathrm{wall}} = 0.1\,\mathrm{mm}$, where we note that the width of the Hull cell is 10 mm. We take T_{wall} to be 298.15 K on the top, left and bottom walls. On the right wall we take T_{wall} to be 327.97 K. Near the vertices of the right wall, we have T_{wall} vary smoothly between the values of 298.15 K and 327.97 K. Note that these Robin-type BCs are implemented in a similar fashion to the Dirichlet BCs on the mole fractions from section 3.5.2, wherein we suitably enlarge the space of test functions and we add appropriate boundary terms in the discretisation (cf. eq. (3.53)).

We solve the discretised anisothermal problem using the same mesh, finite element spaces $(\mathcal{V}_h, \mathcal{P}_h)$ and $(\mathcal{N}_h, \mathcal{X}_h)$ (with $\mathcal{S}_h = \mathbb{CG}_{k-1}$ where $k = 4$), timestepping scheme, and Newton solver, as in section 3.5.3. The nonlinear systems at each timestep consist of 2.1×10^6 unknowns, compared with 1.7×10^6 unknowns in section 3.5.3. The larger degree of freedom count is due to discretisation of the temperature and irreversible entropy flux.

Note that we numerically integrate the governing equations up to a final time of 172800 seconds (two days) using the RadauIIA implicit Runge–Kutta method [120] with two stages, and with 200 timesteps. The molar fluxes and fractions vary non-trivially over the course of these 200 timesteps (cf. fig. 3.4). However, a dimensional analysis reveals that the thermal timescale is much smaller than the diffusive timescale

Figure 4.3: Streamlines of the irreversible heat flux J_q' from the simulation of section 4.4.2 at time $t = 4320\,\mathrm{s}$. The domain is coloured by the temperature T.

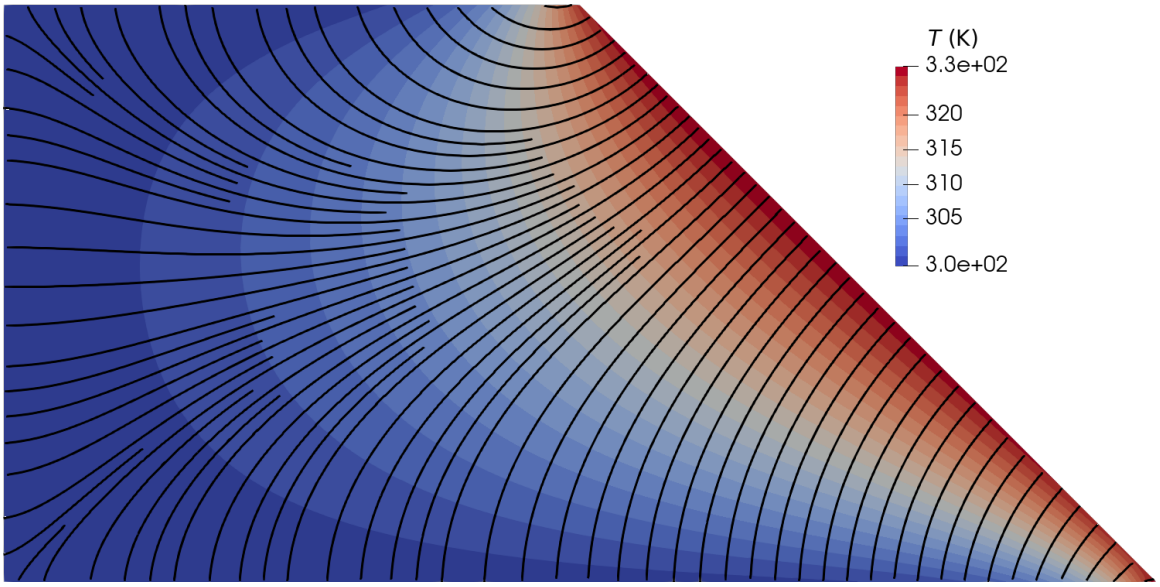

for this problem. In particular, we observe that the temperature field reaches near steady-state conditions within the first two timesteps. This underscores the practical value of using an implicit Runge–Kutta method, which remains stable in the presence of multiple physical processes with disparate timescales.

In fig. 4.3 we plot the computed temperature field T, and streamlines of the irreversible heat flux J_q', at time $t = 4320\,\mathrm{s}$. The qualitative behaviour of these fields matches what one would expect from Robin-type BCs in eq. (4.63), with heat flowing from the hotter right wall to the others. It is also worth noting that the temperature and irreversible heat flux remain well-behaved near the top-right corner, even though the current density becomes singular in this region (cf. fig. 3.1).

4.5 Conclusions

We have demonstrated that the numerical framework from the previous chapters extends readily to the anisothermal setting. If desired, energy preservation and entropy dissipation can simultaneously be enforced using a Lagrange multiplier. We also brought attention to the quantity $\frac{\partial \Phi_Z}{\partial T}$, which appears to have physical importance in the entropy balance for electroneutral flows, and we are not aware of discussions on this in the existing OSM literature. It will be of interest to clarify the meaning of this quantity in future work.

Chapter 5

Conclusions

This thesis has developed a general numerical framework, based on finite element methods, for the simulation of multicomponent flows. The foundation of this framework was established in chapter 2, where we devised a large family of finite element methods for Stokes–OSM flow that are amenable to Newton's method, and in a linearised setting are provably discretely well-posed and quasi-optimal. Chapters 3 and 4 then extended this framework in various directions by systematically incorporating additional physical phenomena, such as transience, Navier–Stokes flow, local electroneutrality and anisothermality. This has ultimately resulted in a large family of finite element algorithms that are capable of solving the Navier–Stokes–OSM equations eqs. (1.50), (1.74), and (1.75) in great generality. The challenges that we faced along the way to accomplishing this have, in many cases, not previously been addressed or even identified in the literature.

The generality of our framework here enables the simulation of scientific applications that were not previously possible. A particularly exciting application is the simulation of battery electrolytes, since these are known to be captured well by OSM theory [23, 86], but for lithium-ion batteries the relevant OSM transport coefficients have only recently been experimentally measured [68, 117]. For systems where transport coefficients are not known, the numerical framework of this thesis opens the door for their estimation using techniques such as inverse modelling and PDE-constrained optimisation.

Of course, while the numerical framework of this thesis is quite general, ample opportunities exist to further improve upon it and extend its scientific applicability. For example, large-scale simulations in three spatial dimensions will necessitate the development of efficient preconditioning strategies, as investigated in other work involving the present author [72]. Another example is that of extreme physical regimes, wherein, for example, the species concentrations may locally vanish (or nearly so),

or where the Reynolds or Péclet numbers become very large. Specialising upon the methods here by efficiently handling these regimes (e.g. with stabilisation schemes) would further increase the scientific applicability of our framework. Finally, one could consider extending upon the governing equations eqs. (1.50), (1.74), and (1.75) themselves, to capture additional physical phenomena, such as chemical reactions [56], nonlinear constitutive laws [91], or violations of local electroneutrality [99].

Ultimately, this thesis represents some of the first work on the development and numerical analysis of algorithms for multicomponent flows in non-idealised physical settings. It is hoped that our work herein will be useful, both for practitioners in the sciences and for other mathematicians studying the numerical analysis of multicomponent fluids.

Appendix

This appendix is adapted from the appendix in [7].

A.1 A problematic model

Consider a binary mixture on a fixed domain Ω with molar concentrations c_1, c_2, total concentration $c_T = c_1 + c_2$ and molar fractions $x_i := c_i/c_T$ with $x_1 + x_2 = 1$. Let $x := x_1$. We assume a volumetric equation of state

$$c_T = A + Bx, \tag{A.1}$$

with A and B non-zero constants satisfying $A > 0$ and $A + B > 0$ so that $c_T > 0$. This seemingly benign equation of state assumes the total concentration is linear in composition; an experimentalist might reasonably make such an approximation by fitting experimental data. Since $c_T = n_T/V$ where n_T is the total number of moles and V is the volume, one can verify that the (non-constant) partial molar volumes (recall eq. (1.10)) are

$$\overline{V_1} = \frac{A + B(2x-1)}{(A+Bx)^2}, \quad \overline{V_2} = \frac{A + 2Bx}{(A+Bx)^2} \quad \text{and} \quad \frac{1}{c_T} = x_1\overline{V_1} + x_2\overline{V_2}.$$

Assume that the total number of moles of each species is conserved, so that

$$\frac{\mathrm{d}}{\mathrm{d}t}\int_\Omega c_i \,\mathrm{d}\Omega = 0 \quad \forall i \in \{1,2\}. \tag{A.2}$$

Since $c_T = c_1 + c_2$, we can use eq. (A.2) and use eq. (A.1) to deduce that

$$\frac{\mathrm{d}}{\mathrm{d}t}\int_\Omega x \,\mathrm{d}\Omega = 0. \tag{A.3}$$

Moreover, since $c_1 = xc_T$ we can use eqs. (A.1) to (A.3) to deduce that

$$\frac{\mathrm{d}}{\mathrm{d}t}\int_\Omega x^2 \,\mathrm{d}\Omega = 0. \tag{A.4}$$

Let $\bar{x} := \int_\Omega x \, \mathrm{d}\Omega / \int_\Omega 1 \, \mathrm{d}\Omega$ denote the spatial mean of x. Since Ω is assumed not to depend on t, eq. (A.3) implies that $\bar{x}$ is a constant. Note that eqs. (A.3) and (A.4) also imply

$$\frac{\mathrm{d}}{\mathrm{d}t} \int_\Omega (x - \bar{x})^2 \, \mathrm{d}\Omega = \frac{\mathrm{d}}{\mathrm{d}t} \Big(\int_\Omega x^2 \, \mathrm{d}\Omega - \int_\Omega \bar{x}^2 \, \mathrm{d}\Omega \Big) = 0.$$

Thus $\int_\Omega (x - \bar{x})^2 \, \mathrm{d}\Omega = C$ for some constant C. Now, if x is initially spatially uniform, then $C = 0$. This then implies that $x = \bar{x}$ a.e. in Ω for all time, and $\bar{x}$ is a constant.

To conclude, any model which assumes equation of state eq. (A.1) and conservation properties eq. (A.2), with Ω independent of t, is seemingly either (i) ill-posed or (ii) well-posed, but incapable of making physically meaningful predictions, since a solution that initially has a spatially uniform composition retains that uniform composition over all time.

Bibliography

[1] P. R. Amestoy, I. S. Duff, J.-Y. L'Excellent, and J. Koster, *A fully asynchronous multifrontal solver using distributed dynamic scheduling*, SIAM J. Matrix Anal. Appl., 23 (2001), pp. 15–41.

[2] P. W. Atkins, J. De Paula, and J. Keeler, *Atkins' Physical Chemistry*, Oxford University Press, Oxford, 12th ed., 2023.

[3] F. R. Aznaran, P. E. Farrell, and R. C. Kirby, *Transformations for Piola-mapped elements*, SMAI J. Comput. Math., 8 (2022), pp. 399–437.

[4] F. R. Aznaran, P. E. Farrell, C. W. Monroe, and A. J. Van-Brunt, *Finite element methods for multicomponent convection-diffusion*, IMA J. Numer. Anal., (2024), p. drae001.

[5] A. Baier-Reinio and P. E. Farrell, *Software used in 'High-order finite element methods for three-dimensional multicomponent convection-diffusion'*. `https://doi.org/10.5281/zenodo.16416180`, 2025.

[6] A. Baier-Reinio and P. E. Farrell, *High-order finite element methods for three-dimensional multicomponent convection-diffusion*, SIAM J. Sci. Comput., 48 (2026), pp. A540–A567.

[7] A. Baier-Reinio, P. E. Farrell, and C. W. Monroe, *Finite element methods for electroneutral multicomponent electrolyte flows*, preprint, 2025. Available at `https://doi.org/10.48550/arXiv.2510.14923`.

[8] K. Balakrishnan, A. L. Garcia, A. Donev, and J. B. Bell, *Fluctuating hydrodynamics of multispecies nonreactive mixtures*, Phys. Rev. E, 89 (2014), p. 013017.

[9] S. Balay and 34 Others, *PETSc/TAO Users Manual*, Tech. Rep. ANL-21/39 - Revision 3.21, Argonne National Laboratory, 2024.

[10] A. J. Bard and L. R. Faulkner, *Electrochemical Methods: Fundamentals and Applications*, John Wiley & Sons, New York, 2nd ed., 2001.

[11] P. N. Bartlett, *Bioelectrochemistry: Fundamentals, Experimental Techniques and Applications*, John Wiley & Sons, Chichester, 2008.

[12] J. Betteridge, P. E. Farrell, M. Hochsteger, C. Lackner, J. Schöberl, S. Zampini, and U. Zerbinati, *ngsPETSc: A coupling between NETGEN/NGSolve and PETSc*, J. Open Source Softw., 9 (2024), p. 7359.

[13] A. K. Bhattacharjee, K. Balakrishnan, A. L. Garcia, J. B. Bell, and A. Donev, *Fluctuating hydrodynamics of multi-species reactive mixtures*, J. Chem. Phys., 142 (2015), p. 224107.

[14] R. B. Bird, W. E. Stewart, and E. N. Lightfoot, *Transport Phenomena*, John Wiley & Sons, 2nd ed., 2002.

[15] A. M. Bizeray, D. A. Howey, and C. W. Monroe, *Resolving a discrepancy in diffusion potentials, with a case study for Li-ion batteries*, J. Electrochem. Soc., 163 (2016), p. E223.

[16] S. W. Boettcher, S. Z. Oener, M. C. Lonergan, Y. Surendranath, S. Ardo, C. Brozek, and P. A. Kempler, *Potentially confusing: potentials in electrochemistry*, ACS Energy Lett., 6 (2020), pp. 261–266.

[17] D. Boffi, *Three-dimensional finite element methods for the Stokes problem*, SIAM J. Numer. Anal., 34 (1997), pp. 664–670.

[18] D. Boffi, F. Brezzi, and M. Fortin, *Mixed Finite Element Methods and Applications*, Springer, Heidelberg, 2013.

[19] L. Bortels, J. Deconinck, and B. Van Den Bossche, *The multi-dimensional upwinding method as a new simulation tool for the analysis of multi-ion electrolytes controlled by diffusion, convection and migration. Part 1. Steady state analysis of a parallel plane flow channel*, J. Electroanal. Chem., 404 (1996), pp. 15–26.

[20] D. Bothe, W. Dreyer, and P.-E. Druet, *Multicomponent incompressible fluids—An asymptotic study*, Appl. Maths Mech./Z. Angew. Math. Mech., 103 (2023), p. e202100174.

[21] M. Braukhoff, I. Perugia, and P. Stocker, *An entropy structure preserving space-time formulation for cross-diffusion systems: analysis and Galerkin discretization*, SIAM J. Numer. Anal., 60 (2022), pp. 364–395.

[22] F. Brezzi, J. Douglas, and L. D. Marini, *Two families of mixed finite elements for second order elliptic problems*, Numer. Math., 47 (1985), pp. 217–235.

[23] F. Brosa Planella, W. Ai, A. M. Boyce, A. Ghosh, I. Korotkin, S. Sahu, V. Sulzer, R. Timms, T. G. Tranter, M. Zyskin, et al., *A continuum of physics-based lithium-ion battery models reviewed*, Prog. Energy, 4 (2022), p. 042003.

[24] A. Brunk, A. Jüngel, and M. Lukáčová-Medvid'ová, *A structure-preserving numerical method for quasi-incompressible Navier–Stokes–Maxwell–Stefan systems*, J. Sci. Comput., 106 (2026), p. 69.

[25] M. Bulíček, A. Jüngel, M. Pokorný, and N. Zamponi, *Existence analysis of a stationary compressible fluid model for heat-conducting and chemically reacting mixtures*, J. Math. Phys., 63 (2022).

[26] E. Burman, A. Ern, and V. Giovangigli, *Bunsen flame simulation by finite elements on adaptively refined, unstructured triangulations*, Combust. Theory Model., 8 (2003), p. 65.

[27] J. A. V. Butler, *Studies in heterogeneous equilibria. Part II.—The kinetic interpretation of the Nernst theory of electromotive force*, Trans. Faraday Soc., 19 (1924), pp. 729–733.

[28] C. Cancès, V. Ehrlacher, and L. Monasse, *Finite volumes for the Stefan–Maxwell cross-diffusion system*, IMA J. Numer. Anal., 44 (2023), pp. 1029–1060.

[29] B. Carnes and G. F. Carey, *Local boundary value problems for the error in FE approximation of non-linear diffusion systems*, Internat. J. Numer. Methods Engrg., 73 (2008), pp. 665–684.

[30] H.-K. Chang, R. C. Tai, and L. E. Farhi, *Some implications of ternary diffusion in the lung*, Resp. Physiol., 23 (1975), pp. 109–120.

[31] Z. Cheng, Y.-J. Huang, B. Zahiri, P. Kwon, P. V. Braun, and D. G. Cahill, *Ionic Peltier effect in Li-ion electrolytes*, Phys. Chem. Chem. Phys., 26 (2024), pp. 6708–6716.

[32] C. I. Correa, G. N. Gatica, and R. Ruiz-Baier, *New mixed finite element methods for the coupled Stokes and Poisson–Nernst–Planck equations in Banach spaces*, ESAIM Math. Model. Numer. Anal., 57 (2023), pp. 1511–1551.

[33] L. D. Dalcin, R. R. Paz, P. A. Kler, and A. Cosimo, *Parallel distributed computing using Python*, Adv. Water Resour., 34 (2011), pp. 1124–1139.

[34] S. R. De Groot and P. Mazur, *Non-Equilibrium Thermodynamics*, Dover Publications, Inc., New York, 1984.

[35] P. Deuflhard, *Newton Methods for Nonlinear Problems*, Springer Science & Business Media, Berlin, Heidelberg, 2011.

[36] E. J. Dickinson and A. J. Wain, *The Butler-Volmer equation in electrochemical theory: Origins, value, and practical application*, J. Electroanal. Chem., 872 (2020), p. 114145.

[37] A. Donev, A. Nonaka, A. K. Bhattacharjee, A. L. Garcia, and J. B. Bell, *Low Mach number fluctuating hydrodynamics of multispecies liquid mixtures*, Phys. Fluids, 27 (2015), p. 037103.

[38] A. Donev, A. Nonaka, Y. Sun, T. Fai, A. Garcia, and J. Bell, *Low Mach number fluctuating hydrodynamics of diffusively mixing fluids*, Commun. Appl. Math. Comput. Sci., 9 (2014), pp. 47–105.

[39] A. Donev, A. J. Nonaka, C. Kim, A. L. Garcia, and J. B. Bell, *Fluctuating hydrodynamics of electrolytes at electroneutral scales*, Phys. Rev. Fluids, 4 (2019), p. 043701.

[40] W. Dreyer, C. Guhlke, and R. Müller, *Overcoming the shortcomings of the Nernst–Planck model*, Phys. Chem. Chem. Phys., 15 (2013), pp. 7075–7086.

[41] P.-É. Druet, *Global–in–time existence for liquid mixtures subject to a generalised incompressibility constraint*, J. Math. Anal. Appl., 499 (2021), p. 125059.

[42] L. Dufour, *Über die Diffusion der Gase durch poröse Wände und die sie begleitenden Temperaturveränderungen*, Ann. Phys. (Berl.), 224 (1873), pp. 490–492.

[43] A. J. Ellingsrud, P. Benedusi, and M. Kuchta, *A splitting, discontinuous Galerkin solver for the cell-by-cell electroneutral Nernst–Planck framework*, SIAM J. Sci. Comput., 47 (2025), pp. B477–B504.

[44] T. Erdey-Grúz and M. Volmer, *Zur Theorie der Wasserstoff Überspannung*, Z. Phys. Chem., 150A (1930), pp. 203–213.

[45] A. Ern and V. Giovangigli, *Multicomponent Transport Algorithms*, vol. 24, Springer Berlin, Heidelberg, 1994.

[46] ——, *Thermal diffusion effects in hydrogen-air and methane-air flames*, Combust. Theory Model., 2 (1998), p. 349.

[47] A. Ern and J.-L. Guermond, *Finite element quasi-interpolation and best approximation*, ESAIM Math. Model. Numer. Anal., 51 (2017), pp. 1367–1385.

[48] ——, *Finite Elements I: Approximation and Interpolation*, Springer, Cham, Switzerland, 2021.

[49] ——, *Finite Elements II: Galerkin Approximation, Elliptic and Mixed PDEs*, Springer, Cham, Switzerland, 2021.

[50] A. Ern, R. Joubaud, and T. Lelièvre, *Mathematical study of non-ideal electrostatic correlations in equilibrium electrolytes*, Nonlinearity, 25 (2012), p. 1635.

[51] P. E. Farrell, R. C. Kirby, and J. Marchena-Menendez, *Irksome: Automating Runge–Kutta time-stepping for finite element methods*, ACM Trans. Math. Softw., 47 (2021), pp. 1–26.

[52] E. Feireisl, D. Hilhorst, H. Petzeltová, and P. Takáč, *Mathematical analysis of variable density flows in porous media*, J. Evol. Equ., 16 (2016), pp. 1–19.

[53] A. Fick, *Über Diffusion*, Ann. Phys. (Berl.), 170 (1855), pp. 59–86.

[54] P. Franke, *Thermodynamic evaluation of five organic carbonates and their mixtures used in lithium ion batteries*, J. Electrochem. Soc., 172 (2025), p. 070520.

[55] W. H. Furry, R. C. Jones, and L. Onsager, *On the theory of isotope separation by thermal diffusion*, Phys. Rev., 55 (1939), pp. 1083–1095.

[56] V. Giovangigli, *Multicomponent Flow Modeling*, Birkhäuser, Boston, 1999.

[57] V. Giovangigli, M. Pokornỳ, and E. Zatorska, *On the steady flow of reactive gaseous mixture*, Analysis (Berlin), 35 (2015), pp. 319–341.

[58] V. Girault and P.-A. Raviart, *Finite Element Methods for Navier–Stokes Equations: Theory and Algorithms*, Springer-Verlag, Berlin, 1986.

[59] P. Goyal and C. W. Monroe, *New foundations of Newman's theory for solid electrolytes: thermodynamics and transient balances*, J. Electrochem. Soc., 164 (2017), pp. E3647–E3660.

[60] D. W. Green and R. H. Perry, *Perry's Chemical Engineers' Handbook*, McGraw Hill Professional, 8th ed., 2007.

[61] E. A. Guggenheim, *Thermodynamics: An Advanced Treatment for Chemists and Physicists*, North-Holland Books, Amsterdam, 5th ed., 1967.

[62] W. W. Hager, *Updating the inverse of a matrix*, SIAM Rev., 31 (1989), pp. 221–239.

[63] D. A. Ham and 26 Others, *Firedrake User Manual*, 1st ed., 2023.

[64] E. Helfand, *On inversion of the linear laws of irreversible thermodynamics*, J. Chem. Phys., 33 (1960), pp. 319–322.

[65] V. John, *Finite Element Methods for Incompressible Flow Problems*, Springer, Cham, Switzerland, 2016.

[66] V. John, A. Linke, C. Merdon, M. Neilan, and L. G. Rebholz, *On the divergence constraint in mixed finite element methods for incompressible flows*, SIAM Rev., 59 (2017), pp. 492–544.

[67] R. Joubaud, O. Bernard, A. Delville, A. Ern, B. Rotenberg, and P. Turq, *Numerical study of density functional theory with mean spherical approximation for ionic condensation in highly charged confined electrolytes*, Phys. Rev. E, 89 (2014), p. 062302.

[68] T. Jung, A. A. Wang, and C. W. Monroe, *Overpotential from cosolvent imbalance in battery electrolytes: LiPF6 in EMC: EC*, ACS Omega, 8 (2023), pp. 21133–21144.

[69] A. Jüngel, *The boundedness-by-entropy method for cross-diffusion systems*, Nonlinearity, 28 (2015), p. 1963.

[70] A. Jüngel and O. Leingang, *Convergence of an implicit Euler Galerkin scheme for Poisson–Maxwell–Stefan systems*, Adv. Comput. Math., 45 (2019), pp. 1469–1498.

[71] R. C. Kirby and S. P. MacLachlan, *Extending Irksome: improvements in automated Runge–Kutta time stepping for finite element methods*, ACM Trans. Math. Softw., 51 (2024), pp. 1–27.

[72] K. Knook, A. Baier-Reinio, and P. E. Farrell, *Preconditioners for the Onsager–Stefan–Maxwell equations for multicomponent diffusion*, preprint, 2026. Available at `https://doi.org/10.48550/arXiv.2604.19230`.

[73] M. N. Kogan, *Rarefied Gas Dynamics*, Plenum, New York, 1969.

[74] G. Kraaijeveld, V. Sumberova, S. Kuindersma, and H. Wesselingh, *Modelling electrodialysis using the Maxwell–Stefan description*, Chem. Eng. J., 57 (1995), pp. 163–176.

[75] G. Kraaijeveld and J. A. Wesselingh, *Negative Maxwell–Stefan diffusion coefficients*, Ind. Eng. Chem. Res., 32 (1993), pp. 738–742.

[76] R. Krishna, *Uphill diffusion in multicomponent mixtures*, Chem. Soc. Rev., 44 (2015), pp. 2812–2836.

[77] ——, *Diffusing uphill with James Clerk Maxwell and Josef Stefan*, Chem. Eng. Sci., 195 (2019), pp. 851–880.

[78] R. Krishna and J. A. Wesselingh, *The Maxwell–Stefan approach to mass transfer*, Chem. Eng. Sci., 52 (1997), pp. 861–911.

[79] E. Lightfoot, E. Cussler Jr, and R. Rettig, *Applicability of the Stefan–Maxwell equations to multicomponent diffusion in liquids*, AIChE J., 8 (1962), pp. 708–710.

[80] A. Longo, M. Barsanti, A. Cassioli, and P. Papale, *A finite element Galerkin/least-squares method for computation of multicomponent compressible–incompressible flows*, Comput. & Fluids, 67 (2012), pp. 57–71.

[81] J. Málek and V. Průša, *Derivation of equations for continuum mechanics and thermodynamics of fluids*, in Handbook of Mathematical Analysis in Mechanics of Viscous Fluids, Y. Giga and A. Novotný, eds., Springer, Cham, 2018, pp. 3–72.

[82] J. C. Maxwell, *On the dynamical theory of gases*, Phil. Trans. R. Soc., (1866), pp. 49–88.

[83] M. McLeod and Y. Bourgault, *Mixed finite element methods for addressing multi-species diffusion using the Maxwell–Stefan equations*, Comput. Meth. Appl. Mech. Eng., 279 (2014), pp. 515–535.

[84] J.-C. Nédélec, *Mixed finite elements in* $\mathbb{R}^3$, Numer. Math., 35 (1980), pp. 315–341.

[85] ——, *A new family of mixed finite elements in* $\mathbb{R}^3$, Numer. Math., 50 (1986), pp. 57–81.

[86] J. Newman and N. P. Balsara, *Electrochemical Systems*, John Wiley & Sons, Hoboken, NJ, 4th ed., 2021.

[87] J. Newman, D. Bennion, and C. W. Tobias, *Mass transfer in concentrated binary electrolytes*, Ber. Bunsenges. Phys. Chem., 69 (1965), pp. 608–612.

[88] L. Onsager, *Reciprocal relations in irreversible processes. I.*, Phys. Rev., 37 (1931), pp. 405–426.

[89] ——, *Reciprocal relations in irreversible processes. II.*, Phys. Rev., 38 (1931), pp. 2265–2279.

[90] ——, *Theories and problems of liquid diffusion*, Ann. N. Y. Acad. Sci., 46 (1945), pp. 241–265.

[91] H. C. Öttinger, *Beyond Equilibrium Thermodynamics*, John Wiley & Sons, Hoboken, NJ, 2005.

[92] J.-P. Péraud, A. Nonaka, A. Chaudhri, J. B. Bell, A. Donev, and A. L. Garcia, *Low Mach number fluctuating hydrodynamics for electrolytes*, Phys. Rev. Fluids, 1 (2016), p. 074103.

[93] B. A. Pethica, *Are electrostatic potentials between regions of different chemical composition measurable? The Gibbs–Guggenheim principle reconsidered, extended and its consequences revisited*, Phys. Chem. Chem. Phys., 9 (2007), pp. 6253–6262.

[94] C. Phelan, J. Swallow, and R. Weatherup, *Applying the Maxwell–Stefan diffusion framework to multicomponent battery electrolytes*, preprint, 2024. Available at `https://doi.org/10.26434/chemrxiv-2024-70tj6`.

[95] A. Prohl and M. Schmuck, *Convergent finite element discretizations of the Navier–Stokes–Nernst–Planck–Poisson system*, ESAIM Math. Model. Numer. Anal., 44 (2010), pp. 531–571.

[96] P.-A. Raviart and J.-M. Thomas, *A mixed finite element method for 2-nd order elliptic problems*, in Mathematical Aspects of Finite Element Methods, vol. 606 of Lecture Notes in Math., Springer, Berlin, 1977, pp. 292–315.

[97] G. W. Richardson, J. M. Foster, R. Ranom, C. P. Please, and A. M. Ramos, *Charge transport modelling of Lithium-ion batteries*, European J. Appl. Math., 33 (2022), pp. 983–1031.

[98] T. Roy, J. Andrej, and V. A. Beck, *A scalable DG solver for the electroneutral Nernst–Planck equations*, J. Comput. Phys., 475 (2023), p. 111859.

[99] R. Rungta and C. W. Monroe, *Nernst–Planck laws, distilled from Onsager–Stefan–Maxwell theory*, J. Chem. Phys., 164 (2026), p. 144907.

[100] R. Rungta, P. Slowikowski, A. Gardner, D. Persa, and C. W. Monroe, *Quantifying volumetric expansion and bulk moduli of carbonate cosolvents with lithium salts*, in preparation.

[101] J. Schöberl, *NETGEN: An advancing front 2D/3D-mesh generator based on abstract rules*, Computing and Visualization in Science, 1 (1997), pp. 41–52.

[102] L. R. Scott and M. Vogelius, *Norm estimates for a maximal right inverse of the divergence operator in spaces of piecewise polynomials*, ESAIM Math. Model. Numer. Anal., 19 (1985), pp. 111–143.

[103] J. H. Seinfeld and S. N. Pandis, *Atmospheric Chemistry and Physics: From Air Pollution to Climate Change*, John Wiley & Sons, Hoboken, NJ, 3rd ed., 2016.

[104] R. Sijabat, M. De Groot, S. Moshtarikhah, and J. Van Der Schaaf, *Maxwell–Stefan model of multicomponent ion transport inside a monolayer Nafion membrane for intensified chlor-alkali electrolysis*, J. Appl. Electrochem., 49 (2019), pp. 353–368.

[105] C. Soret, *Sur l'état d'équilibre que prend, au point de vue de sa concentration, une dissolution saline primitivement homogène, dont deux parties sont portées à des températures différentes*, Arch. Sci. Phys. Nat., 2 (1879), pp. 48–61.

[106] I. Srivastava, D. R. Ladiges, A. J. Nonaka, A. L. Garcia, and J. B. Bell, *Staggered scheme for the compressible fluctuating hydrodynamics of multispecies fluid mixtures*, Phys. Rev. E, 107 (2023), p. 015305.

[107] J. Stefan, *Über das Gleichgewicht und die Bewegung, insbesondere die Diffusion von Gasgemengen*, Sitzber. Akad. Wiss. Wien., 63 (1871), pp. 63–124.

[108] Z. Sun, J. A. Carrillo, and C.-W. Shu, *An entropy stable high-order discontinuous Galerkin method for cross-diffusion gradient flow systems*, Kinet. Relat. Models, 12 (2019), pp. 885–908.

[109] C. Taylor and P. Hood, *A numerical solution of the Navier–Stokes equations using the finite element technique*, Comput. & Fluids, 1 (1973), pp. 73–100.

[110] D. C. Thorstenson and D. W. Pollock, *Gas transport in unsaturated zones: Multicomponent systems and the adequacy of Fick's laws*, Water Resour. Res., 25 (1989), pp. 477–507.

[111] C. Tsallis, *Introduction to Nonextensive Statistical Mechanics: Approaching a Complex World*, Springer, New York, 1st ed., 2009.

[112] A. Van-Brunt, P. E. Farrell, and C. W. Monroe, *Augmented saddle-point formulation of the steady-state Stefan–Maxwell diffusion problem*, IMA J. Numer. Anal., 42 (2022), pp. 3272–3305.

[113] ——, *Consolidated theory of fluid thermodiffusion*, AIChE J., 68 (2022), p. e17599.

[114] ——, *Structural electroneutrality in Onsager–Stefan–Maxwell transport with charged species*, Electrochim. Acta, 441 (2023), p. 141769.

[115] I. M. J. J. van de Ven-Lucassen, T. J. H. Vlugt, A. J. J. van der Zanden, and P. J. A. M. Kerkhof, *Using molecular dynamics to obtain Maxwell–Stefan diffusion coefficients in liquid systems*, Mol. Phys., 94 (1998), pp. 495–503.

[116] V. K. Vanag and I. R. Epstein, *Cross-diffusion and pattern formation in reaction–diffusion systems*, Phys. Chem. Chem. Phys., 11 (2009), pp. 897–912.

[117] A. A. Wang, A. B. Gunnarsdóttir, J. Fawdon, M. Pasta, C. P. Grey, and C. W. Monroe, *Potentiometric MRI of a superconcentrated lithium electrolyte: testing the irreversible thermodynamics approach*, ACS Energy Lett., 6 (2021), pp. 3086–3095.

[118] A. A. Wang, T. Hou, M. Karanjavala, and C. W. Monroe, *Shifting-reference concentration cells to refine composition-dependent transport characterization of binary lithium-ion electrolytes*, Electrochim. Acta, 358 (2020), p. 136688.

[119] P. C. Wankat, *Separation Process Engineering: Includes Mass Transfer Analysis*, Pearson, 5th ed., 2022.

[120] G. Wanner and E. Hairer, *Solving Ordinary Differential Equations II*, vol. 375, Springer Berlin Heidelberg, 1996.

[121] A. Z. Weber, R. L. Borup, R. M. Darling, P. K. Das, T. J. Dursch, W. Gu, D. Harvey, A. Kusoglu, S. Litster, M. M. Mench, et al., *A critical review of modeling transport phenomena in polymer-electrolyte fuel cells*, J. Electrochem. Soc., 161 (2014), p. F1254.

[122] A. Z. Weber and C. Delacourt, *Mathematical modelling of cation contamination in a proton-exchange membrane*, Fuel Cells, 8 (2008), pp. 459–465.

[123] J. Wesselingh and R. Krishna, *Mass Transfer in Multicomponent Mixtures*, Delft University Press, Delft, Netherlands, 2000.

[124] D. Xie and B. Lu, *An effective finite element iterative solver for a Poisson–Nernst–Planck ion channel model with periodic boundary conditions*, SIAM J. Sci. Comput., 42 (2020), pp. B1490–B1516.

[125] S. Xu, A. J. Hutchinson, M. Taheri, B. Corry, and J. F. Torres, *Thermodiffusive desalination*, Nat. Commun., 15 (2024), pp. 1–13.

[126] S. Zhang, *A new family of stable mixed finite elements for the 3D Stokes equations*, Math. Comp., 74 (2005), pp. 543–555.